Magnetism to Spintronics
Spintronic materials and device
Micro-magnetics and Spintronics

Shang-Fan Lee (李尚凡)
Institute of Physics, Academia Sinica

J. J. Liang (梁君致)
Dept. of Physics, Fu Jen University

D. S. Hung(洪東興)
Dept. of Info. Telecom. Eng.
Ming Chuan University

S. Y. Huang (黃斯衍), C. Yu (于 淳), J. C. Lee(李榮銓), L. J. Chang (張良君), T. W. Chiang (江典蔚), L. K. Lin (林呂圭), Faris B.

Introduction to Solid State Physics

Chap. 11-13, Kittel 8th ed

Condensed Matter Physics

Chap. 24-26, Marder 2nd ed

Supported by the Academia Sinica and NSC

Cooperative phenomena

- Elementary excitations in solids describe the response of a solid to a perturbation
  - Quasiparticles

    usually fermions, resemble the particles that make the system, e.g. quasi-electrons
  - Collective excitations

    usually bosons, describe collective motions

    use second quantization with Fermi-Dirac of Bose-Einstein statistics

Magnetism

- Origin of the magnetic moment:
  – Electron spin $\vec{S}$
  – Electron orbital momentum $\vec{L}$
- From (macroscopic) response to external magnetic field $\vec{H}$
  – Diamagnetism $\chi < 0$, $\chi \sim 1 \times 10^{-6}$, insensitive to temperature
  – Paramagnetism $\chi > 0$, $\chi = \frac{C}{T}$

$$\chi = \frac{C}{T+\Delta}$$

  – Ferromagnetism exchange interaction (quantum)

- Classical and quantum theory for diamagnetism
  - Calculate $\langle r^2 \rangle$
- Classical and quantum theory for paramagnetism
  - Superparamagnetism, Langevin function
  - Hund's rules
  - Magnetic state $^{2S+1}L_J$
  - Crystal field
  - Quenching of orbital angular momentum L_z
  - Jahn-Teller effect
  - Paramagnetic susceptibility of conduction electrons

- Ferromagnetism
  - Microscopic – ferro, antiferro, ferri magnetism
  - Exchange interaction
  - Exchange splitting – source of magnetization

    two-electron system spin-independent Schrodinger equation
  - Type of exchange: direct exchange, super exchange, indirect exchange, itinerant exchange
  - Spin Hamiltonian and Heisenberg model
  - Molecular-field (mean-field) approximation

- Stoner band ferromagnetism

Demagnetization factor D

can be solved analytically in some cases, numerically in others

For an ellipsoid $D_x + D_y + D_z = 1$ (SI units) $D_x + D_y + D_z = 4\pi$ (cgs units)

Solution for Spheroid $a = b \neq c$

1. Prolate spheroid (football shape) $c/a = r > 1$; $a = b$, In cgs units

$$D_c = \frac{4\pi}{r^2-1}\left[\frac{r}{\sqrt{r^2-1}}\ln\left(r+\sqrt{r^2-1}\right)-1\right]$$

$$D_a = D_b = \frac{4\pi - D_c}{2}$$

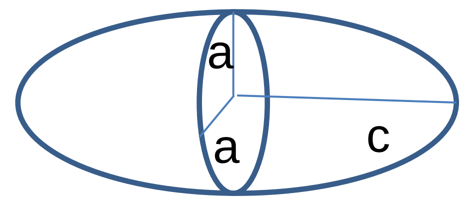

Limiting case r >> 1 (long rod)

$$D_c = \frac{4\pi}{r^2}\left[\ln(2r) - 1\right] \ll 1$$

$$D_a = D_b = 2\pi$$

Note: you measure $2\pi M$ *without* knowing the sample

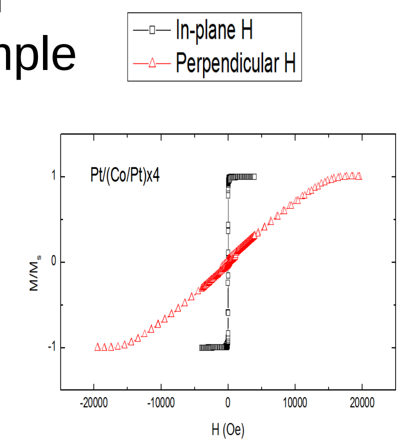

2. Oblate Spheroid (pancake shape) $c/a = r < 1$; $a = b$

$$D_c = \frac{4\pi}{1-r^2}\left[1 - \frac{r}{\sqrt{1-r^2}}\cos^{-1} r\right]$$

$$D_a = D_b = \frac{4\pi - D_c}{2}$$

Limiting case r >> 1 (flat disk)

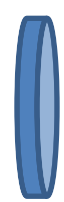

$$D_c = 4\pi$$

$$D_a = D_b = \pi\,{}^2 r \ll 1$$

Note: you measure $4\pi M$ *without* knowing the sample

Ferromagnetic domains

$$E = E_{exchange} + E_{Zeeman} + E_{mag} + E_{anisotropy} + \cdots$$

- $E_{ex} : \sum 2J\vec{S_i} \cdot \vec{S_j}$
- $E_{Zeeman} : \vec{M} \cdot \vec{H}$
- $E_{mag} : \frac{1}{8\pi}\int B^2 dV$
- $E_{anisotropy}$

  For hcp Co$= K_1' \sin^2\theta + K_2{}' \sin^4\theta$

  For bcc Fe $= K_1(\alpha_1^2\alpha_2^2 + \alpha_2^2\alpha_3^2 + \alpha_3^2\alpha_1^2) + K_2(\alpha_1^2\alpha_2^2\alpha_3^2)$

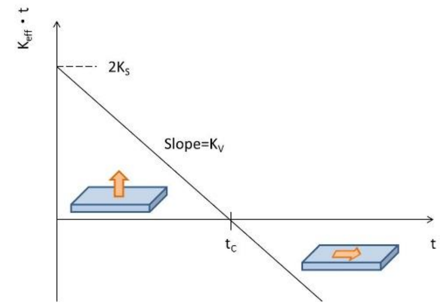

α_i : directional cosines

Surface anisotropy $K_{\text{eff}} = \frac{2K_S}{t} + K_V$ ➔ $K_{\text{eff}} \cdot t = 2K_S + K_V \cdot t$

For a 180° Bloch wall rotated in N+1 atomic planes, $N\Delta E_{ex} = N(JS^2\left(\frac{\pi}{N}\right)^2)$

Wall energy density $\sigma_w = \sigma_{ex} + \sigma_{anis} \approx JS^2\pi^2/(Na^2) + KNa$ $\quad a$: lattice constant

$\partial\sigma_w/\partial N \equiv 0,$ $\quad N = \sqrt{[JS^2\pi^2/(Ka^3)]} \approx 300$ in Fe

$\sigma_w = 2\pi\sqrt{KJS^2/a} \approx$ 1 erg/cm^2 in Fe

Wall width $\quad Na = \pi\sqrt{JS^2/Ka} \equiv \pi\sqrt{\frac{A}{K}}$, $\quad A = JS^2/a$ Exchange stiffness constant

Domain wall energy γ versus thickness D of $Ni_{80}Fe_{20}$ thin films

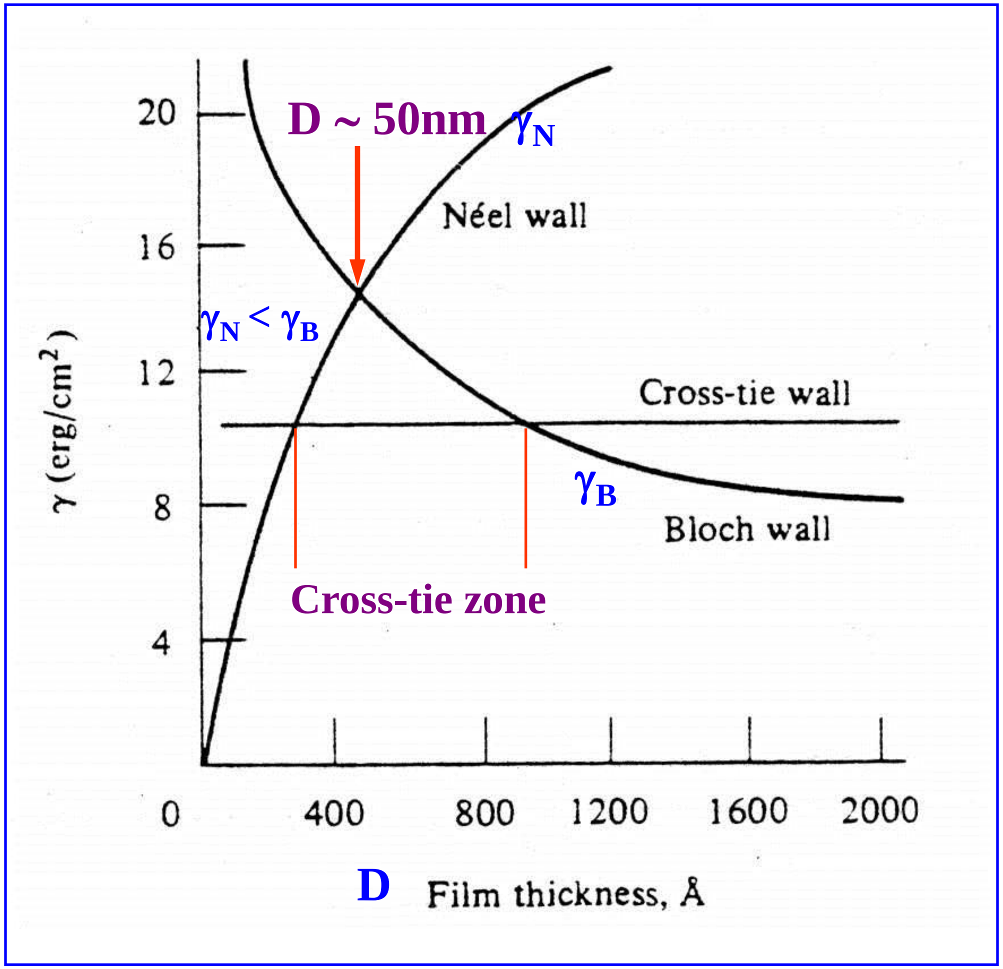

$A=10^{-6}$ erg/cm

$K=1500$ erg/cm^3

When D < 50 nm，

$\gamma_N < \gamma_B$。

From Bloch wall in ‘thick’ film to Neel wall in ‘thin’ film, there is a transition region of ‘Cross-tie’ wall.

Magnetic Resonance

- Nuclear Magnetic Resonance (NMR)
  - Line width
  - Hyperfine Splitting, Knight Shift
  - Nuclear Quadrupole Resonance (NQR)
- Ferromagnetic Resonance (FMR)
  - Shape Effect
  - Spin Wave resonance (SWR)
- Antiferromagnetic Resonance (AFMR)
- Electron Paramagnetic Resonance (EPR or ESR)
  - Exchange narrowing
  - Zero-field Splitting
- Maser

What we can learn:

- From absorption fine structure ➔ electronic structure of single defects
- From changes in linewidth ➔ relative motion of the spin to the surroundings
- From resonance frequency ➔ internal magnetic field
- Collective spin excitations

FMR

Equation of motion of a magnetic moment $\boldsymbol{\mu}$ in an external field B_0

$$\frac{\hbar d\boldsymbol{I}}{dt} = \boldsymbol{\mu} \times \boldsymbol{B} \qquad \boldsymbol{\mu} = \gamma \hbar \boldsymbol{I} \qquad \frac{d\boldsymbol{\mu}}{dt} = \gamma \boldsymbol{\mu} \times \boldsymbol{B} \qquad \frac{d\boldsymbol{M}}{dt} = \gamma \boldsymbol{M} \times \boldsymbol{B}$$

Landau-Lifshitz-Gilbert (LLG) equation

$$\frac{d\boldsymbol{M}}{dt} = -\gamma \boldsymbol{M} \times \boldsymbol{H}_{\text{eff}} + \alpha \boldsymbol{M} \times \frac{d\boldsymbol{M}}{dt}$$

Shape effect:

internal magnetic field

$$B_x^i = B_x^0 - N_x M_x \qquad B_y^i = B_y^0 - N_y M_y \qquad B_z^i = B_z^0 - N_z M_z$$

$$\frac{dM_x}{dt} = \gamma\left(M_y B_z^i - M_z B_y^i\right) = \gamma\left[B_0 + \left(N_y - N_z\right)M\right]M_y$$

$$\frac{dM_y}{dt} = \gamma[M(-N_x M_x) - M_x(B_0 - N_z M)] = -\gamma[B_0 + (N_x - N_z)M]M_x$$

To first order $\dfrac{dM_z}{dt} = 0 \qquad M_z = M$

$$\begin{vmatrix} i\omega & \gamma\left[B_0 + \left(N_y - N_z\right)M\right] \\ -\gamma[B_0 + (N_x - N_z)M] & i\omega \end{vmatrix} = 0$$

$$\omega_0^2 = \gamma^2\left[B_0 + \left(N_y - N_z\right)M\right][B_0 + (N_x - N_z)M]$$

Uniform mode

Uniform mode

Sphere | flat plate with perpendicular field | flat plate with in-plane field

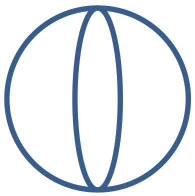

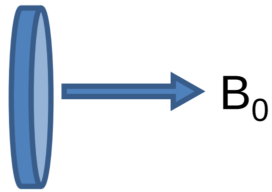

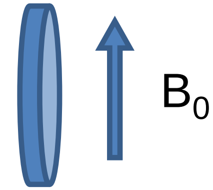

$N_x = N_y = N_z$ | $N_x = N_y = 0 \quad N_z = 4\pi$ | $N_x = N_z = 0 \quad N_y = 4\pi$

$\omega_0 = \gamma\, B_0$ | $\omega_0 = \gamma\,(B_0 - 4\pi M)$ | $\omega_0 = \gamma\,[B_0(B_0 + 4\pi M)]^{1/2}$

Spin wave resonance; Magnons

Consider a one-dimensional spin chain with only nearest-neighbor interactions.

$U = -2J \sum \vec{S_i} \cdot \vec{S_j}$ We can derive $\hbar\omega = 4JS(1 - \cos ka)$

When $ka << 1$ $\quad \hbar\omega \cong (2JSa^2)k^2$

flat plate with perpendicular field $\quad \omega_0 = \gamma\,(B_0 - 4\pi M) + Dk^2$

Quantization of (uniform mode) spin waves, then consider the thermal excitation of Mannons, leads to Bloch $T^{3/2}$ law. $\quad \Delta M/M(0) \propto T^{3/2}$

AFMR

Spin wave resonance; Antiferromagnetic Magnons

Consider a one-dimensional antiferromangetic spin chain with only nearest-neighbor interactions. Treat sublattice A with up spin S and sublattice B with down spin –S, J<0.

$U = -2J\sum \vec{S_i} \cdot \vec{S_j}$ We can derive $\hbar\omega = -4JS|\sin ka|$

When $ka << 1$ $\hbar\omega \cong (-4JS)|ka|$

AFMR

exchange plus anisotropy fields on the two sublattices

$\boldsymbol{B}_1 = -\lambda \boldsymbol{M}_2 + B_A \hat{\boldsymbol{z}}$ on $\mathbf{M}_1$ $\boldsymbol{B}_2 = -\lambda \boldsymbol{M}_1 - B_A \hat{\boldsymbol{z}}$ on $\mathbf{M}_2$

$M_1^z \equiv M$ $M_2^z \equiv -M$ $M_1^+ \equiv M_1^x + iM_1^y$ $M_2^+ \equiv M_2^x + iM_2^y$ $B_E \equiv \lambda M$

$$\frac{dM_1^+}{dt} = -i\gamma[M_1^+(B_A + B_E) + M_2^+ B_E]$$

$$\frac{dM_2^+}{dt} = -i\gamma[M_2^+(B_A + B_E) + M_1^+ B_E]$$

$$\begin{vmatrix} \gamma(B_A + B_E) - \omega & \gamma B_E \\ B_E & \gamma(B_A + B_E) + \omega \end{vmatrix} = 0$$

$\omega_0^2 = \gamma^2 B_A(B_A + 2B_E)$ Uniform mode

outline

- Giant Magnetoresistance, Tunneling Magnetoresistance
- Pure Spin current (no net charge current)
    - Spin Hall, Inverse Spin Hall effects
    - Spin Pumping effect
    - Spin Seebeck effect
- Spin Transfer Torque
- Micro and nano Magnetics

Spintronics :

Electronics with electron spin as an extra degree of freedom
Generate, inject, process, and detect spin currents

- **Generation: ferromagnetic materials, spin Hall effect, spin pumping effect etc.**
- **Injection: interfaces, heterogeneous structures, tunnel junctions**
- **Process: spin transfer torque**
- **Detection: Giant Magnetoresistance, Tunneling MR**

科學月刊 **38**, 898 (2007).
物理雙月刊 **30**, 116 (2008).
科學人 **87**, 82 (2009).

鐵磁性元素 : 鐵 Fe, 鈷 Co, 鎳 Ni, 釓 Gd, 鏑 Dy,
錳 Mn, 鈀 Pd ??

Elements with ferromagnetic properties

合金, alloys

錳氧化物 MnOx

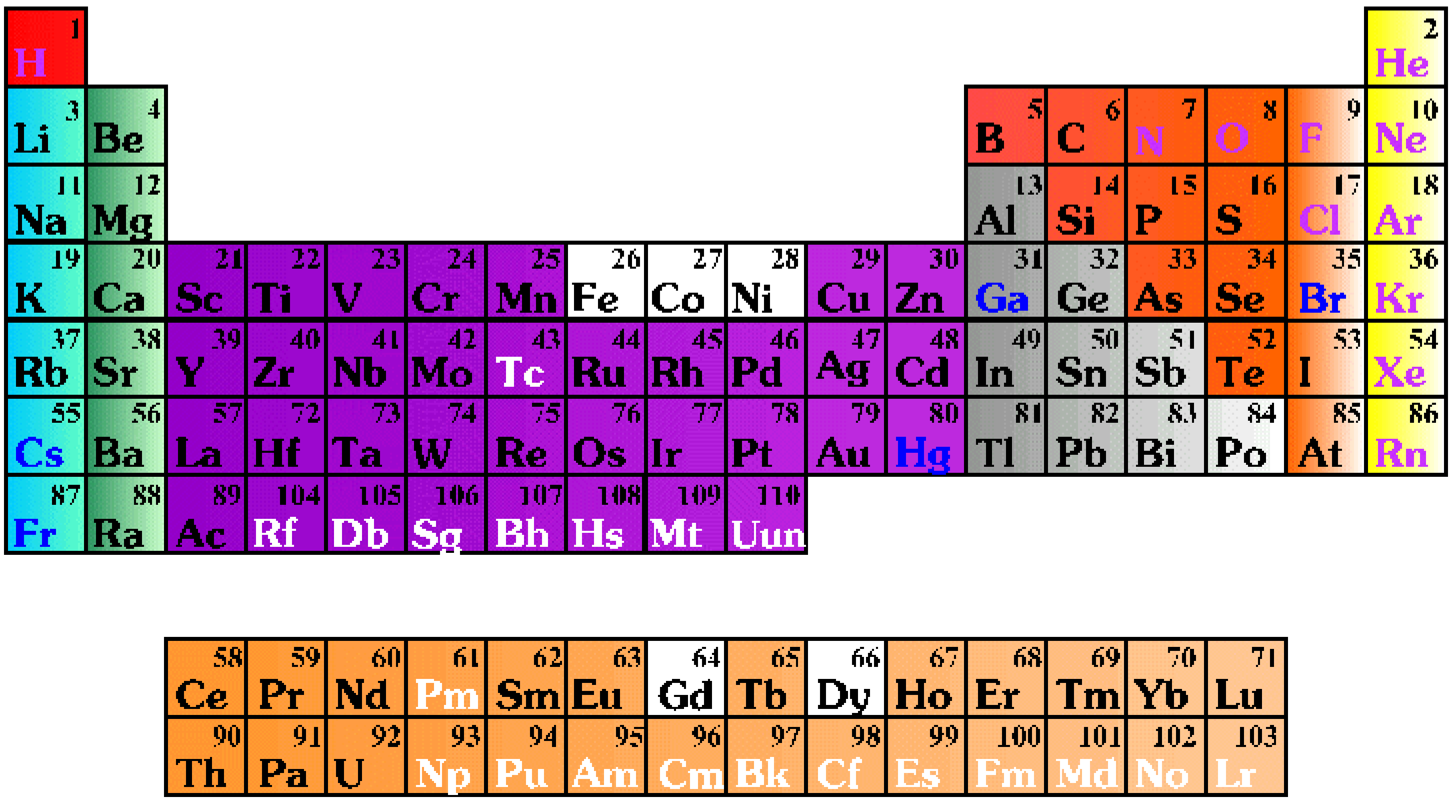

Solar system

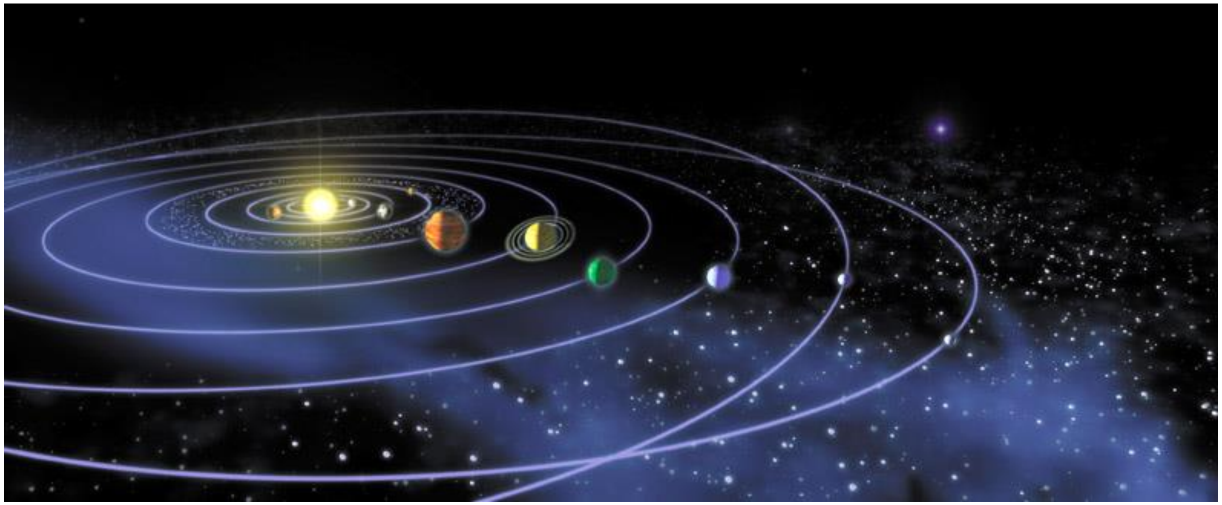

s, p electron orbital

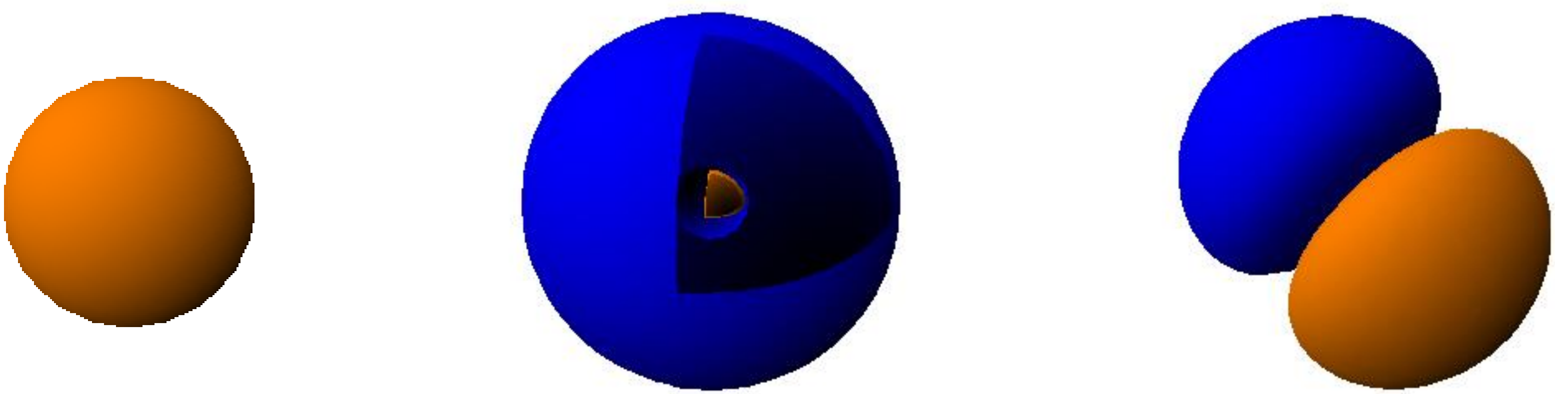

Orbital viewer

Platonic solid

From Wikipedia

In geometry, a Platonic solid is a convex polyhedron that is regular, in the sense of a regular polygon. Specifically, the faces of a Platonic solid are congruent regular polygons, with the same number of faces meeting at each vertex; thus, all its edges are congruent, as are its vertices and angles.
There are precisely five Platonic solids (shown below):

The name of each figure is derived from its number of faces: respectively 4, 6, 8, 12, and 20.

The aesthetic beauty and symmetry of the Platonic solids have made them a favorite subject of geometers for thousands of years. They are named for the ancient Greek philosopher Plato who theorized that the classical elements were constructed from the regular solids.

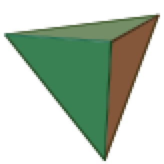 Tetrahedron	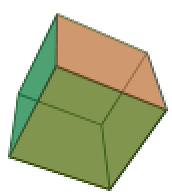 Cube hexahedron	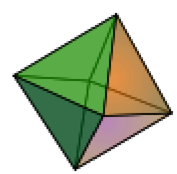 Octahedron	 Dodecahedron	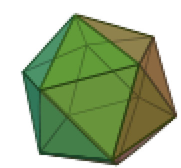 Icosahedron

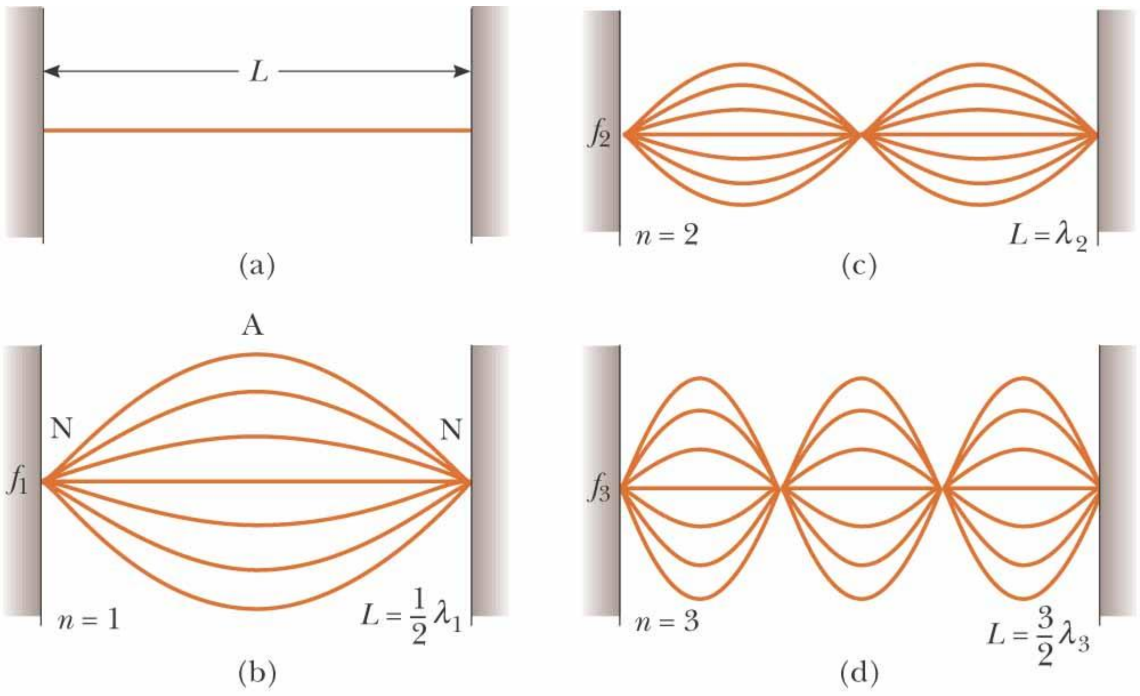

One-dimensional resonance

Two-dimensional resonance

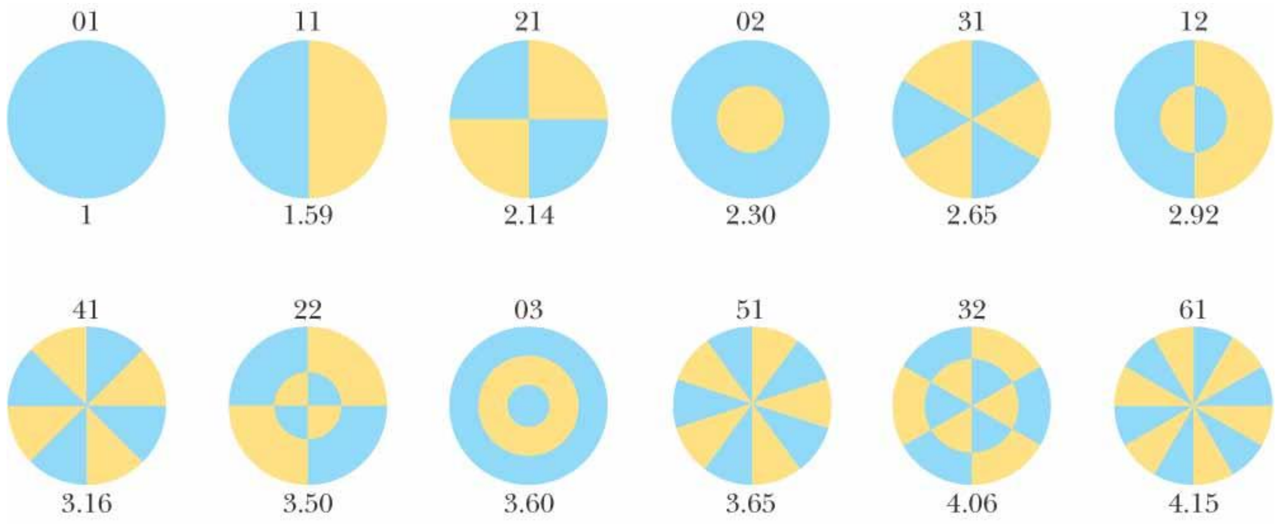

3d transition metals:

Mn atom has 5 d ↑ electrons

Bulk Mn is NOT magnetic.

3d electron distribution in real space

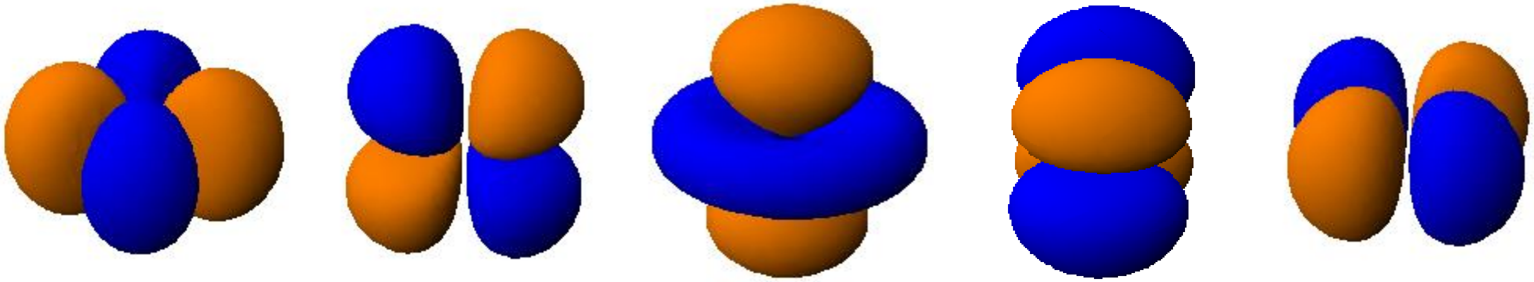

Co atom has 5 d ↑electrons and 2 d ↓ electrons

Bulk Co is magnetic.

Stoner criterion for ferromagnetism:

$I\,N(E_F) > 1$, I is the Stoner exchange parameter and $N(E_F)$ is the density of states at the Fermi energy.

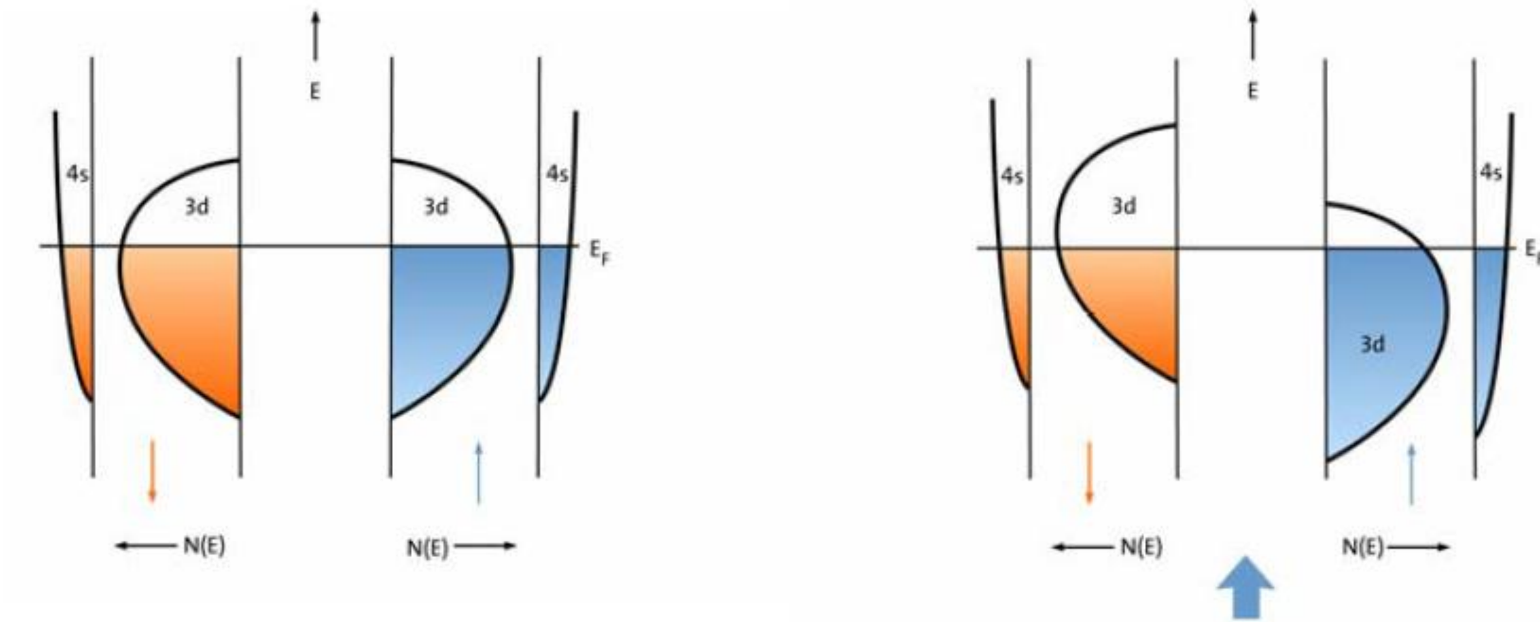

For the non-magnetic state there are identical density of states for the two spins.

For a ferromagnetic state, $N\uparrow > N\downarrow$. The polarization is indicated by the thick blue arrow.

Schematic plot for the energy band structure of 3d transition metals.

RKKY (*Ruderman-Kittel-Kasuya-Yosida*) interaction

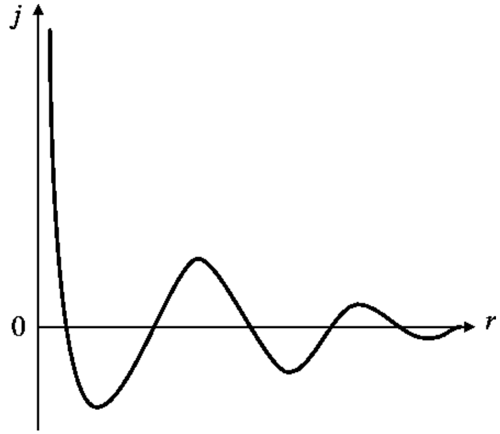

coupling coefficient

$$j\left(\boldsymbol{R}_l - \boldsymbol{R}_{l'}\right) = 9\pi \left(\frac{j^2}{\epsilon_F}\right) F\left(2k_F|\boldsymbol{R}_l - \boldsymbol{R}_{l'}|\right)$$

$$F(x) = \frac{x\cos x - \sin x}{x^4}$$

Magnetic coupling in superlattices

- Long-range incommensurate magnetic order in a Dy-Y multilayer
  M. B. Salamon, Shantanu Sinha, J. J. Rhyne, J. E. Cunningham, Ross W. Erwin, Julie Borchers, and C. P. Flynn, Phys. Rev. Lett. **56**, 259 - 262 (1986)
- Observation of a Magnetic Antiphase Domain Structure with Long-Range Order in a Synthetic Gd-Y Superlattice
  C. F. Majkrzak, J. W. Cable, J. Kwo, M. Hong, D. B. McWhan, Y. Yafet, and J. V. Waszczak,C. Vettier, Phys. Rev. Lett. **56**, 2700 - 2703 (1986)
- Layered Magnetic Structures: Evidence for Antiferromagnetic Coupling of Fe Layers across Cr Interlayers
  P. Grünberg, R. Schreiber, Y. Pang, M. B. Brodsky, and H. Sowers, Phys. Rev. Lett. **57**, 2442 - 2445 (1986)

Magnetic coupling in multilayers

•Long-range incommensurate magnetic order in a Dy-Y multilayer
M. B. Salamon, Shantanu Sinha, J. J. Rhyne, J. E. Cunningham, Ross W. Erwin, Julie Borchers, and C. P. Flynn, Phys. Rev. Lett. 56, 259 - 262 (1986)

•Observation of a Magnetic Antiphase Domain Structure with Long- Range Order in a Synthetic Gd-Y Superlattice
C. F. Majkrzak, J. W. Cable, J. Kwo, M. Hong, D. B. McWhan, Y. Yafet, and J. V. Waszczak,C. Vettier, Phys. Rev. Lett. 56, 2700 - 2703 (1986)

•Layered Magnetic Structures: Evidence for Antiferromagnetic Coupling of Fe Layers across Cr Interlayers
P. Grünberg, R. Schreiber, Y. Pang, M. B. Brodsky, and H. Sowers, Phys. Rev. Lett. 57, 2442 - 2445 (1986)

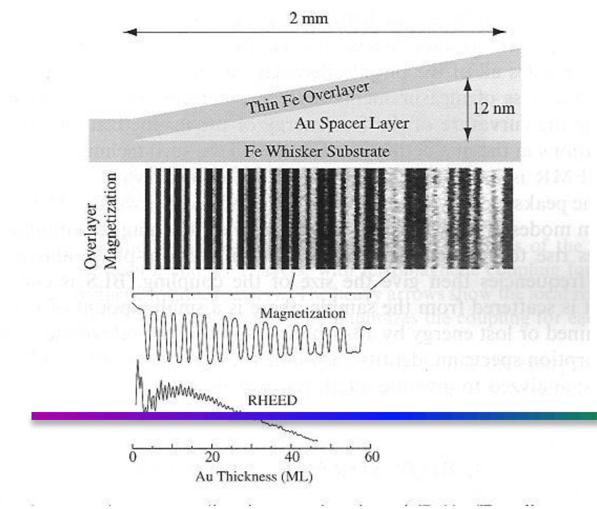

Coupling in **wedge-shaped**
Fe/Cr/Fe
Fe/Au/Fe
Fe/Ag/Fe
J. Unguris, R. J. Celotta, and D. T. Pierce

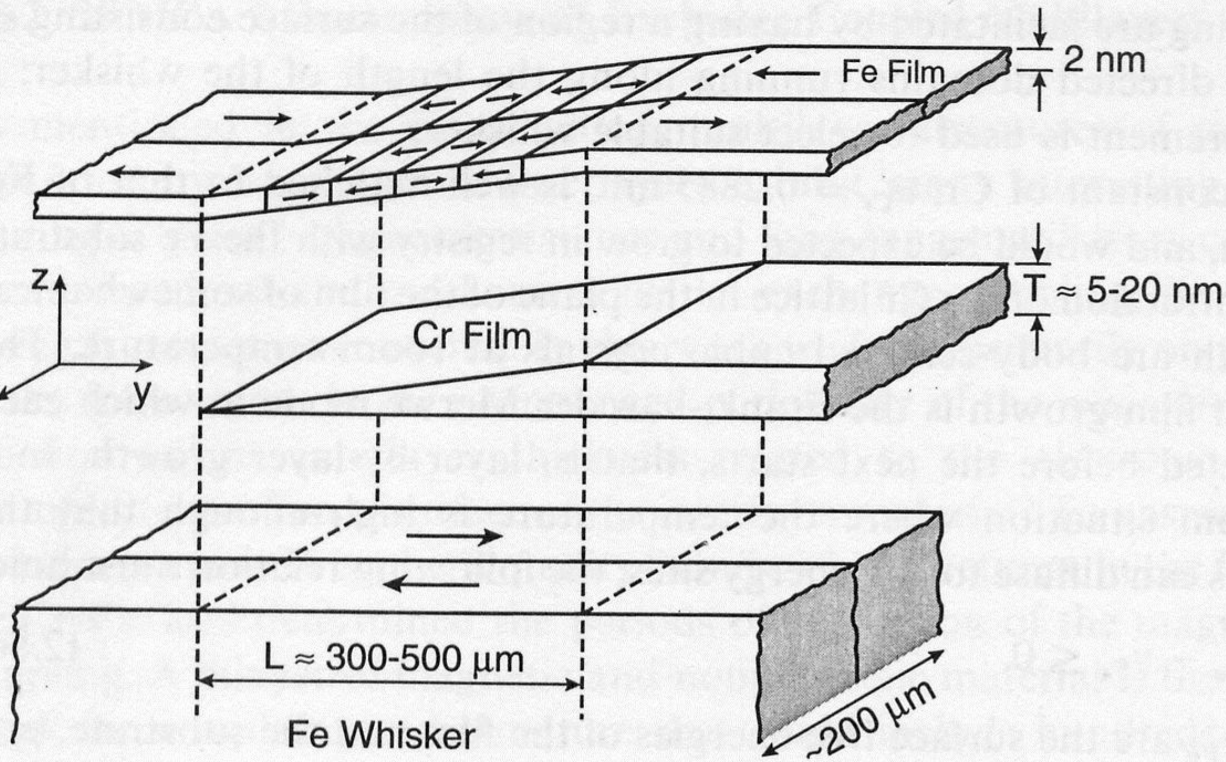

Fig. 2.41. A schematic expanded view of the sample structure showing the Fe(0 0 1) single-crystal whisker substrate, the evaporated Cr wedge, and the Fe overlayer. The arrows in the Fe show the magnetization direction in each domain. The z-scale is expanded approximately 5000 times. (From [2.206])

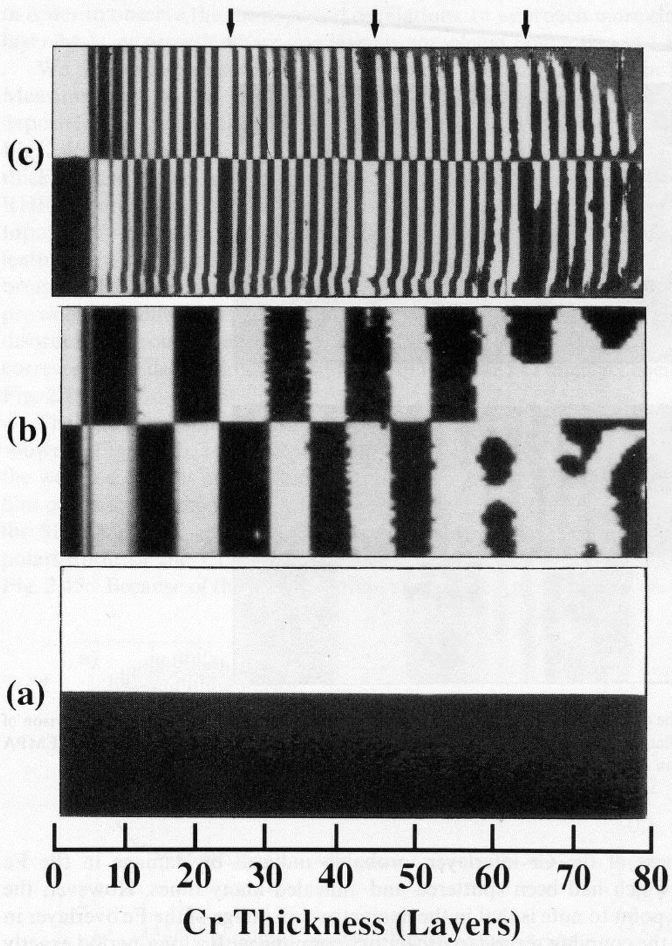

Fig. 2.43. SEMPA image of the magnetization M_y (axes as in Fig. 2.41) showing domains in (**a**) the clean Fe whisker, (**b**) the Fe layer covering the Cr spacer layer evaporated at 30 °C, and (**c**) the Fe layer covering a Cr spacer evaporated on the Fe whisker held at 350 °C. The scale at the bottom shows the increase in the thickness of the Cr wedge in (**b**) and (**c**). The arrows at the top of (**c**) indicate the Cr thicknesses where there are phase slips. The region of the whisker imaged is about 0.5 mm long

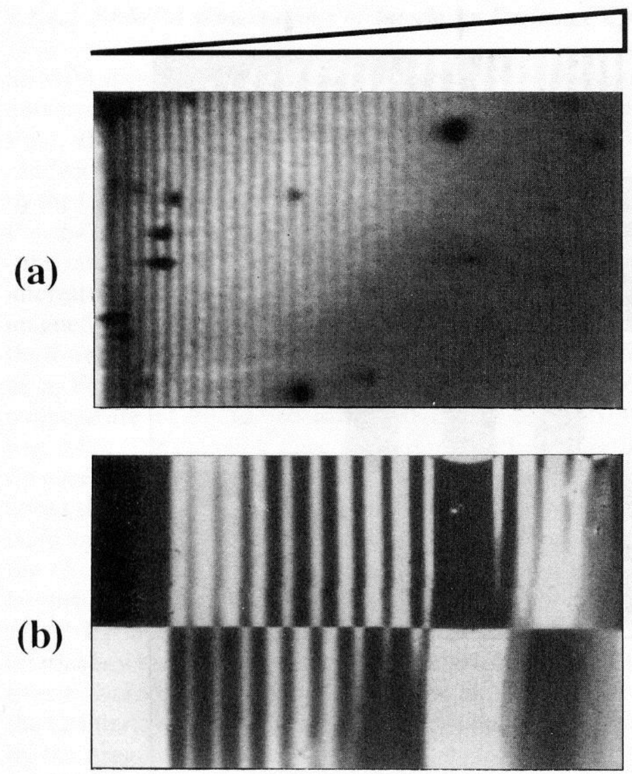

Fig. 2.44. The effect of roughness on the inertlayer exchange coupling is shown by a comparison of (**a**) the oscillations of the RHEED intensity along the bare Cr wedge with (**b**) the SEMPA magnetization image over the same part of the wedge

Oscillatory magnetic coupling in multilayers

Ru interlayer has the largest coupling strength

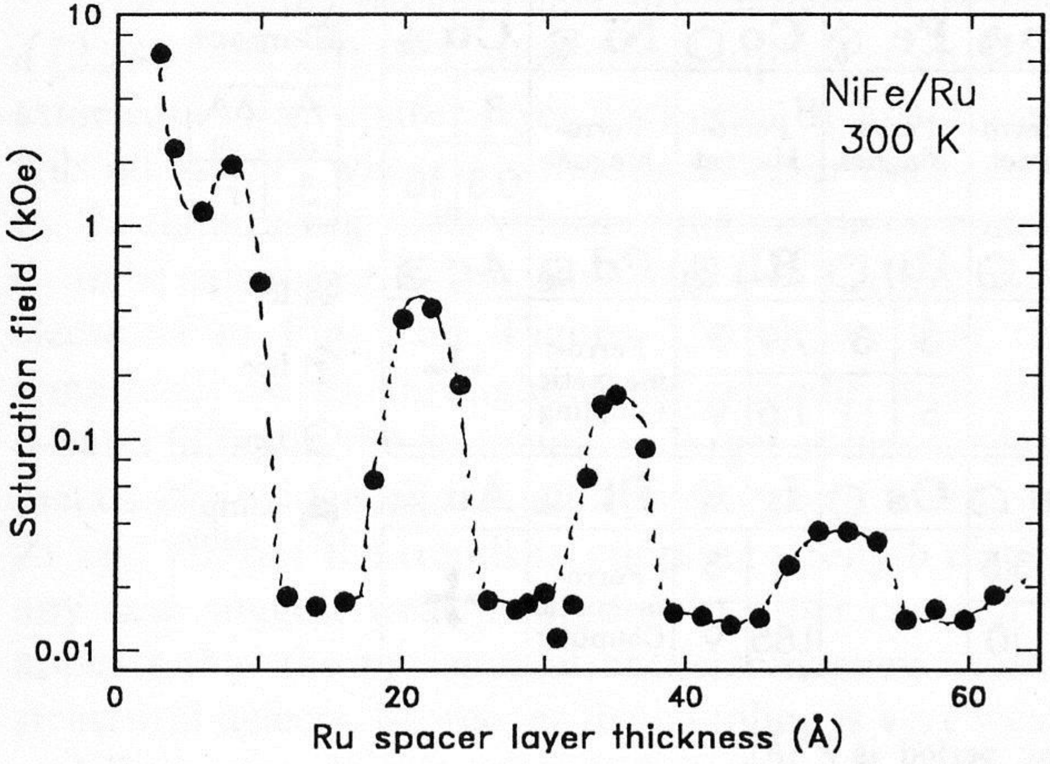

S. S. P. Parkin

Fig. 2.58. Dependence of saturation field on Ru spacer layer thickness for several series of $Ni_{81}Fe_{19}$/Ru multilayers with structure, 100 Å Ru/[30 Å $Ni_{81}Fe_{19}$/Ru(t_{Ru})]$_{20}$, where the topmost Ru layer thickness is adjusted to be $\simeq$25 Å for all samples

Kwo et al, PRB **35** 7295 (1987)
Modulated magnetic properties in synthetic rare-earth Gd-Y superlattices

Spin-dependent conduction in Ferromagnetic metals (Two-current model)

First suggested by Mott (1936)

Experimentally confirmed by I. A. Campbell and A. Fert (~1970)

At low temperature

$$\rho = \frac{\rho_{\uparrow}\rho_{\downarrow}}{\rho_{\uparrow} + \rho_{\downarrow}}$$

At high temperature

$$\rho = \frac{\rho_{\uparrow}\rho_{\downarrow} + \rho_{\uparrow\downarrow}(\rho_{\uparrow} + \rho_{\downarrow})}{\rho_{\uparrow} + \rho_{\downarrow} + 4\rho_{\uparrow\downarrow}}$$

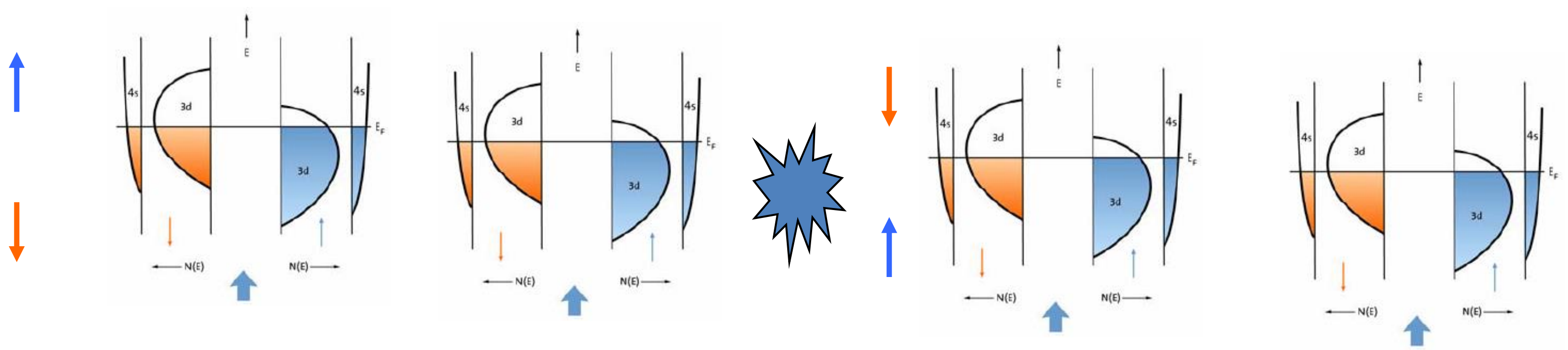

Spin mixing effect equalizes two currents

Two Current Model

s **electrons carry the electric current**

resistivity (spin-dependent *s* → *d* scattering)

$$R^S = \text{const. } N_d^S$$

number of empty *d* states

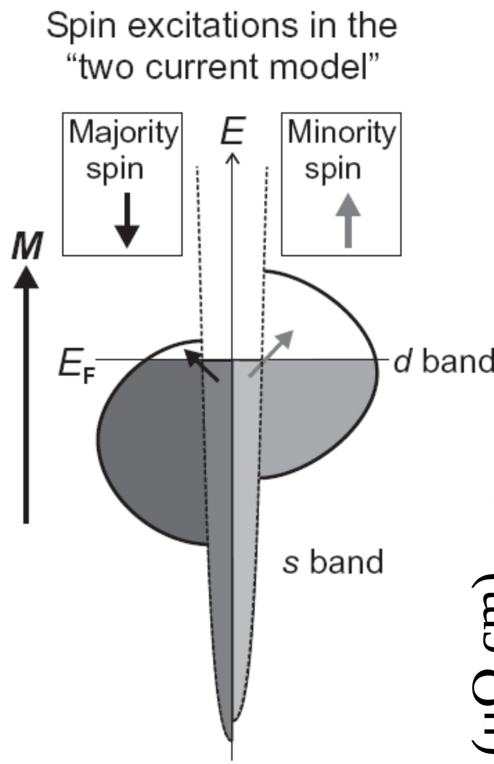

spin selective scattering

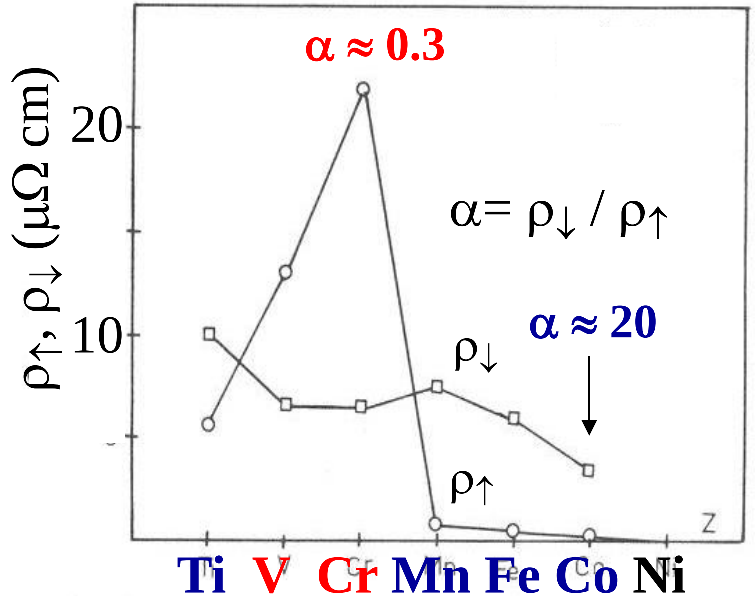

element	$N_{\rm h}^{d}$ [a]	$\lvert\boldsymbol{m}\rvert$ $[\mu_{\rm B}]$	R [b] $[\Omega\,{\rm m}]$
Fe (bcc)	3.90	2.216	9.71×10^{-8}
Co (hcp)	2.80	1.715	6.25×10^{-8}
Ni (fcc)	1.75	0.616	6.84×10^{-8}
Cu (fcc)	0.50	–	1.68×10^{-8}

A. Fert, I.A. Campbell, PRL **21**, 1190 (1968)

Anisotropic magnetoresistance (AMR)

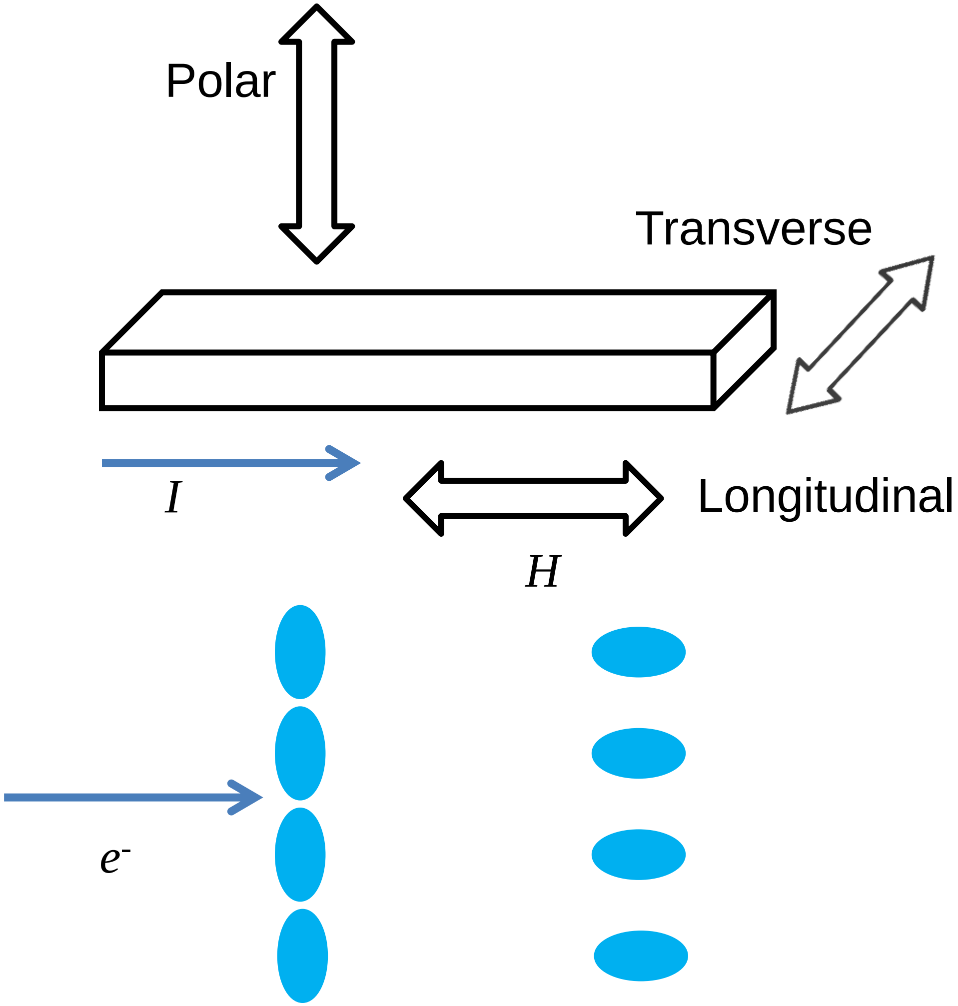

$$R_{Long.} > R_{Trans.}, R_{Pol.}$$

Geometrical size effect

Fe 100nm 10K

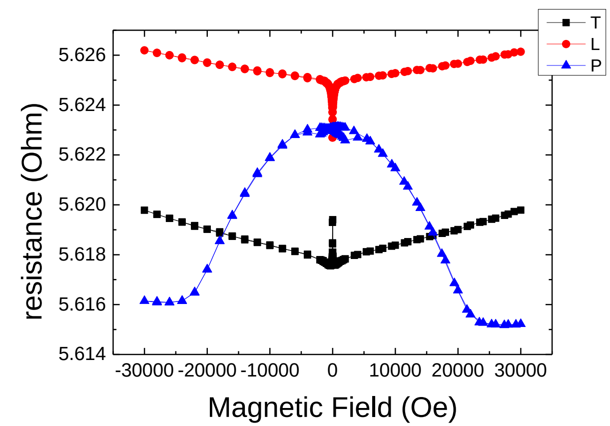

Ni 100nm 10K

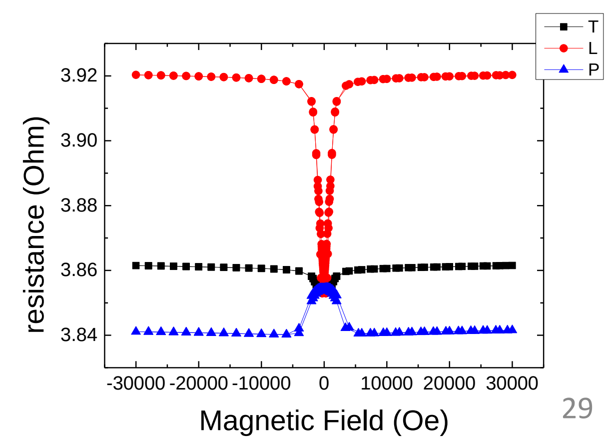

outline

- Giant Magnetoresistance, Tunneling Magnetoresistance
- Pure Spin current (no net charge current)
  - Spin Hall, Inverse Spin Hall effects
  - Spin Pumping effect
  - Spin Seebeck effect
- Spin Transfer Torque
- Micro and nano Magnetics

2007 Nobel prize in Physics

2007年諾貝爾物理獎得主 左 亞伯・費爾(Albert Fert)
與右彼得・葛倫貝格(Peter Grünberg)

(圖片資料來源：Copyright © Nobel Web AB 2007/ Photo: Hans Mehlin)

Giant Magnetoresistance
Tunneling Magnetoresistance

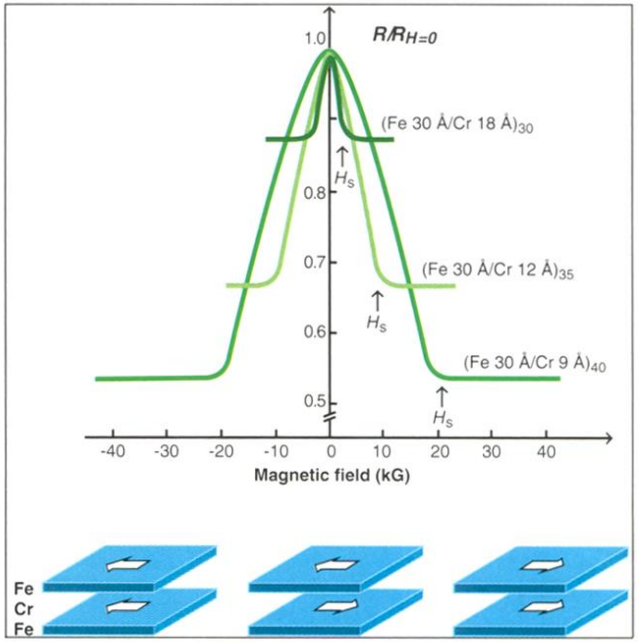

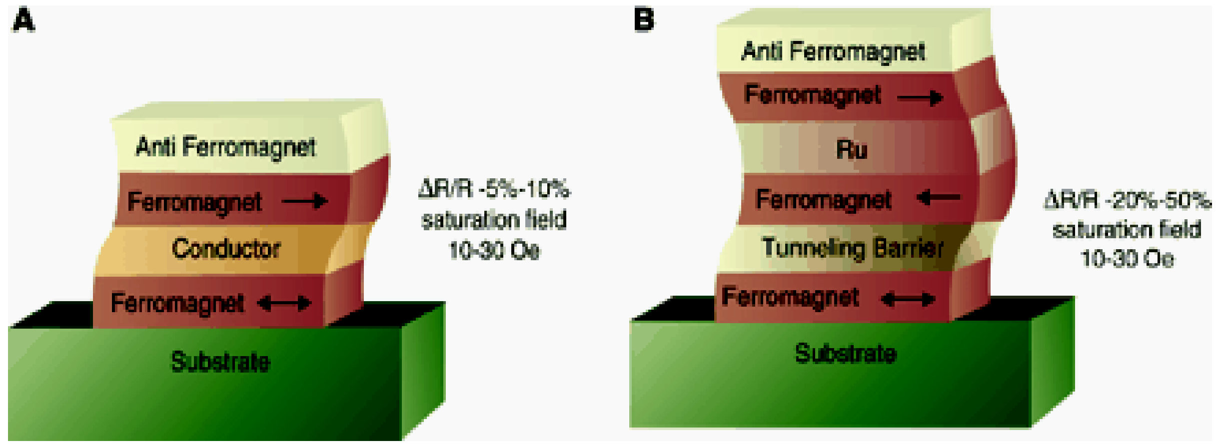

Discovery of Giant MR -- Two-current model combines with magnetic coupling in multilayers

Spin-dependent transport structures. (A) Spin valve. (B) Magnetic tunnel junction. (from Science)

Moodera's group, PRL **74**, 3273 (1995)

Fert's group, PRL **61**, 2472 (1988)

Miyazaki's group, JMMM **139**, L231(1995)

Transport geometry

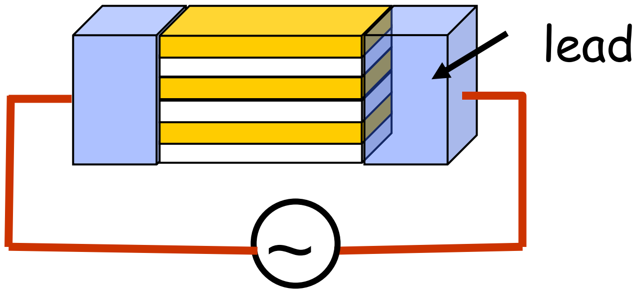

CIP geometry

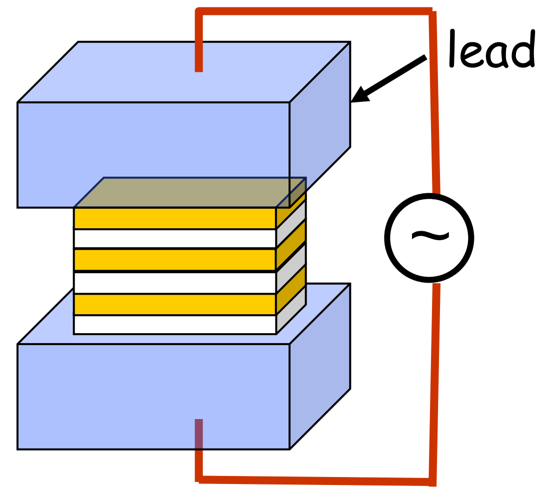

CPP geometry

- In metallic multilayers, CIP resistance can be measured easily, CPP resistance needs special techniques.
- From CPP resistance in metallic multilayers, one can measure interface resistances, spin diffusion lengths, and polarization in ferromagnetic materials, etc.

Valet and Fert model of (CPP-)GMR

Based on the Boltzmann equation

A semi-classical model with spin taken into consideration

$$j_{+(-)} = \frac{1}{e\rho_{+(-)}} \frac{\partial \mu_{+(-)}}{\partial x}$$

$$j_+ + j_- = j_e$$

$$\frac{\partial (j_+ - j_-)}{\partial x} = \frac{2eN(E_F)\Delta\mu}{\tau_{sf}}$$

$$\frac{\partial^2 \mu_{+(-)}}{\partial z^2} = \frac{\mu_{+(-)}}{l_{sf}^2} \qquad l_{sf}^F = \left[\lambda_{sf}^F / 3(\lambda_\uparrow^{-1} + \lambda_\downarrow^{-1})\right]^{1/2}, \quad l_{sf}^N = \left[\lambda_{sf}^N \lambda / 6\right]^{1/2}$$

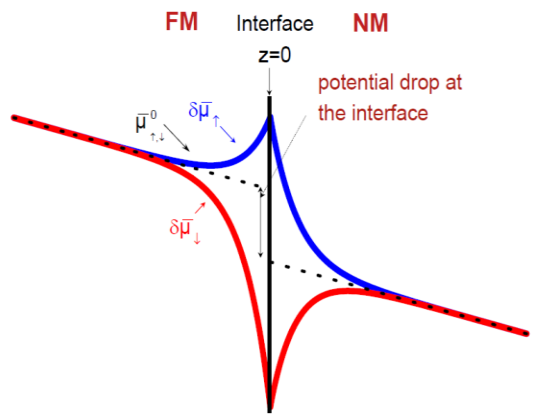

$\Delta\mu$ for antiparallel aligned multilayers

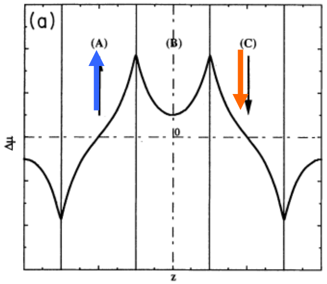

$\Delta\mu$ for parallel aligned multilayers

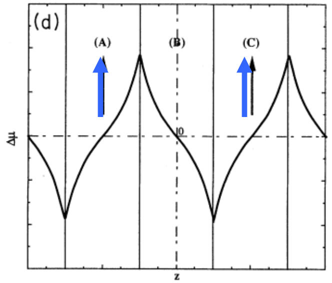

Spin imbalance induced charge accumulation at the interface is important

Spin diffusion length, instead of mean free path, is the dominant physical length scale

Spin valve –

a sandwich structure with a free ferromagnetic layer (F) and a fixed F layer pinned by an antiferromagnetic (AF) layer

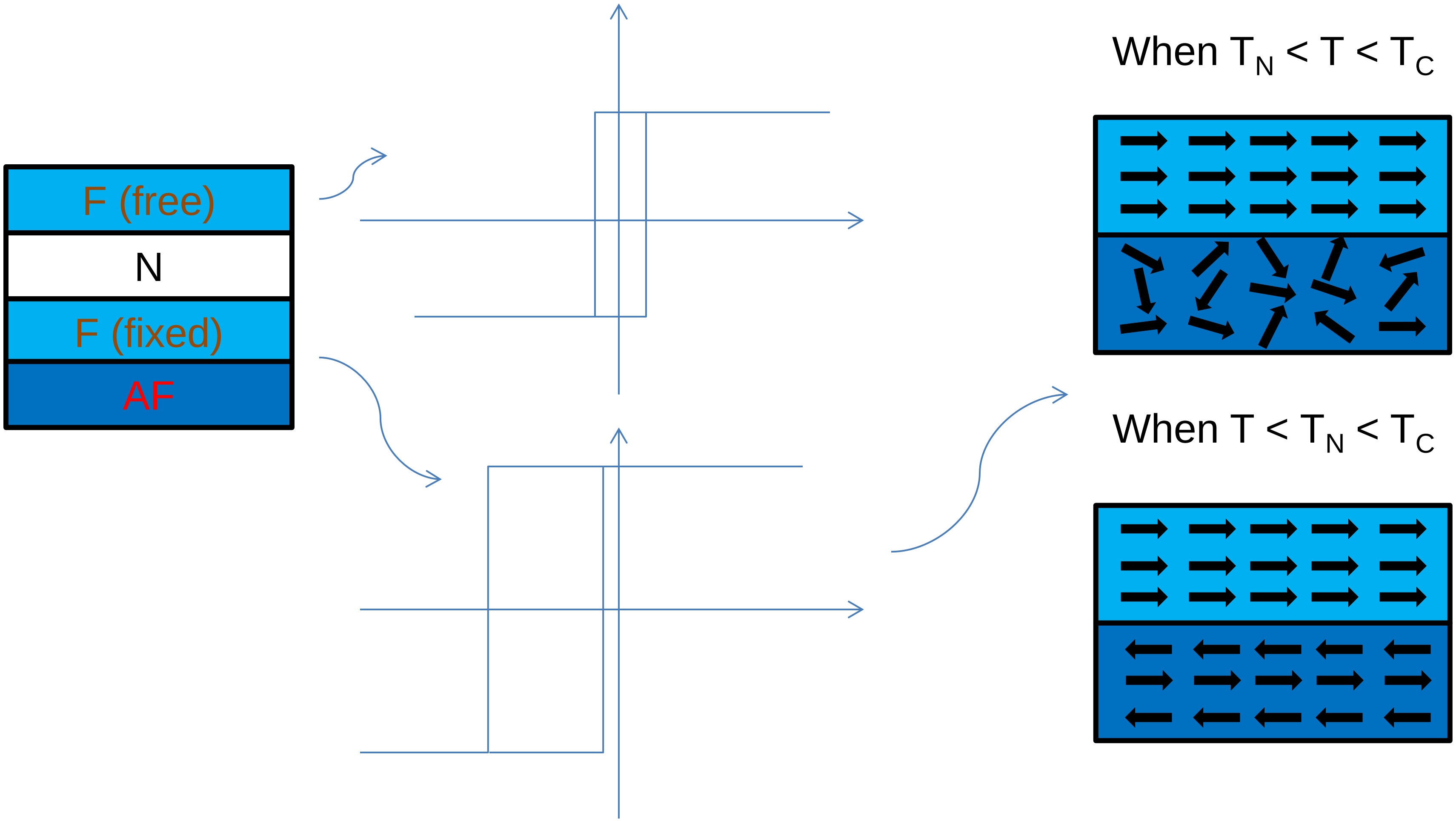

Types of antiferromagnet

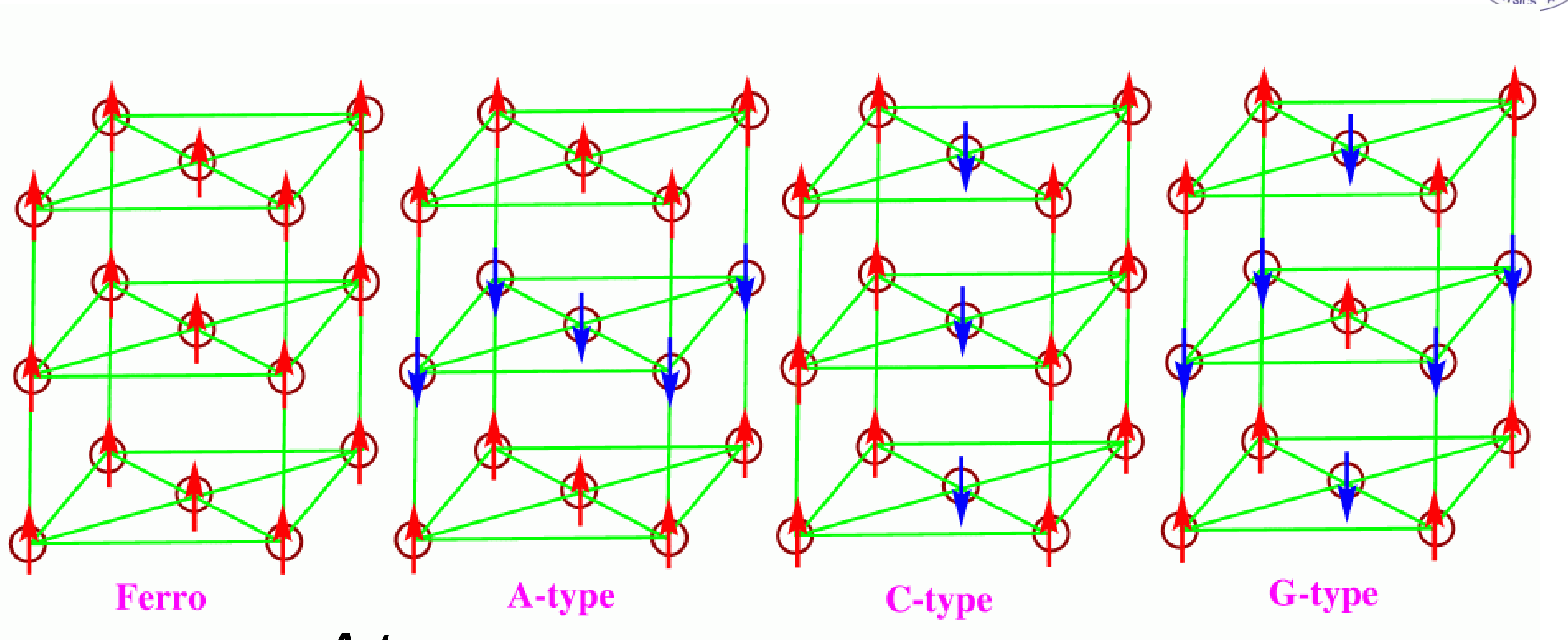

A-type:

Intra-plane F coupling, Inter-plane AF coupling.

C-type:

Intra-plane AF coupling, Inter-plane F coupling.

G-type:

Both intra-plane and inter-plane are AF coupling.

Spin Diffusion: The Johnson Transistor
non-local measurement

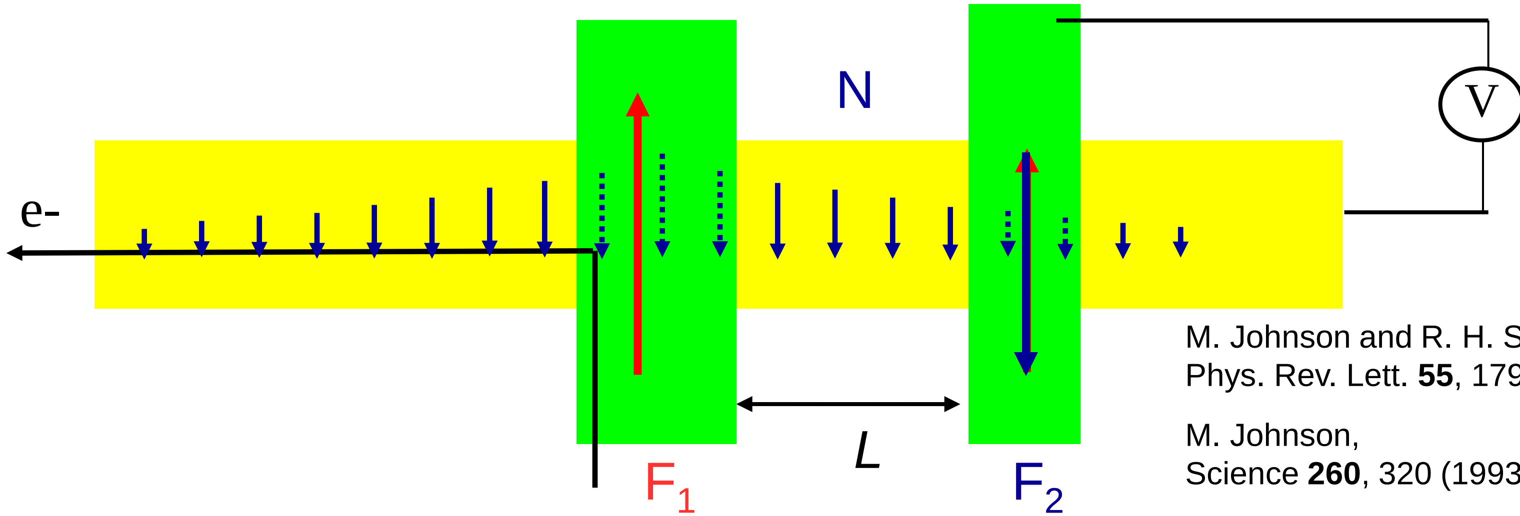

M. Johnson and R. H. Silsbee, Phys. Rev. Lett. **55**, 1790 (1985)

M. Johnson, Science **260**, 320 (1993)

First Experimental Demonstrations

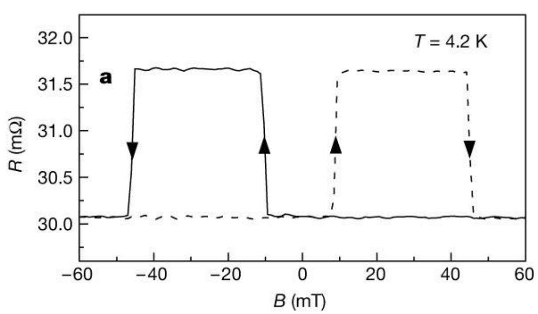

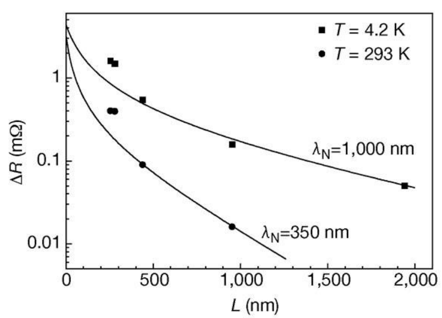

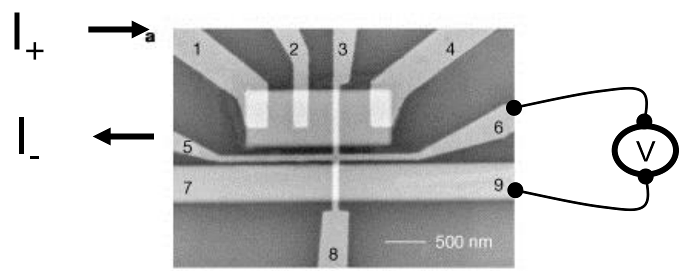

Cu film: $\lambda_s = 1\ \mu m$ (4.2 K)

Jedema *et al.*, Nature **410**, 345 (2001)

outline

- Giant Magnetoresistance, Tunneling Magnetoresistance
- Pure Spin current (no net charge current)
  - Spin Hall, Inverse Spin Hall effects
  - Spin Pumping effect
  - Spin Seebeck effect
- Spin Transfer Torque
- Micro and nano Magnetics

Pure Spin Current

-- with no accompanying net charge current

- Theoretically
  - $J_S = \hat{s}\cdot\vec{v} \;\rightarrow J_S = \frac{d}{dt}(\hat{s}\cdot\vec{r})$

- Experimentally
  - Spin Hall, Inverse Spin Hall effects
  - Spin Pumping effect
  - Spin Seebeck effect

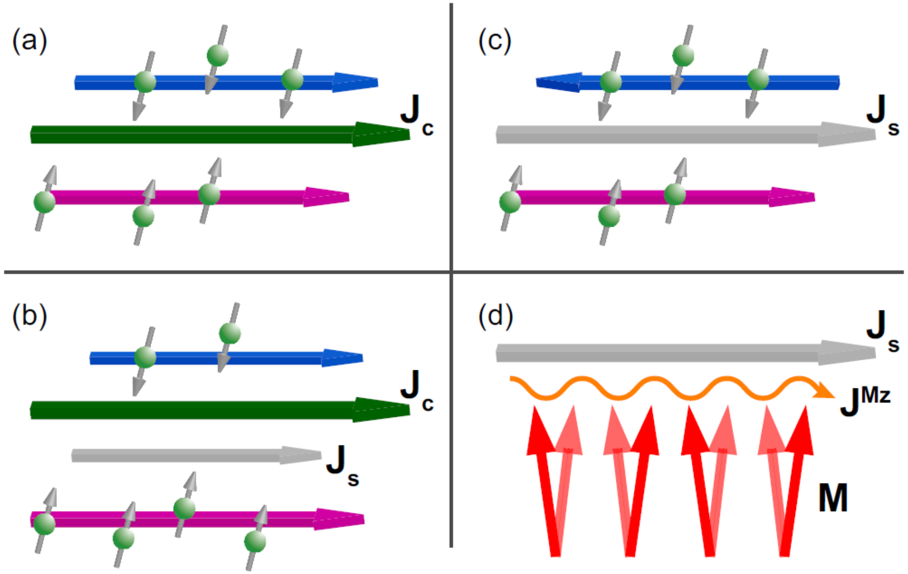

Spin Current

Proper Definition of Spin Current in Spin-Orbit Coupled Systems

Junren Shi,[1,2] Ping Zhang,[2,3] Di Xiao,[2] and Qian Niu[2]

[1]*Institute of Physics and ICQS, Chinese Academy of Sciences, Beijing 100080, People's Republic of China*
[2]*Department of Physics, The University of Texas at Austin, Austin, Texas 78712, USA*
[3]*Institute of Applied Physics and Computational Mathematics, Beijing 100088, People's Republic of China*

(Received 19 April 2005; revised manuscript received 18 November 2005; published 24 February 2006)

The conventional definition of spin current is incomplete and unphysical in describing spin transport in systems with spin-orbit coupling. A proper and measurable spin current is established in this study, which fits well into the standard framework of near-equilibrium transport theory and has the desirable property to vanish in insulators with localized orbitals. Experimental implications of our theory are discussed.

$$J_S = \hat{s} \cdot \vec{v} \quad \rightarrow \quad J_S = \frac{d}{dt}(\hat{s} \cdot \vec{r}) = \hat{s} \cdot \vec{v} + \frac{d}{dt}\hat{s} \cdot \vec{r}$$

torque dipole term

1. spin current is not conserved
2. can even be finite in insulators with localized eigenstates only
3. not in conjugation with any mechanical or thermodynamic force, not fitted into the standard near-equilibrium transport theory

1. spin current conserved
2. vanishes identically in insulators with localized orbitals
3. in conjugation with a force given by the gradient of the Zeeman field or spin-dependent chemical potential

Spin Current

Advances in Physics
Vol. 59, No. 3, May–June 2010, 181–255

Taylor & Francis
Taylor & Francis Group

Spin currents and spin superfluidity

E.B. Sonin*

Racah Institute of Physics, Hebrew University of Jerusalem, Jerusalem 91904, Israel

(*Received 3 September 2009; final version received 1 February 2010*)

The present review analyses and compares various types of dissipationless spin transport: (1) Superfluid transport, when the spin-current state is a metastable state (a local but not the absolute minimum in the parameter space). (2) Ballistic spin transport, when spin is transported without losses simply because the sources of dissipation are very weak. (3) Equilibrium spin currents, i.e. genuine persistent currents. (4) Spin currents in the spin Hall effect. Since superfluidity is frequently connected with Bose condensation, recent debates about magnon Bose condensation are also reviewed. For any type of spin currents simplest models were chosen for discussion in order to concentrate on concepts rather than the details of numerous models. The various hurdles on the way of using the concept of spin current (absence of the spin-conservation law, ambiguity of spin current definition, etc.) were analysed. The final conclusion is that the spin-current concept can be developed in a fully consistent manner, and is a useful language for the description of various phenomena in spin dynamics.

4. Conclusions

The present review focused on four types of dissipationless spin transport: (1) superfluid transport, when the spin-current state is a metastable state (a local but not the absolute minimum in the parameter space); (2) Ballistic spin transport, when spin is transported without losses simply because the sources of dissipation are very weak; (3) equilibrium spin currents, i.e. genuine persistent currents and (4) spin currents in the spin Hall effect. The dissipationless spin transport was a matter of debate for decades, though sometimes they were to some extent semantic. Therefore, it was important to analyse what physical phenomenon was hidden under this or that name remembering that any choice of terminology is inevitably subjective and is a matter of taste and convention. The various hurdles on the way of using the concept of spin current (absence of the spin-conservation law, ambiguity of spin current definition, etc.) were analysed. The final conclusion is that the spin-current concept can be developed in a fully consistent manner, though this is not an obligatory language of description: spin currents are equivalent to deformations of the spin structure, and one may describe the spin transport also in terms of deformations and spin stiffness.

The recent revival of interest to spin transport is motivated by the emerging of spintronics and high expectations of new applications based on spin manipulation. This is far beyond the scope of the present review, but hopefully the review could justify using of the spin-current language in numerous investigations of spin-dynamics problems, an important example of which is the spin Hall effect.

Spin Hall effect

Spin Hall Effect: Electron flow generates transverse spin current

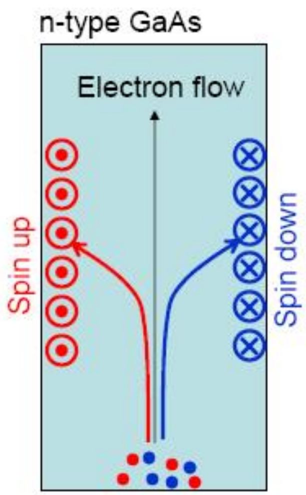

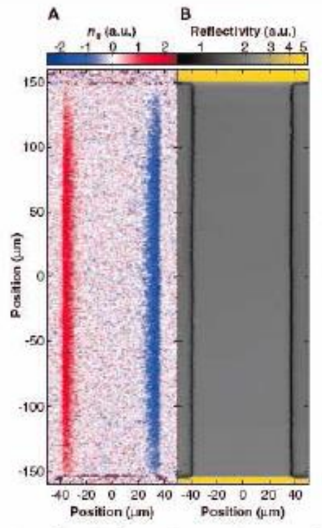

SHE observed in GaAs using Kerr effect to measure spin

Kato et.al. (Awschalom), Science 306, 1910 (2004)

Now observed at room temperature in ZnSe

M. I. Dyakonov and V. I. Perel, *JETP* **13** 467 (1971)

J. E. Hirsch, *Phys. Rev. Lett.* **83** 1834 (1999)

Guo *et al*, PRL **100** 096401 (2008)

The Intrinsic SHE is due to topological band structures

Berry curvature

$$\dot{\vec{r}} = \frac{1}{\hbar}\frac{\partial \varepsilon_n(\vec{k})}{\partial \vec{k}} + \frac{e}{\hbar}\vec{E}\times\vec{\Omega}(\vec{k})$$

The extrinsic SHE is due to asymmetry in electron scattering for up and down spins. – spin dependent probability difference in the electron trajectories

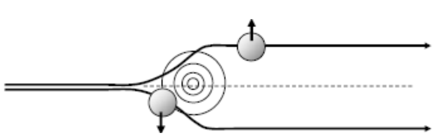

Side jump

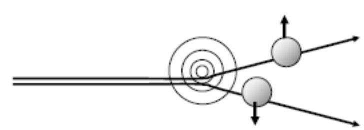

Skew scattering

Inverse Spin Hall effect

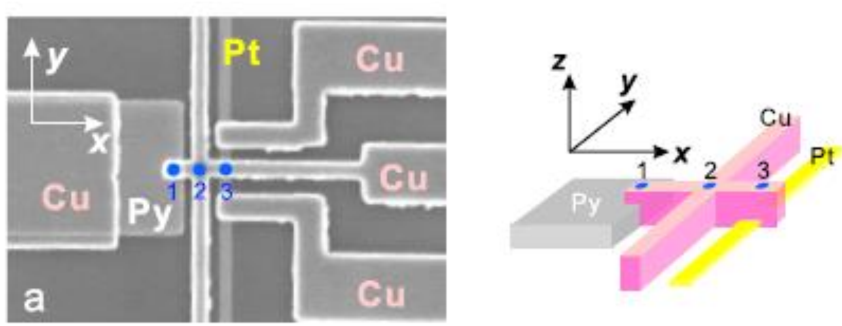

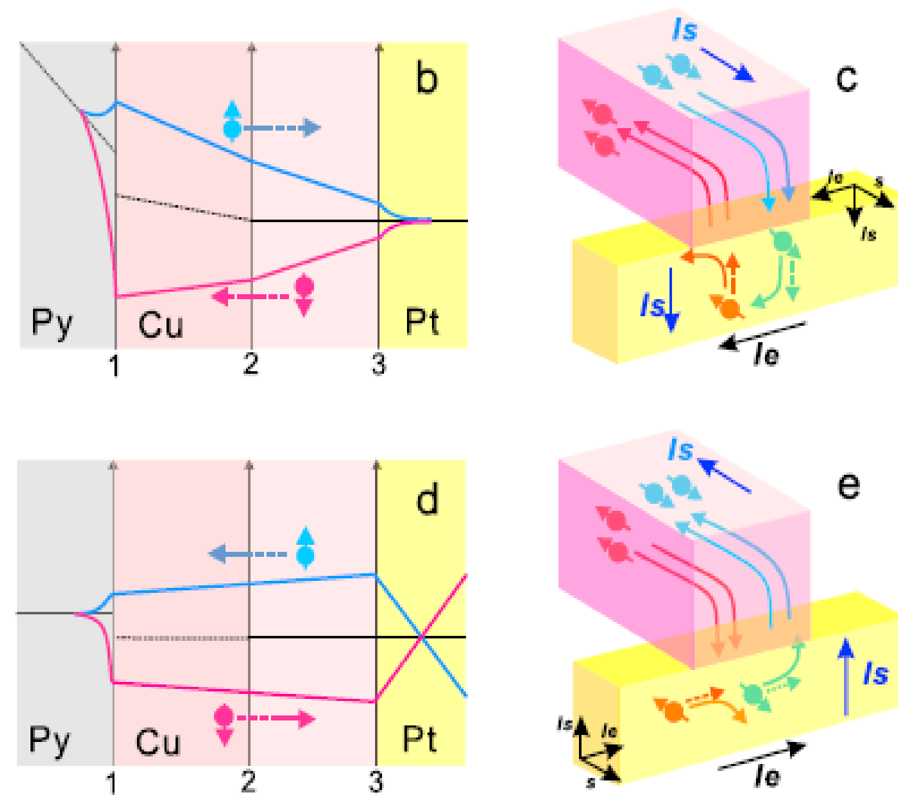

FIG. 1 (color online). (a) Scanning electron microscope (SEM) image of the fabricated spin Hall device together with a schematic illustration of the fabricated device. (b) Schematic spin dependent electrochemical potential map indicating spin accumulation in Cu and Pt induced by the spin injection from the Py pad. Dashed line represents the equilibrium position. (c) Schematic illustration of the charge accumulation process in the Pt wire, where I_S and I_e denote injected pure spin current and induced charge current, respectively. (d) Spin dependent electrochemical potential map for the charge to spin-current conversion and (e) corresponding schematic illustration.

Kimura *et al*, PRL **98**, 156601 (2007)

Guo *et al*, PRL **100** 096401 (2008)

Spin Pumping

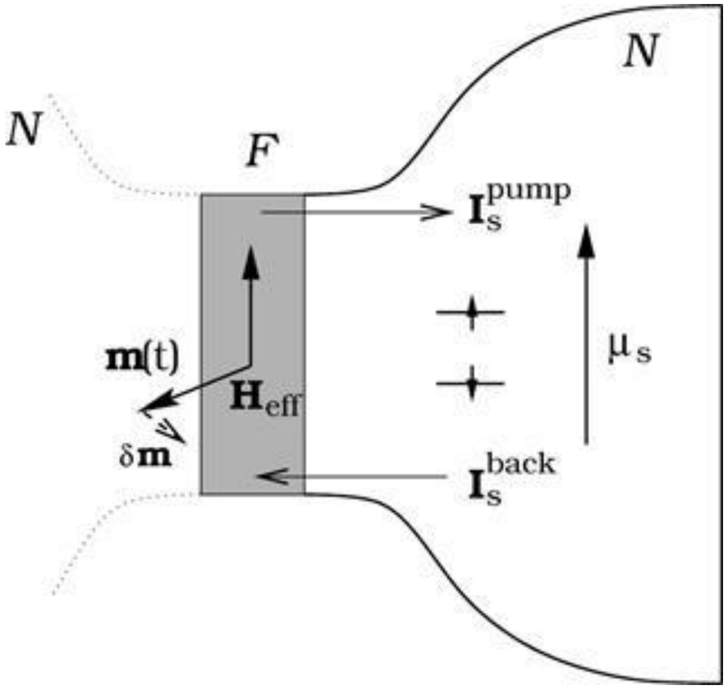

A ferromagnetic film *F* sandwiched between two nonmagnetic reservoirs *N*. For simplicity of the discussion in this section, we mainly focus on the dynamics in one (right) reservoir while suppressing the other (left), e.g., assuming it is insulating. The spin-pumping current $\mathbf{I}_s$ and the spin accumulation μ_s in the right reservoir can be found by conservation of energy, angular momentum, and by applying circuit theory to the steady state $\mathbf{I}_s^{pump} = \mathbf{I}_s^{back}$.

$$\mathbf{I}_s^{pump} = \frac{\hbar}{4\pi}\left(A_r \mathbf{m} \times \frac{d\mathbf{m}}{dt} - A_i \frac{d\mathbf{m}}{dt}\right).$$

Tserkovnyak *et al*, PRL **88**, 117601 (2002), Enhanced Gilbert Damping in Thin Ferromagnetic Films

Brataas *et al*, PRB **66**, 060404(R) (2002), Spin battery operated by ferromagnetic resonance

Tserkovnyak *et al*, PRB **66**, 224403 (2002), Spin pumping and magnetization dynamics in metallic multilayers

Rev Mod Phys **77**, 1375 (2005) Nonlocal magnetization dynamics in ferromagnetic heterostructures

Spin Pumping

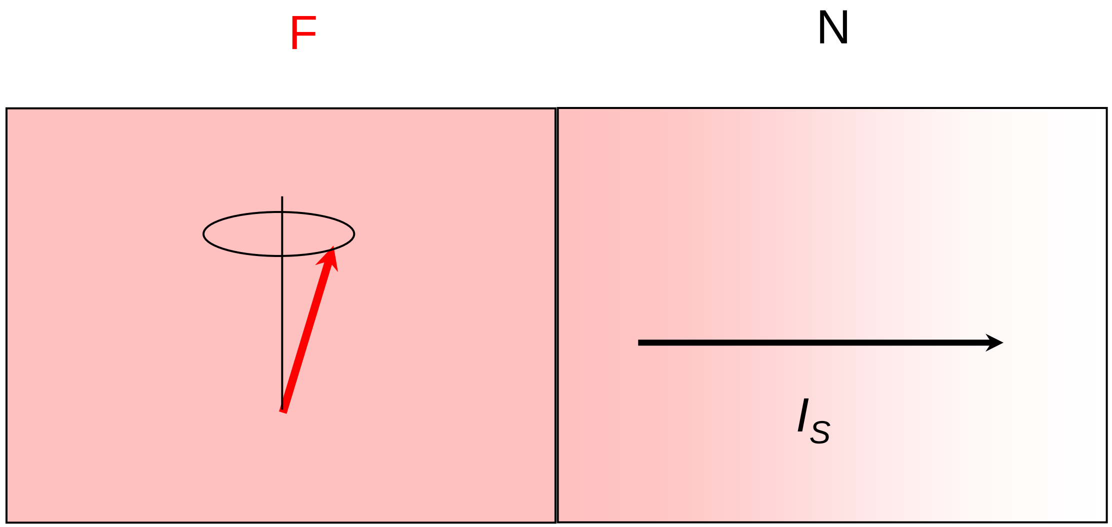

- Landau-Lifshitz-Gilbert

$$\dot{\mathbf{m}} = -\gamma \mathbf{m} \times \mathbf{H}_{\text{eff}} + \mathbf{m} \times (\tilde{\alpha} \dot{\mathbf{m}})$$

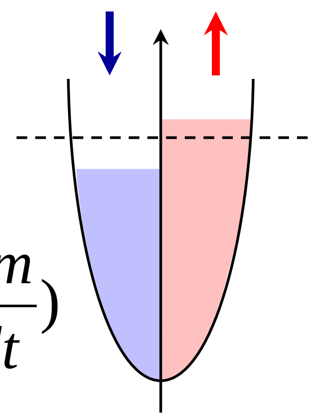

$$I_S^{pump} = \frac{\hbar}{4\pi} \left(\mathrm{Re}\, g^{\downarrow\uparrow} m \times \frac{dm}{dt} + \mathrm{Im}\, g^{\downarrow\uparrow} \frac{dm}{dt} \right)$$

Spin accumulation gives rise to spin current in neighboring normal metal

In the FMR condition, the steady magnetization precession in a F is maintained by balancing the absorption of the applied microwave and the dissipation of the spin angular momentum --the transfer of angular momentum from the local spins to conduction electrons, which polarizes the conduction-electron spins.

Combining Spin Pumping and Inverse Spin Hall Effect

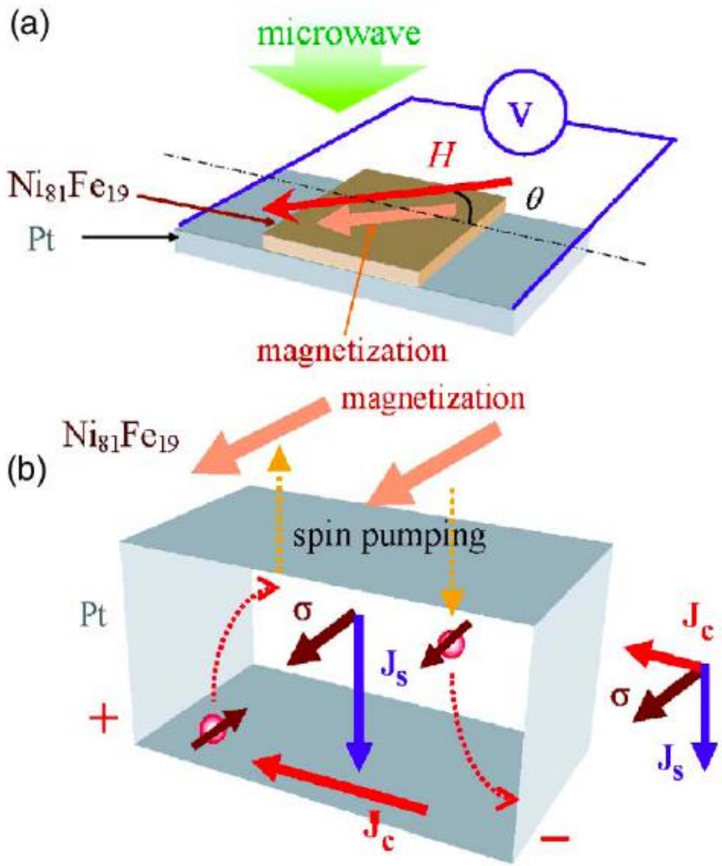

FMR

⇓

Spin Current

in adjacent

normal metal

⇓

Transverse

Charge Current

The spin-orbit interaction bends these two electrons in the same direction and induces a charge current transverse to Js,

$$\mathbf{J}_c = D_{\mathrm{ISHE}} \mathbf{J}_s \times \boldsymbol{\sigma}.$$

The surface of the Py layer is of a 1×1 mm^2 square shape. Two electrodes are attached to both ends of the Pt layer.

Saitoh *et al*, APL **88**, 182509 (2006)

Kimura *et al*, PRL **98**, 156601 (2007)

Combining Spin Pumping and Inverse Spin Hall Effect

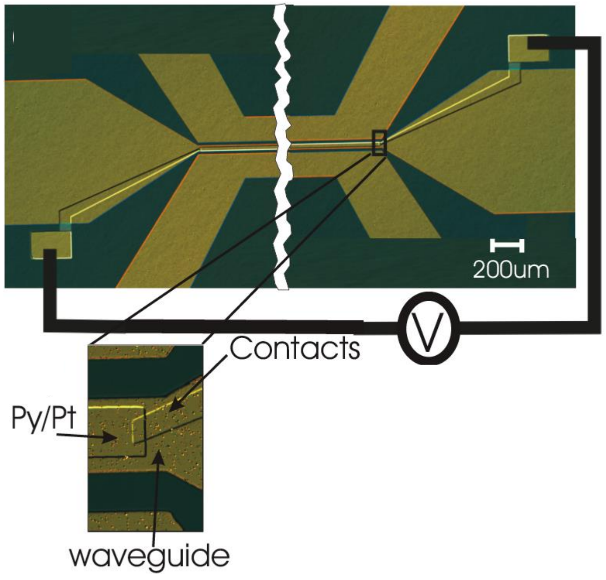

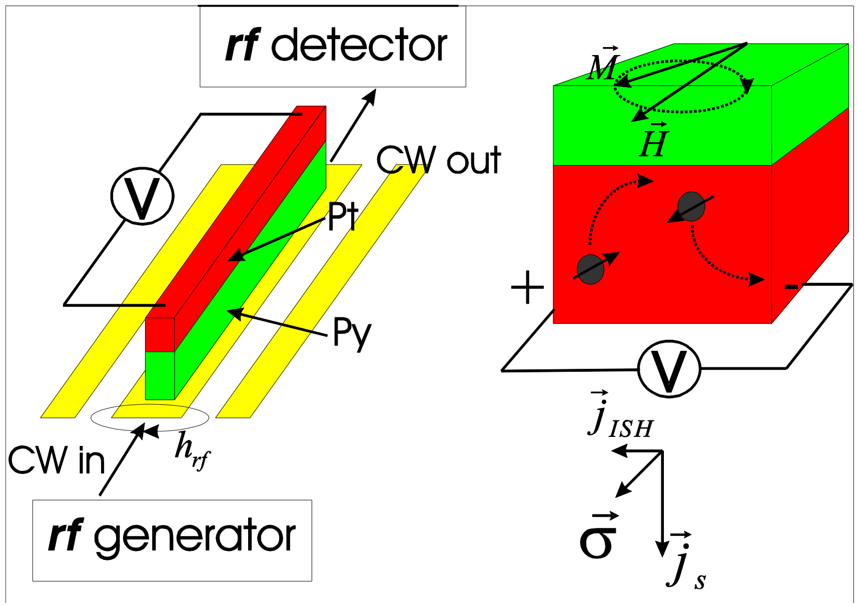

- **Use Spin Pumping to Generate Pure Spin Current**
- **Quantify Spin Current from FMR**
- **Measured Voltage Directly Determines Spin Hall Conductivity**
- **Key Advantage: Signal Scales with Device Dimension**

Mosendz *et al*, PRL **104**, 046601 (2010)

Determine Spin Hall Angle for Many Materials

$$\gamma = \frac{\sigma_{SH}}{\sigma_c}$$

σ_{SH} ⟵ **spin Hall conductivity**

σ_c ⟵ **charge conductivity**

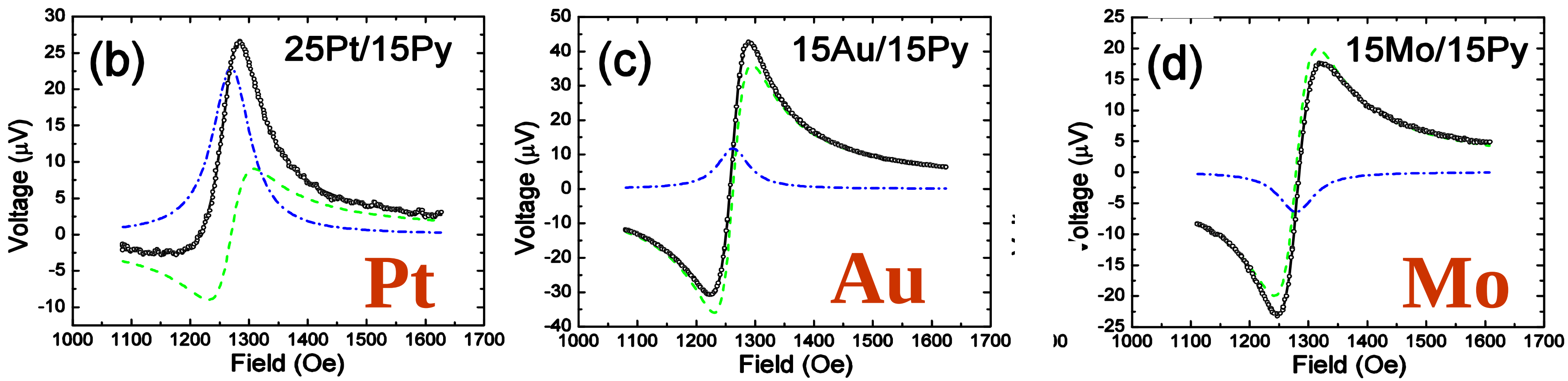

γ = 0.0120±0.0001 **γ = 0.0025±0.0006** **γ = -0.00096±0.00007**

$$V_{\mathrm{AMR}} = I_{\mathrm{rf}}^{m} \frac{R_{\mathrm{wg}}}{R_S} \Delta R_{\mathrm{AMR}} \frac{\sin(2\theta)}{2} \frac{\sin(2\alpha)}{2} \cos\varphi_0,$$

$$V_{\mathrm{ISH}} = -\frac{\gamma g_{\uparrow\downarrow} e L \lambda_{\mathrm{sd}} \omega}{2\pi\sigma_N t_N} \sin\alpha \sin^2\theta \tanh\left(\frac{t_N}{2\lambda_{\mathrm{sd}}}\right).$$

Hoffmann *et al*

Spin Seebeck effect

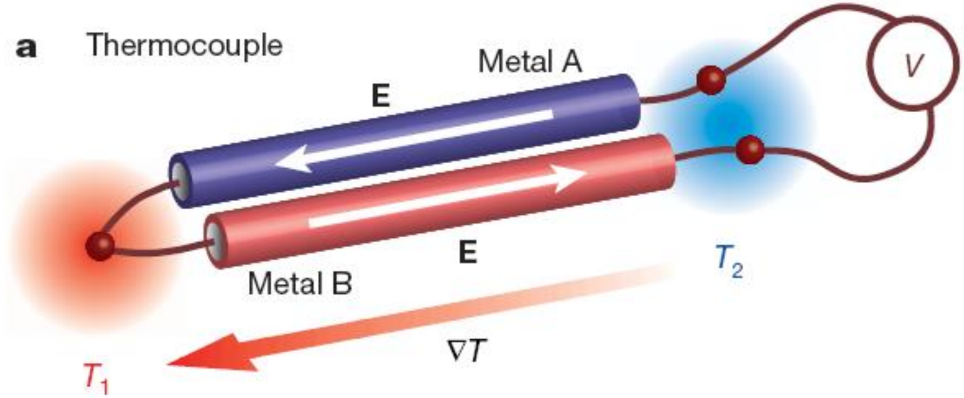

$$\delta V = S\delta T$$

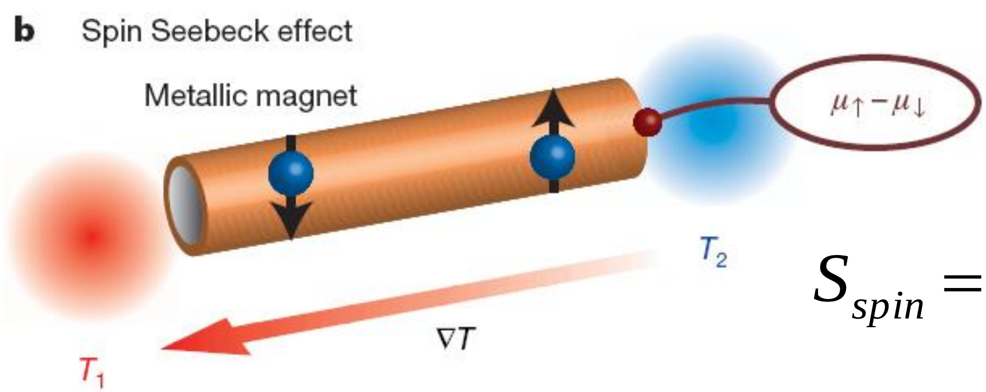

$$\delta V_{spin} = S_{spin}\delta T$$

$$S_{spin} = (1/e)[\partial \mu^c{}_\uparrow / \partial T - \partial \mu^c{}_\downarrow / \partial T]$$

Uchida *et al.*, Nature **455**, 778 (2008)

Spin Seebeck effect

In a ferromagnetic metal, **up- spin and down-spin conduction** electrons have **different scattering rates and densities**, and thus have different Seebeck coefficients.

$$\boldsymbol{j}_s = \boldsymbol{j}_\uparrow - \boldsymbol{j}_\downarrow = (\sigma_\uparrow S_\uparrow - \sigma_\downarrow S_\downarrow)(-\nabla T)$$

This **spin current** flows **without accompanying charge currents** in the open-circuit condition, and the up-spin and down-spin currents flow **in opposite directions** along the temperature gradient

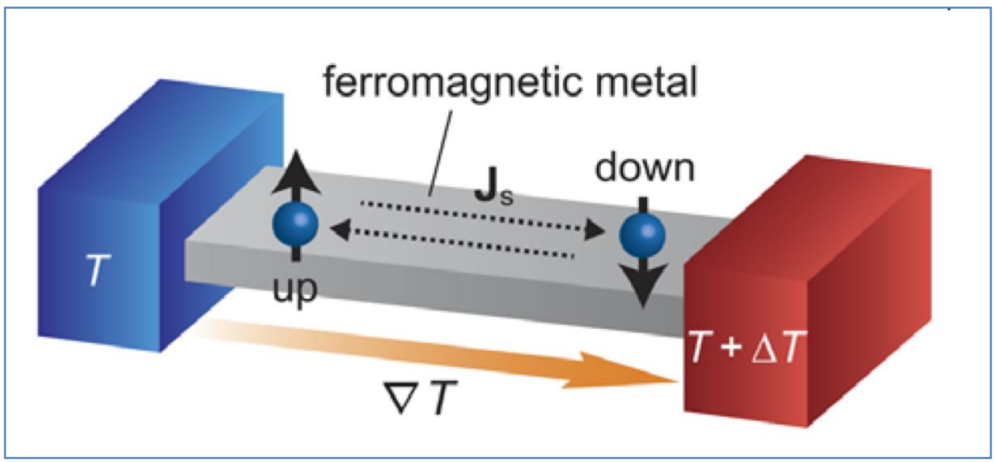

How to detect j_S ?

Inverse Spin Hall Effect coverts j_S into j_C

Solid State Communications **150**, 524 (2010)

Detection of Spin Current by Inverse Spin Hall Effect

The ISHE converts a spin current into an **electromotive force** E_{SHE} by means of spin–orbit scattering.

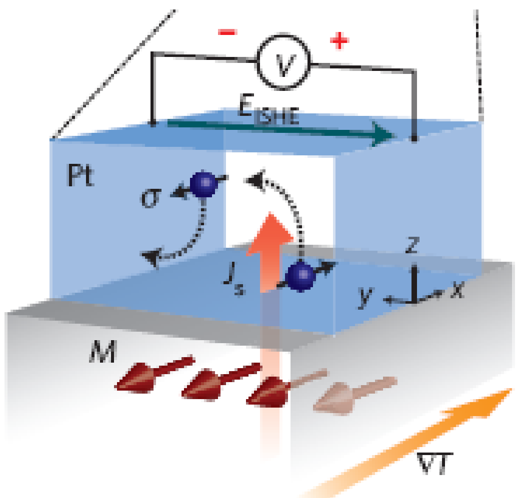

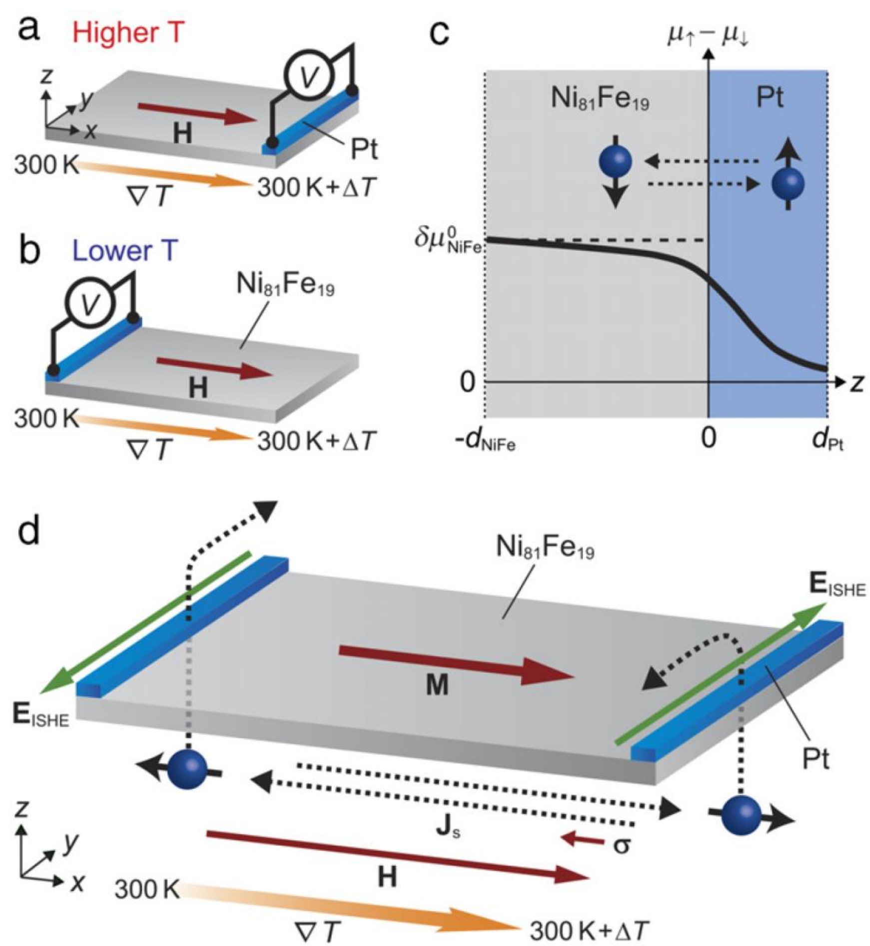

$$E_y = E_{SHE} = D_{ISHE} J_S \times \sigma$$

A spin current carries a spin-polarization vector σ along a spatial direction J_S.

Solid State Communications **150**, 524 (2010)

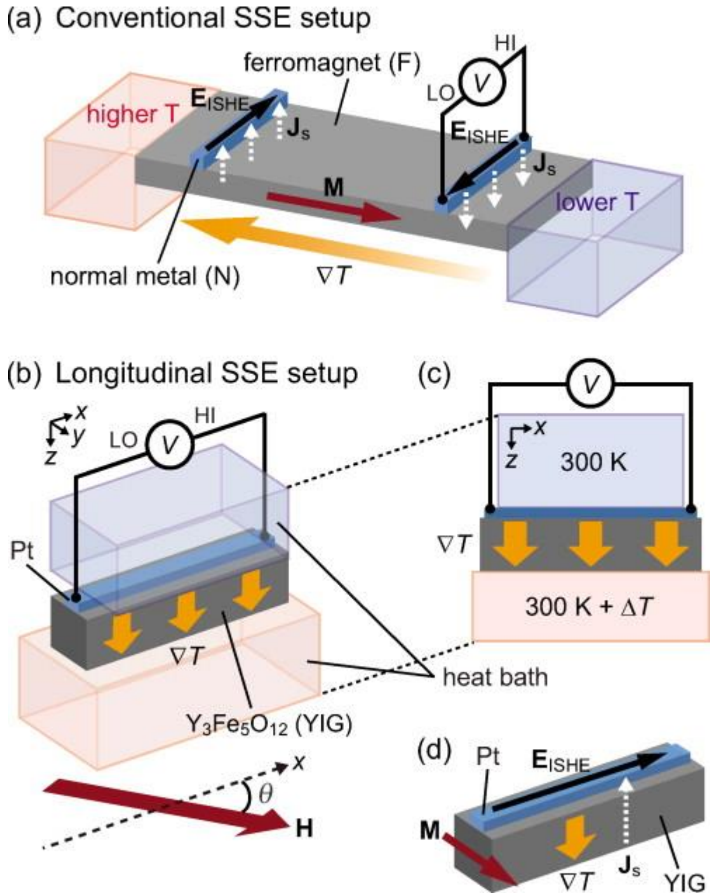

(a) A schematic of the conventional setup for measuring the ISHE induced by the SSE. Here, ∇T, M, Js, and EISHE denote a temperature gradient, the magnetization vector of a ferromagnet (F), the spatial direction of the spin current flowing across the F/no...

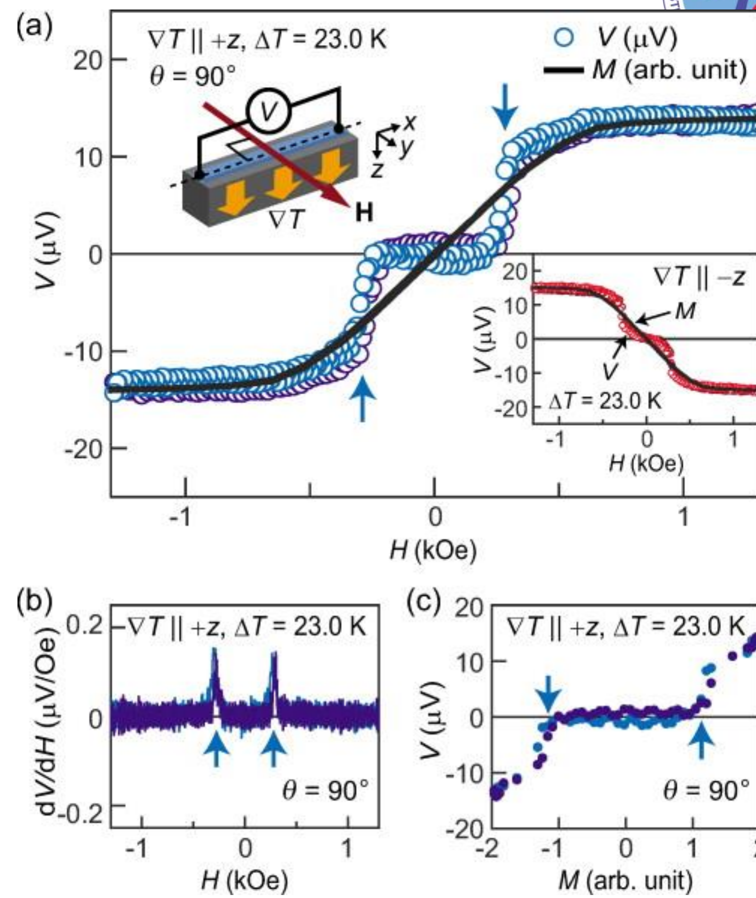

(a) Comparison between the H dependence of V at ΔT = 23.0 K in the YIG/Pt system and the magnetization M curve of the YIG. During the V measurements, ∇T was applied along the +z direction [the −z direction for the inset to (a)] and H was applied along the...

Uchida et al, APL 97, 172505 (2010)

sound waves

JOURNAL OF APPLIED PHYSICS 111, 053903 (2012)

Acoustic spin pumping: Direct generation of spin currents from sound waves in Pt/$Y_3Fe_5O_{12}$ hybrid structures

K. Uchida,[1,2,a)] H. Adachi,[2,3] T. An,[1,2] H. Nakayama,[1,2] M. Toda,[4] B. Hillebrands,[5]
S. Maekawa,[2,3] and E. Saitoh[1,2,3]

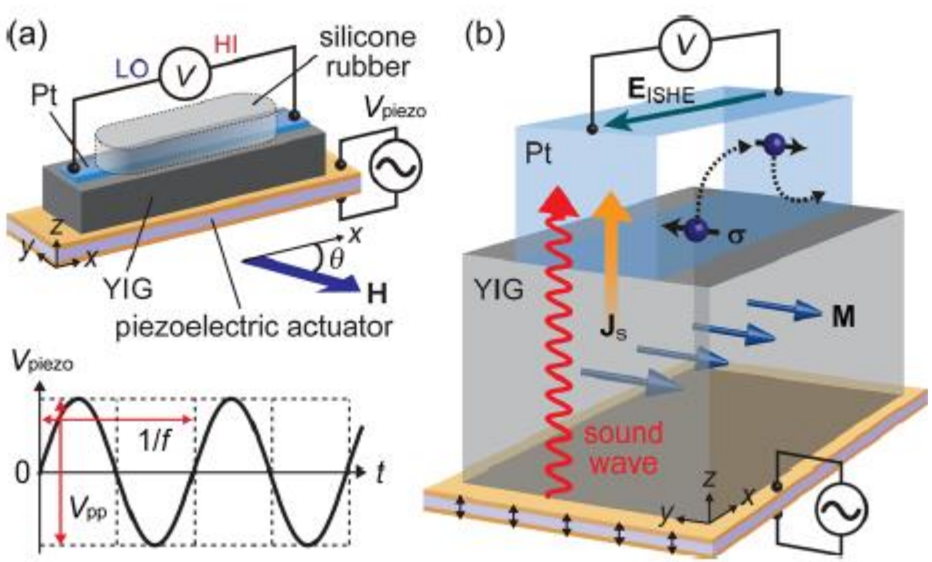

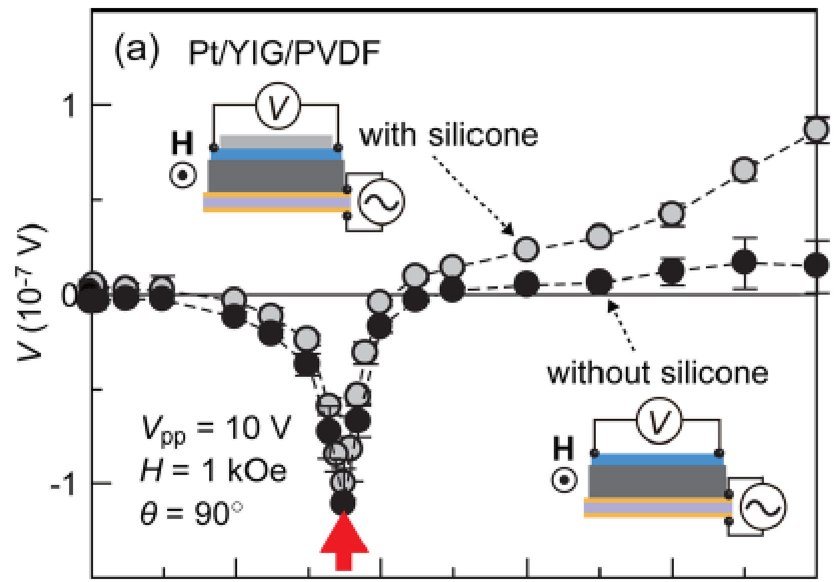

circularly polarized light

APPLIED PHYSICS LETTERS **96**, 082502 (2010)

Photoinduced inverse spin-Hall effect: Conversion of light-polarization information into electric voltage

K. Ando,[1,2,a)] M. Morikawa,[2] T. Trypiniotis,[3] Y. Fujikawa,[1] C. H. W. Barnes,[3] and E. Saitoh[1,2,4]

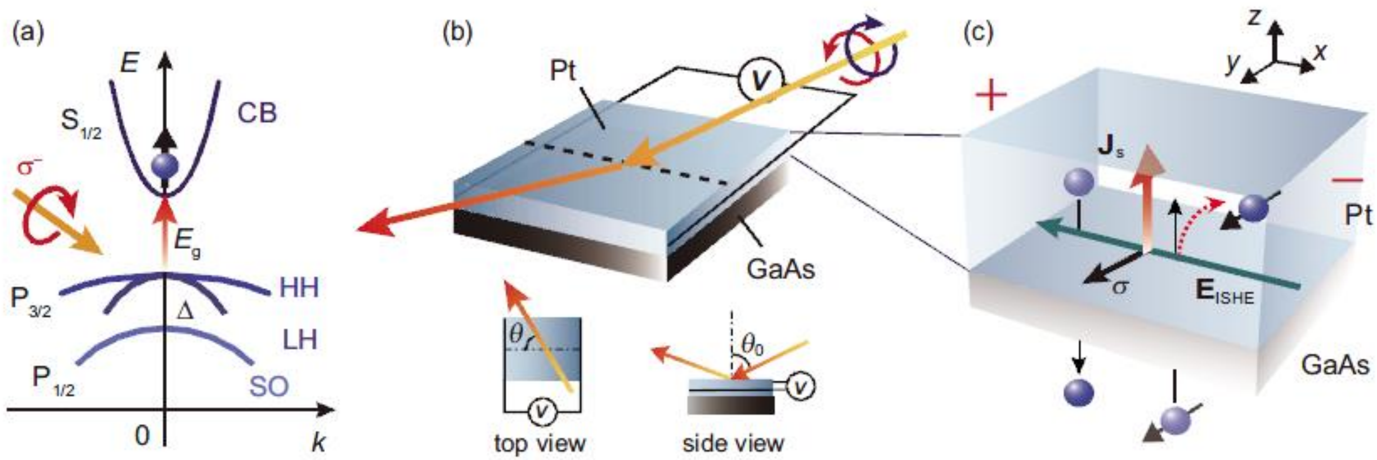

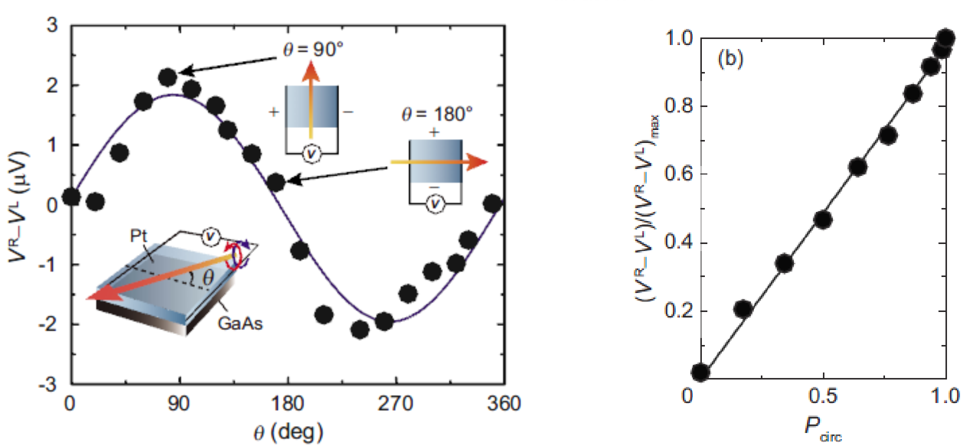

$$P_{\mathrm{circ}} \equiv \frac{I^+ - I^-}{I^+ + I^-}$$

Thermoelectric effect:

The thermoelectric effect is the direct conversion of temperature differences to electric voltage and vice-versa.

Seebeck effect (1821):

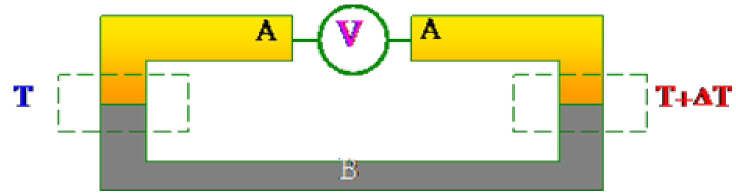

$\Delta T \rightarrow V$

Peltier effect (1823):

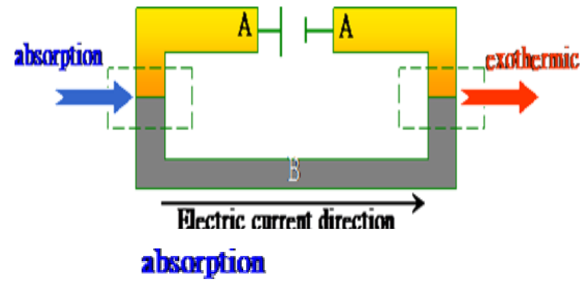

$I \rightarrow Q$

Thomson effect (1851):

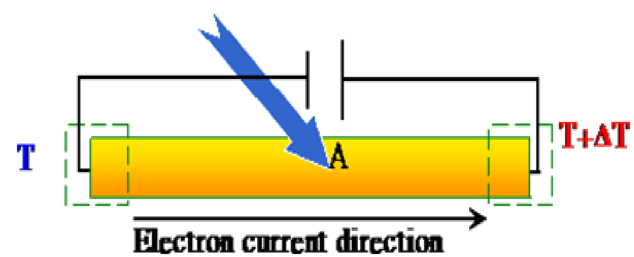

$I + \Delta T \rightarrow Q$

Nernst effect：

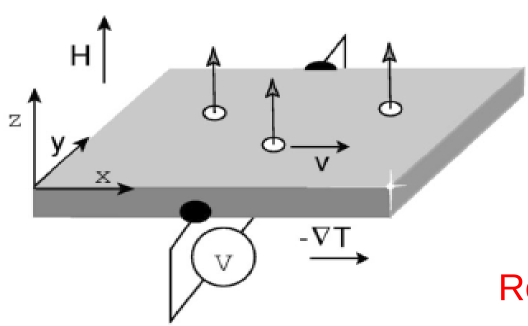

When a sample is subjected to a magnetic field and a temperature gradient normal (perpendicular) to each other, an electric field will be induced normal to both.

Ref: http://web.nchu.edu.tw/~lschang/Thermoelectric.htm

Mystery 1:
Transmission of Spin Current in Metal and Insulator

Over macroscopic distance (mm's >> spin diffusion length) without dissipation ?

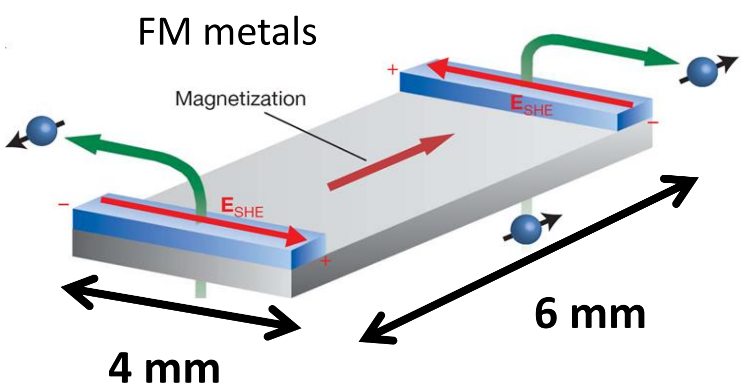

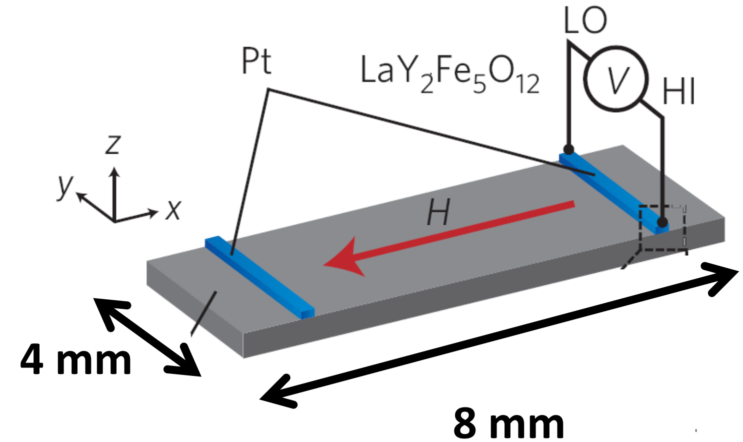

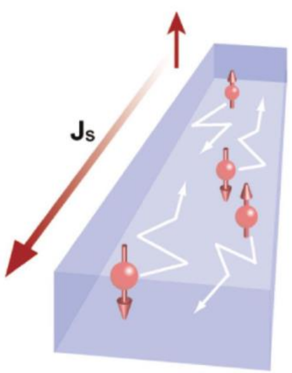

Conduction-electron spin current

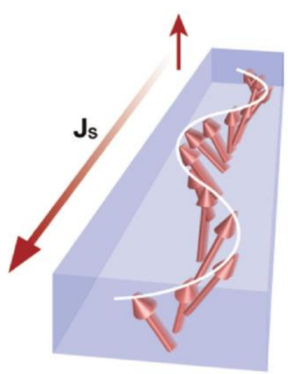

Spin-wave spin current

Resolution: Transmission of spin currents by magnons (spin waves) in either FM metals or FM insulators

Uchida *et al.*, Nature **455**, 778 (2008); Nature Mater. **9**,894 (2010), Kajiwara *et al.*, Nature 464, 262 (2010)

Mystery 2:
Spin Seebeck effect in broken FM semiconductor

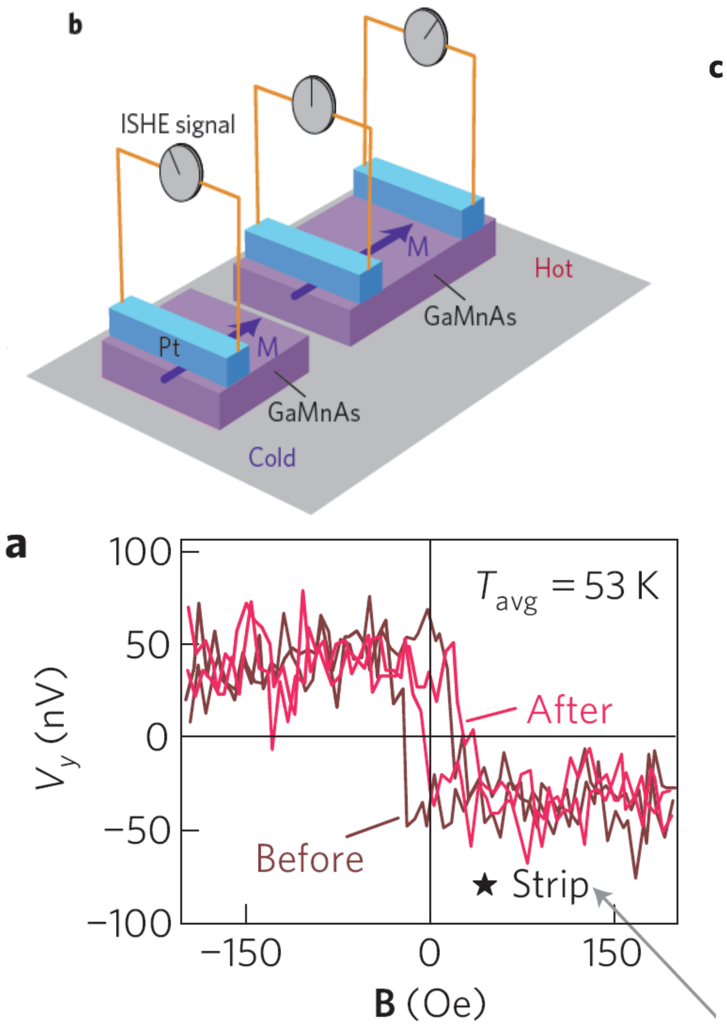

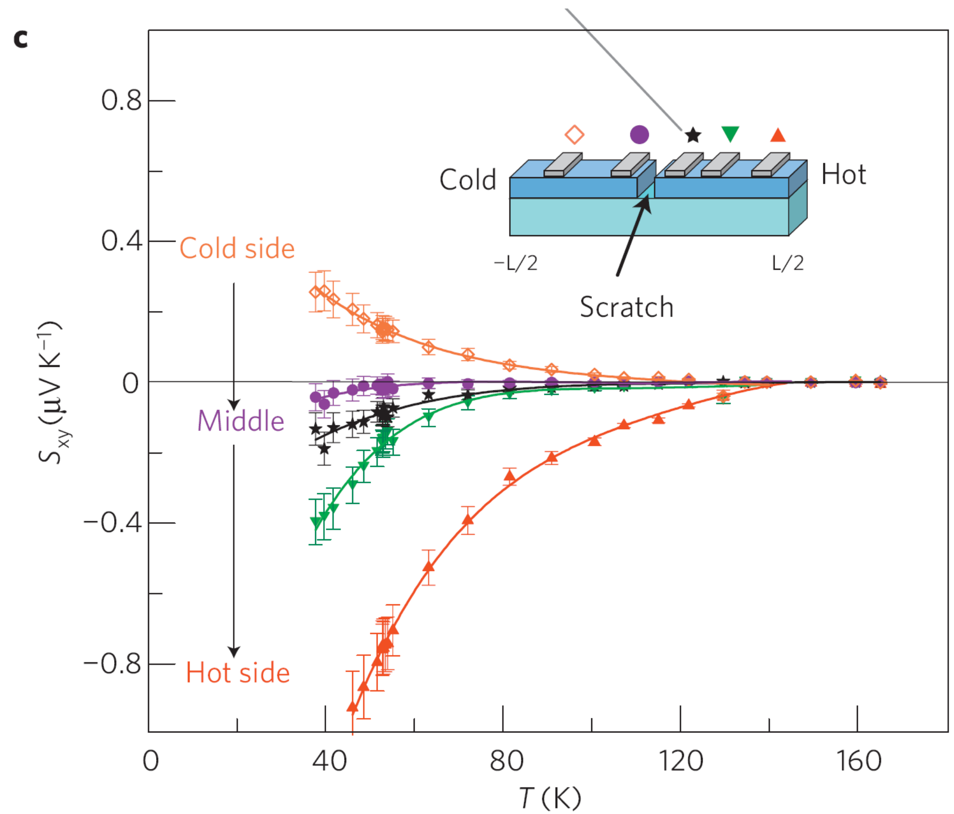

Transmission of spin currents ?

Jaworski *et al.*, Nature Materials **9**, 898 (2010)

Intrinsic Caloritronic effects (not substrate dominated) ?

Intrinsic spin Seebeck effect ?

Intrinsic spin-dependent thermal transport ?

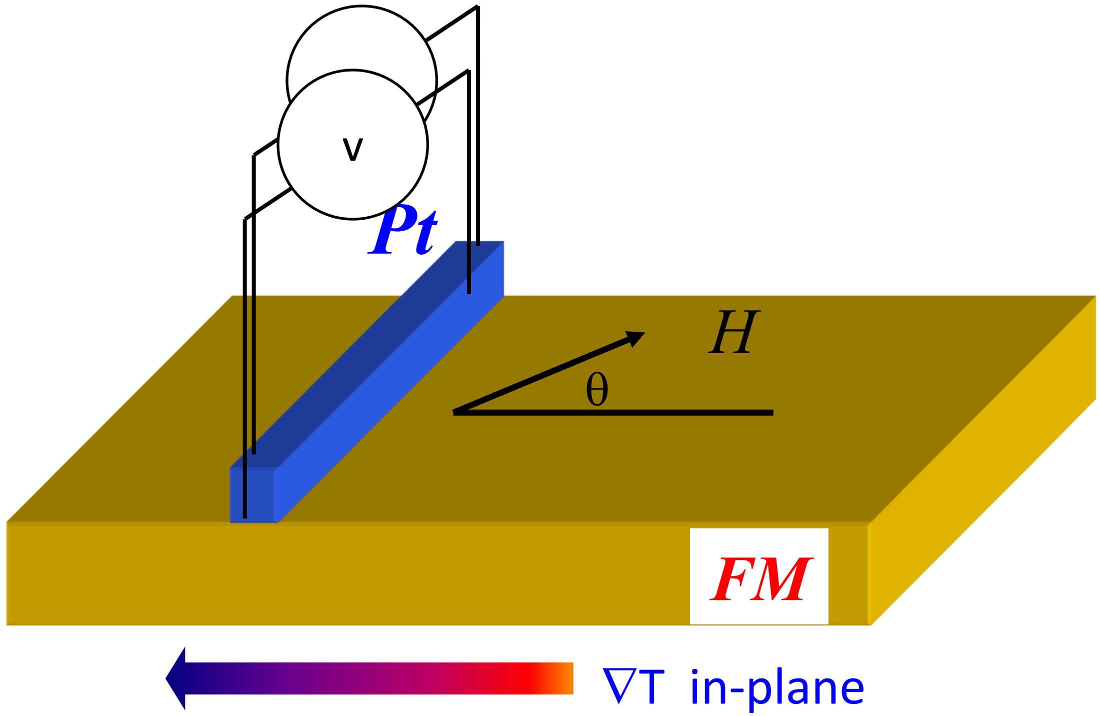

Huang, Wang, Lee, Kwo, and CLC,

"Intrinsic spin-dependent thermal transport," PRL **107**, 216604 (2011).

Spin-Dependent Thermal Transport

Longitudinal thermal voltage V_x

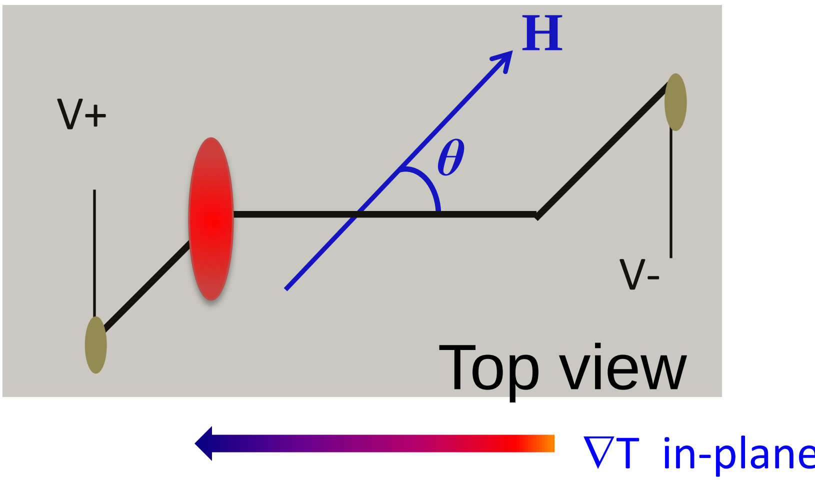

Transverse thermal voltage V_y

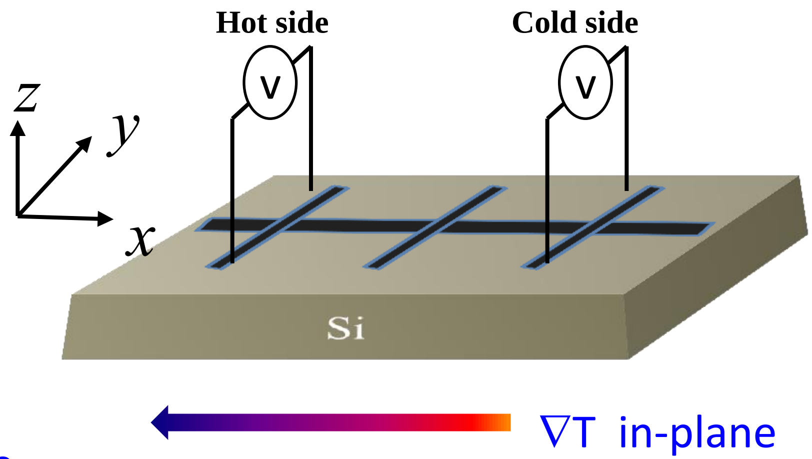

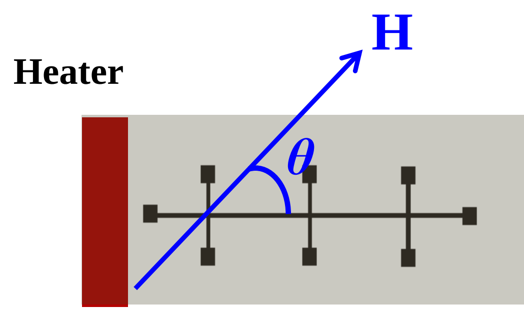

Patterned Py wire on Si substrate

Width: 50-100 μm, Thickness: 20-300 nm

Length: 5 mm   Heater power: 1W

$$V_{th} = V_o + \Delta V_{th}(H, \theta)$$

Angular and Field dependence of $\Delta V_{th}(H, \theta)$?

Consistent, Robust, but Strange $\Delta V_{th}(H,\theta)$ Results

Asymmetric in H

$\Delta V \propto \sin\theta$

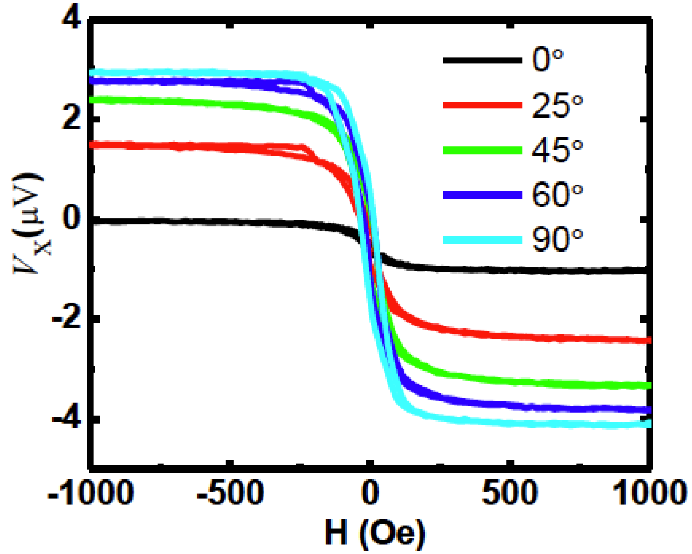

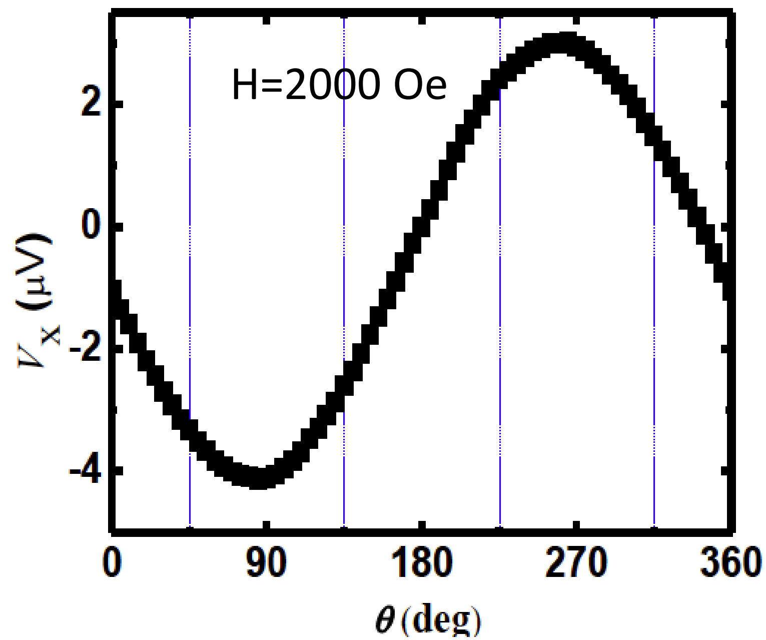

But this is physically impossible !

e.g., ***opposite*** signals at θ = 90° and θ = 270° .

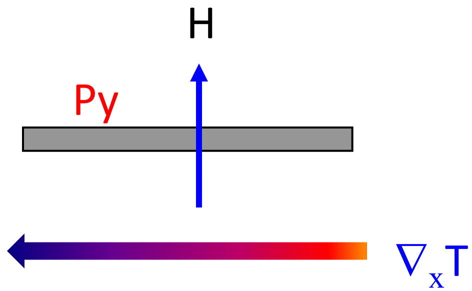

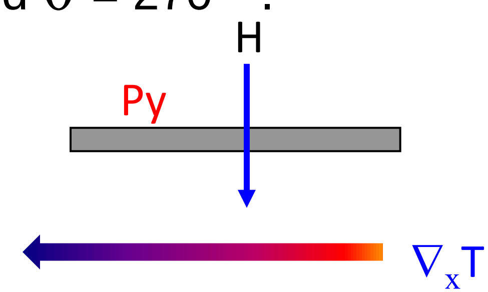

Reversed ∇T, *Same ΔV* !!

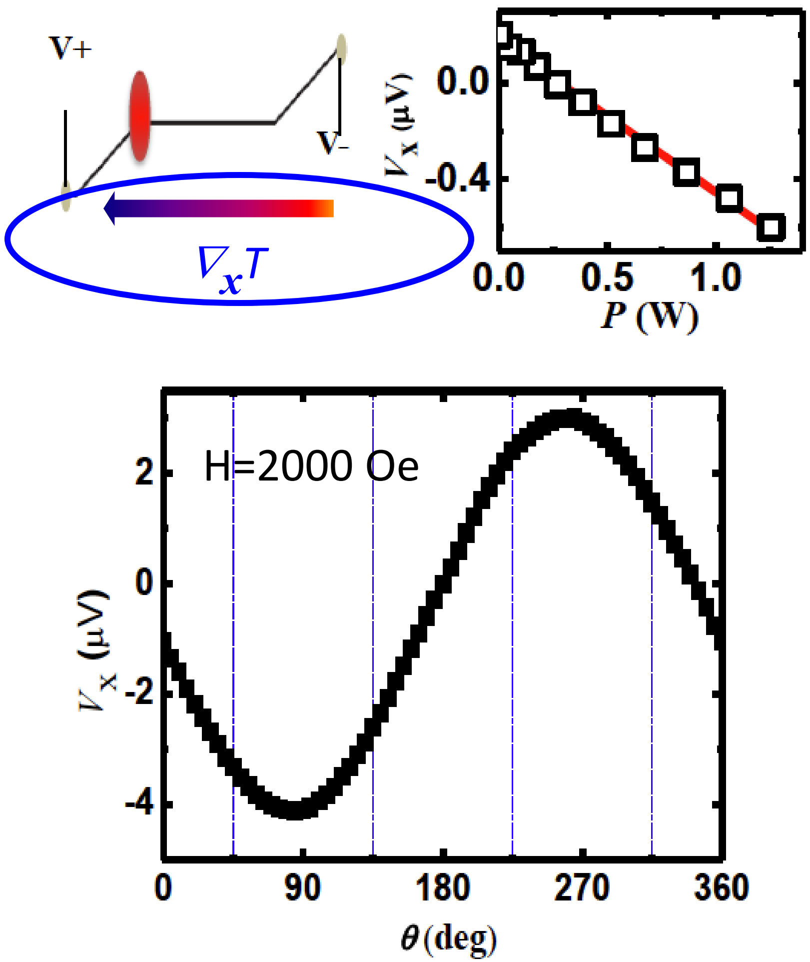

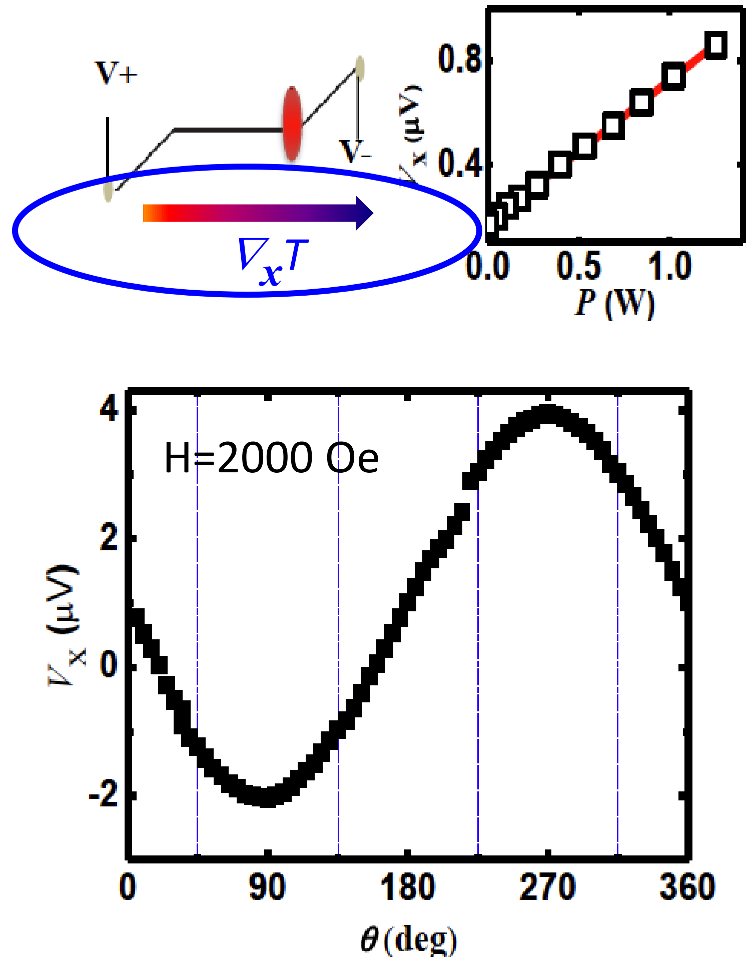

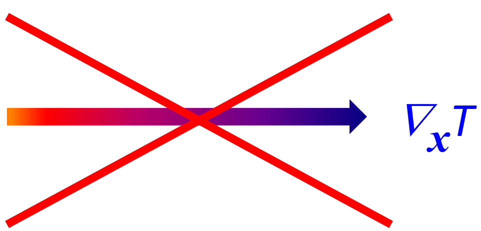

Effective ∇T is not in-plane !

Out-of-plane $\nabla_z T$!!

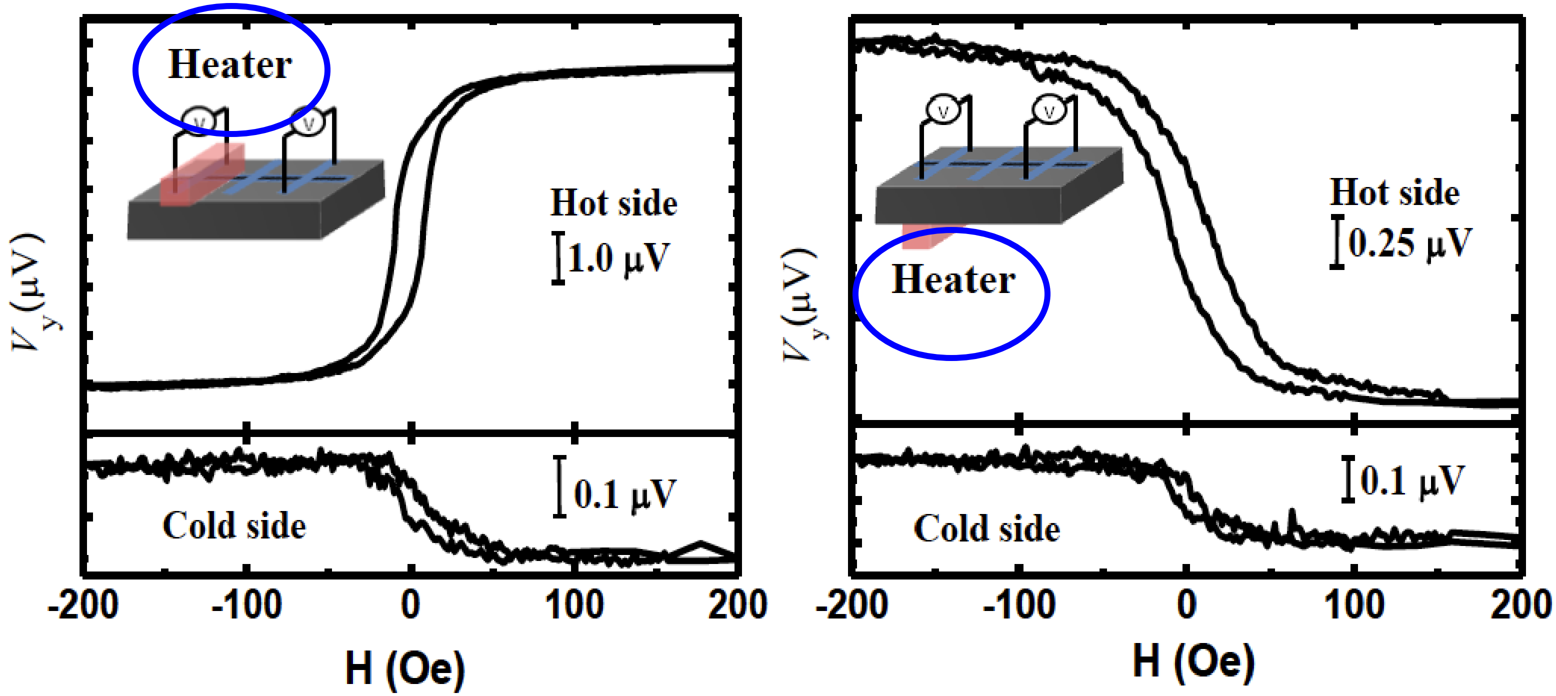

Sign change **No sign change**

This is **anomalous Nernst effect** with perpendicular $\nabla_z T$!!

$\nabla_z T \odot$

(Top view)

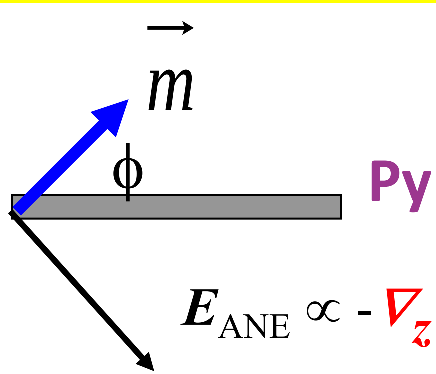

$\vec{E}_{ANE} \propto -\nabla_z T \times \vec{m}$

$$E_{ANE} \propto -\nabla_z T \times \vec{m}$$

Projection along Py wire direction: $\sin\phi$

Only $\nabla_z T$!!

Uniform Heating from substrate

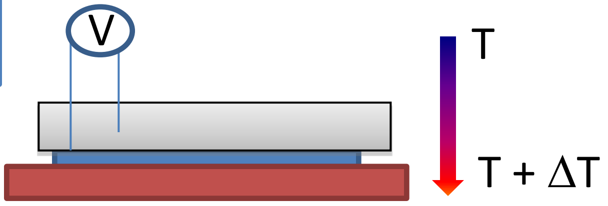

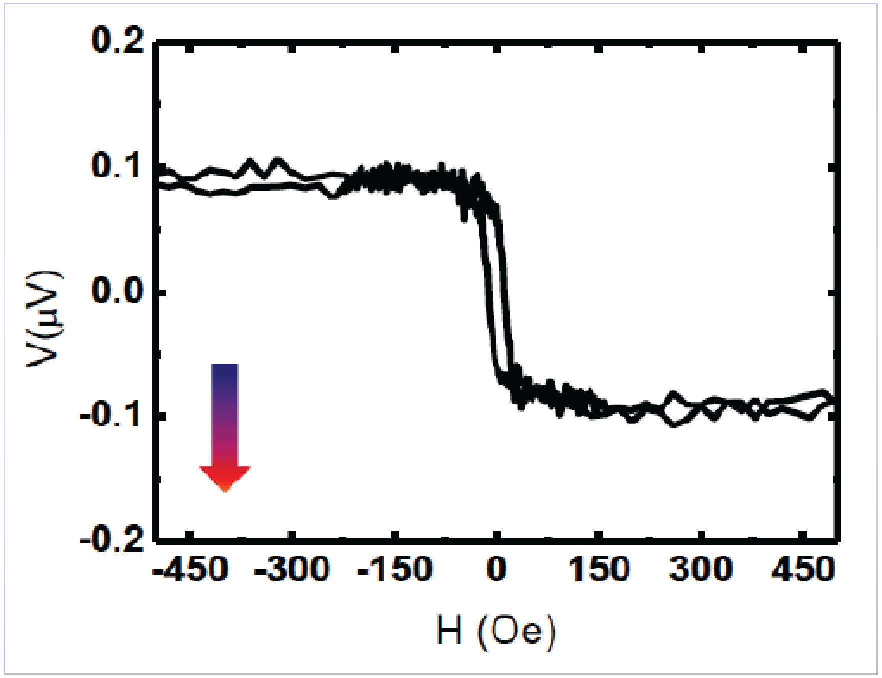

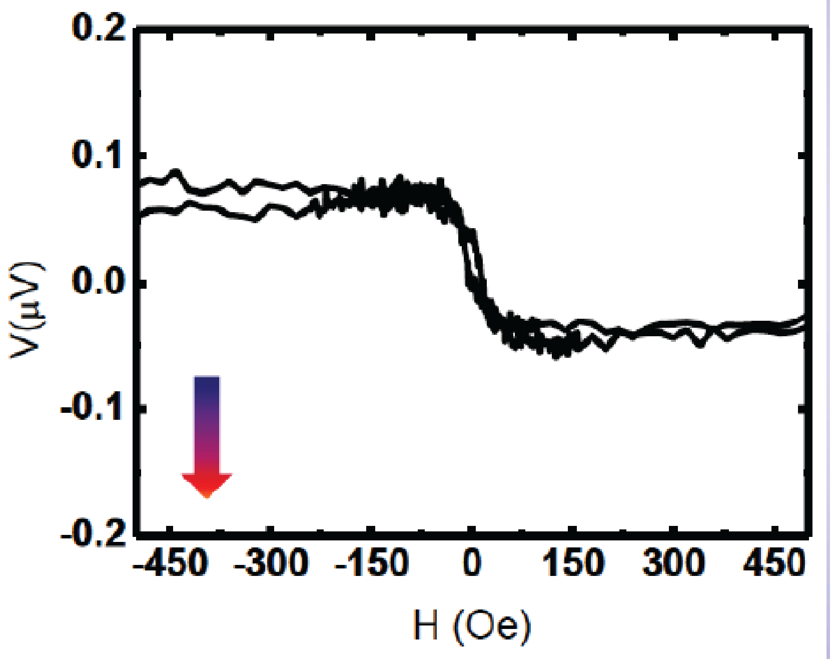

Same ANE sign everywhere with similar magnitude

Thin film on substrate: in-plane and out-of-plane gradient

Anomalous Nernst effect: sensitive detector of ΔT_z and $\nabla_z T$

$$\boldsymbol{E}_{\mathrm{ANE}} \propto \nabla_z T \times \boldsymbol{m}$$

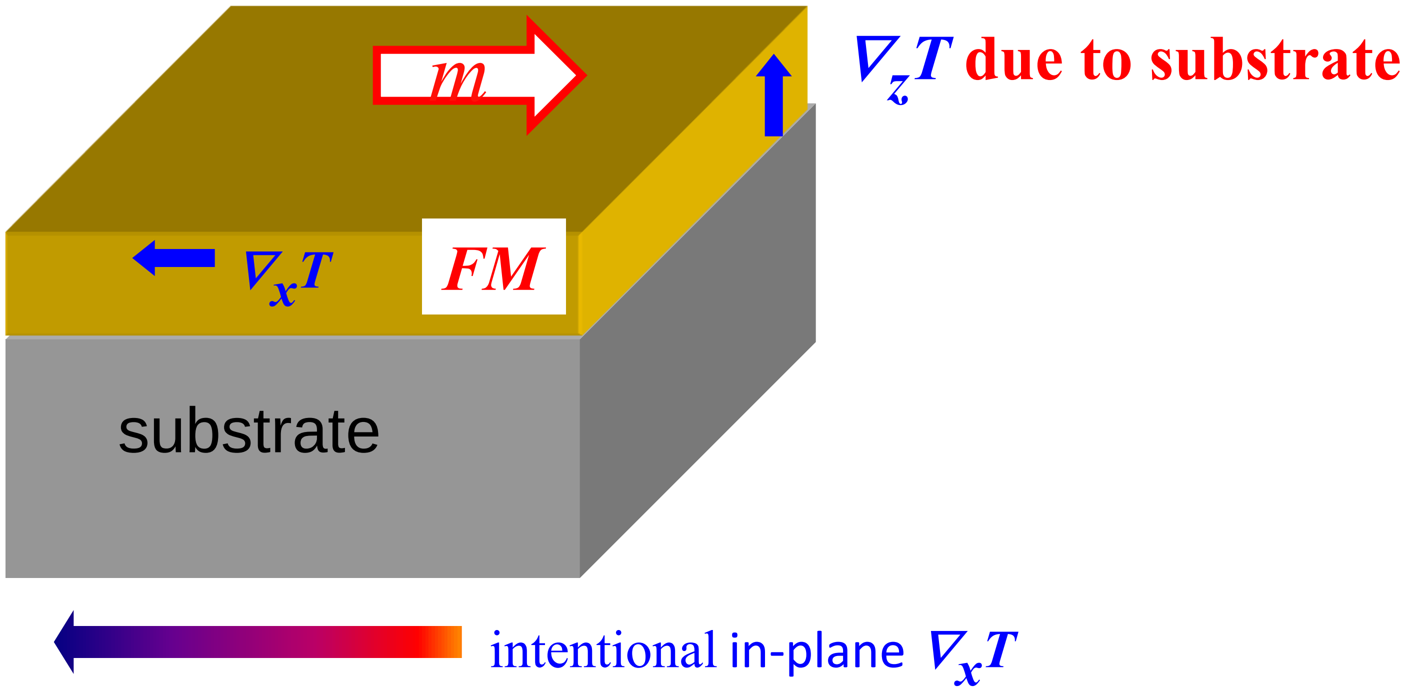

Entanglement of ANE (due to $\nabla_z T$) and SSE (due to $\nabla_x T$)

Anomalous Nernst Effect (ANE)

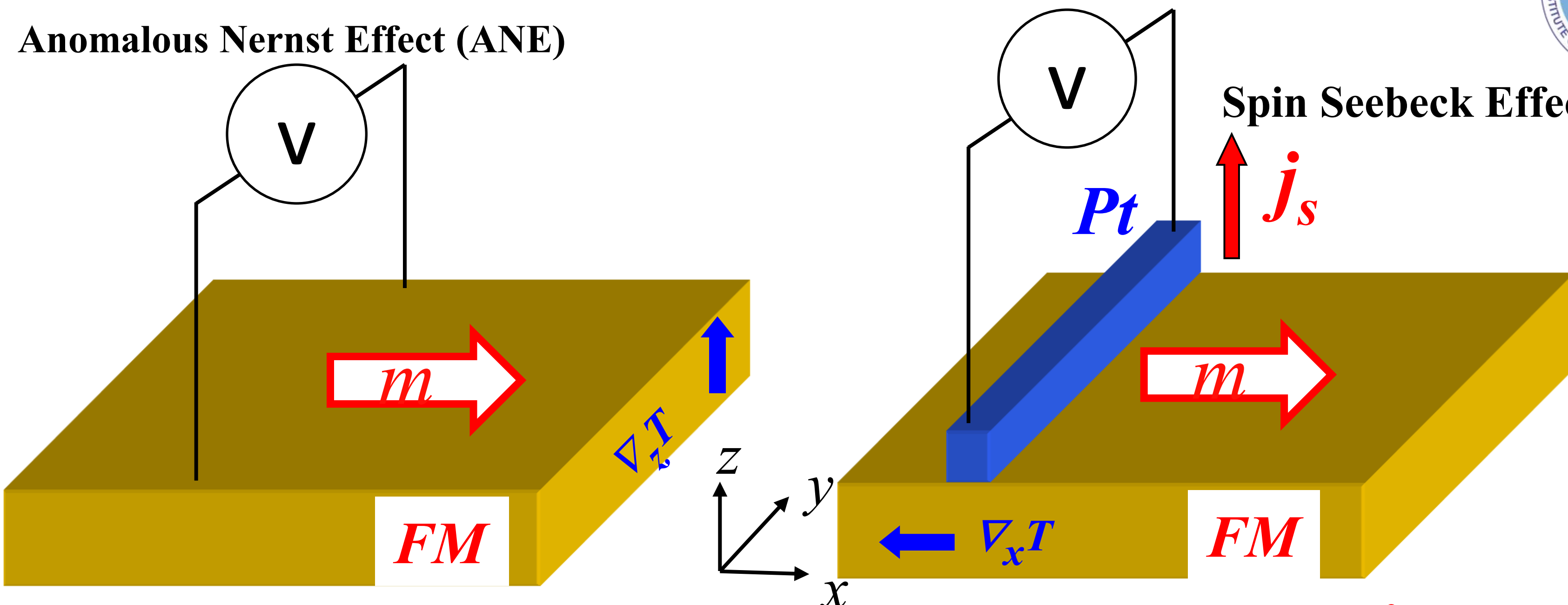

$E_{\text{ANE}} \propto \nabla_z T \times m$

Both along y

$(E_{\text{SSE}})_{\text{Pt}} \propto j_s \times m$

V_{ANE} and $(V_{\text{SSE}})_{\text{Pt}}$ **additive**, both are asymmetric in ***m (or H)***

$(V_{\text{SSE}})_{\text{Pt}} > V_{\text{ANE}}$, one concludes SSE

If V_{ANE} unknown, $(V_{\text{SSE}})_{\text{Pt}}$ uncertain

If $(V_{\text{SSE}})_{\text{Pt}} < V_{\text{ANE}}$, Any SSE ??

Can we eliminate ANE (due to $\nabla_z T$) ?

SSE in FM Metal

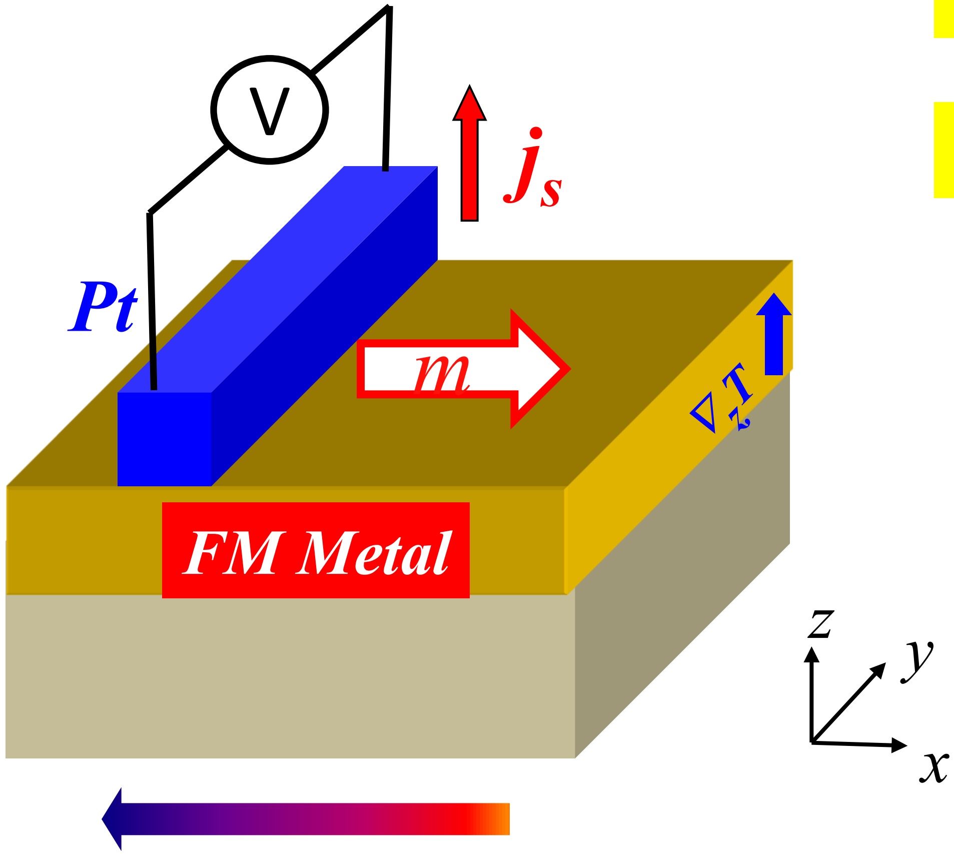

intentional in-plane $\nabla_x T$

SSE + ANE

- **Pt shorts out ANE**
- **Thermally matched substrate**

(Both have been claimed)

Does thin Pt layer short out ANE ?

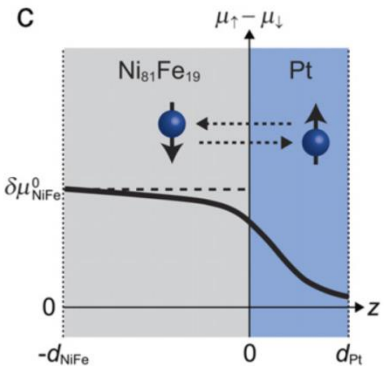

Spin diffusion length of Pt ~ 5 nm

Pt layer shorts out ANE claimed in SSE studies.

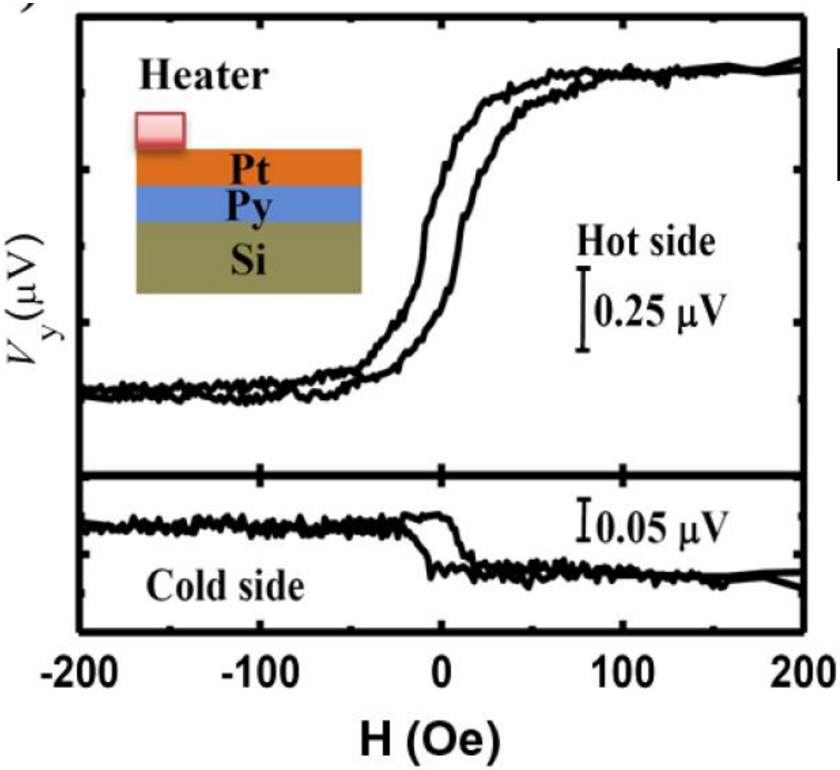

continuous
Pt 10 nm

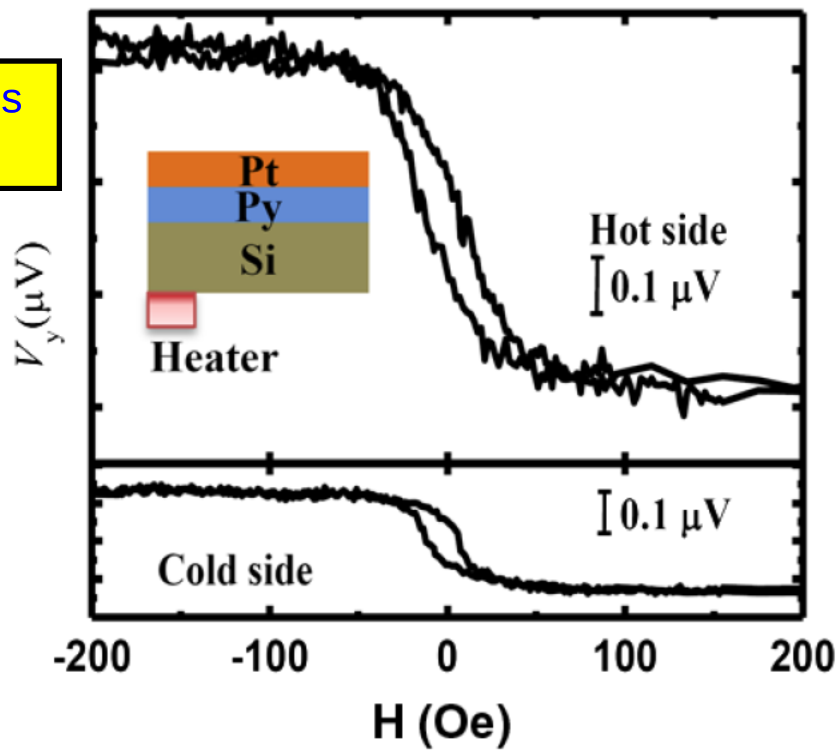

Thin Pt layer reduces, but does not eliminate ANE.

Py on different substrates

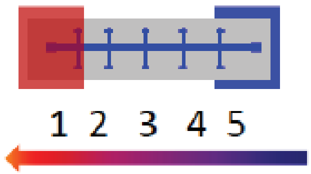

ANE and $\nabla_z T$ in every case

κ(Py)/κ(MgO) ~0.5
Py 50 nm
Heater on top of 1

κ(Py)/κ(GaAs) ~0.54
Py 50 nm
Heater on top of 1

κ(Py)/κ(Glass) ~30
Py 190 nm
Heater on top of 1

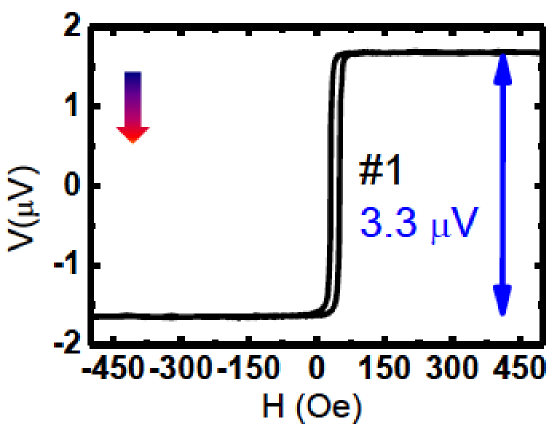

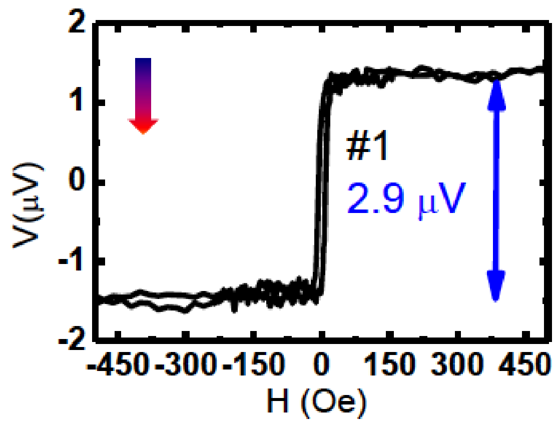

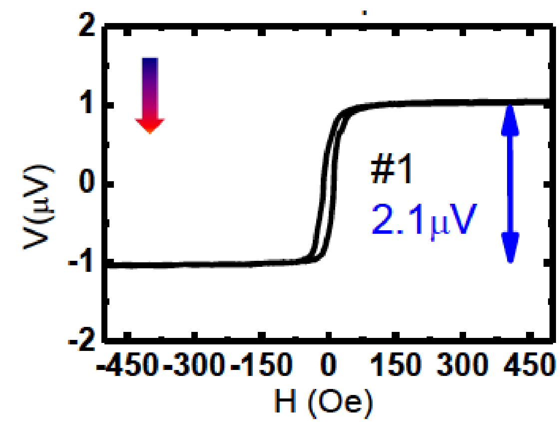

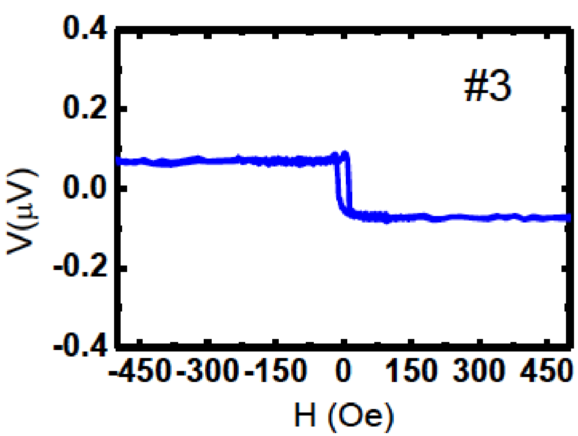

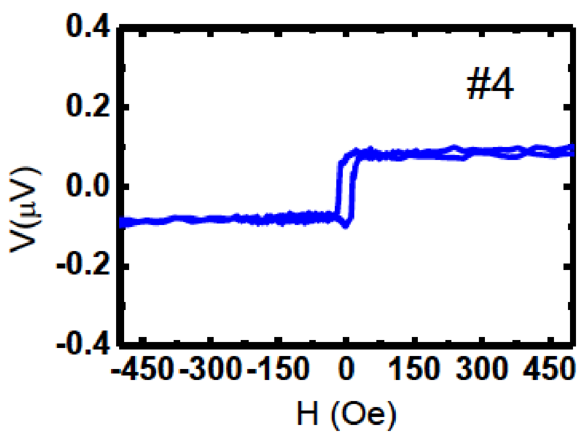

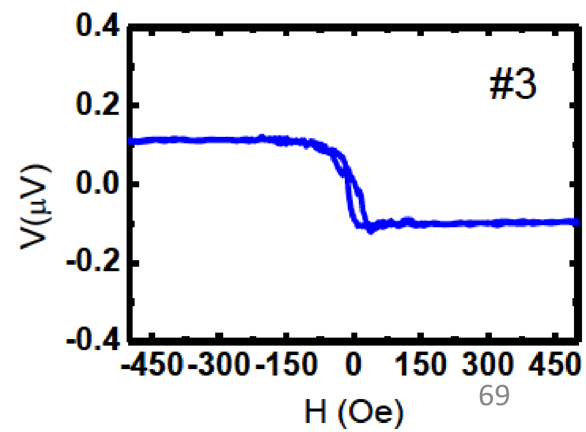

FM on different substrates

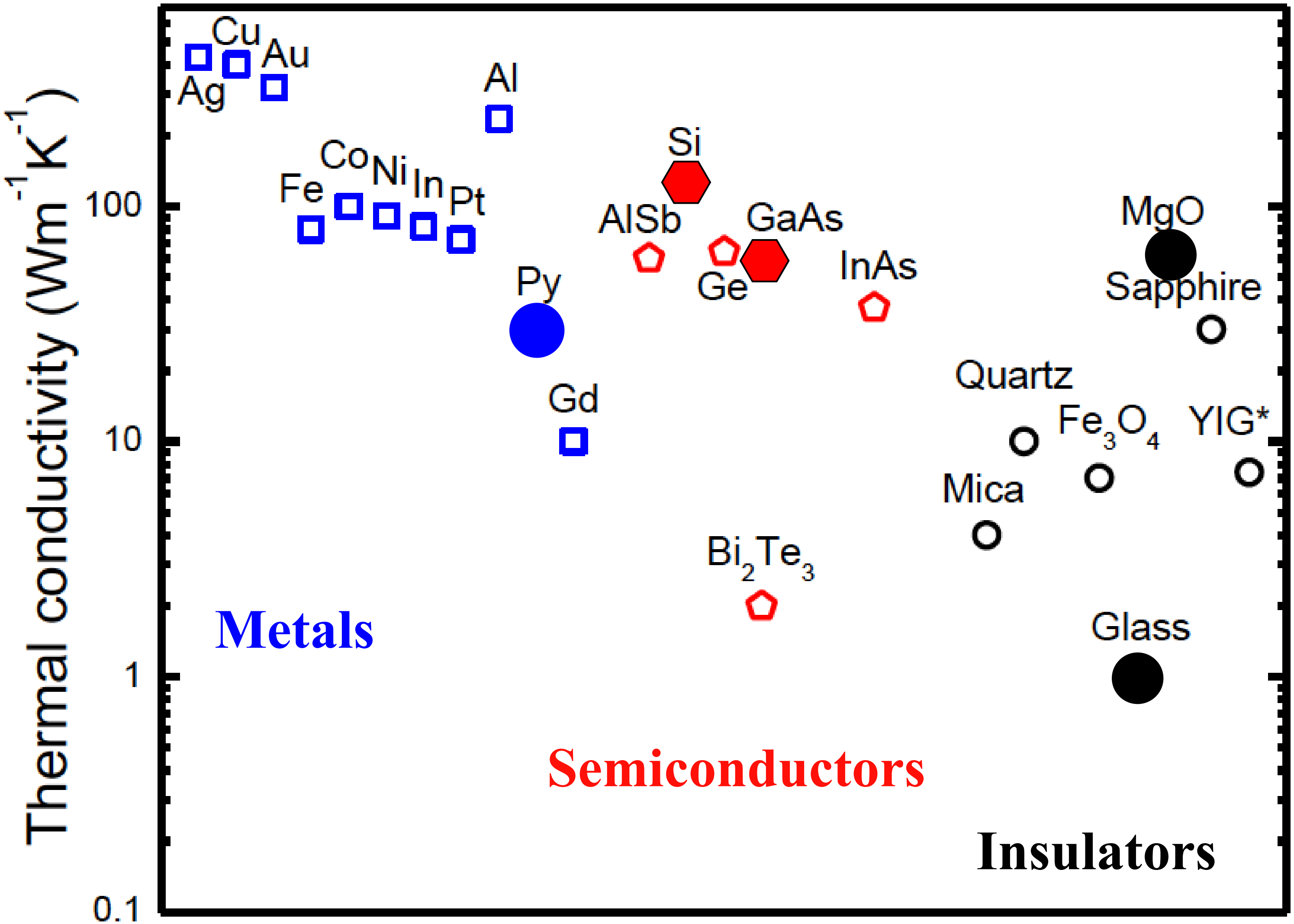

Out-of-plane $\nabla_z T$ exists in all substrates

Intrinsic spin-dependent **Longitudinal** thermal transport in **substrate-free** samples

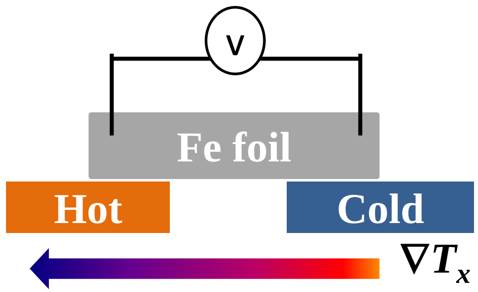

Symmetric in H !

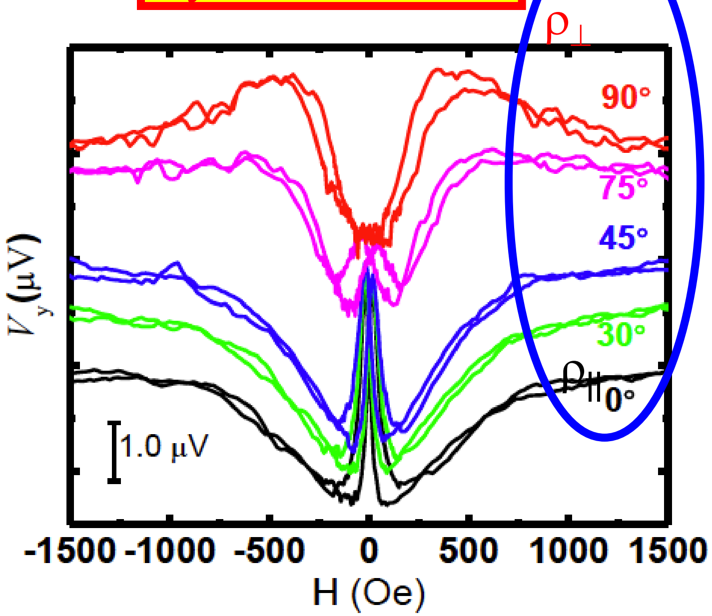

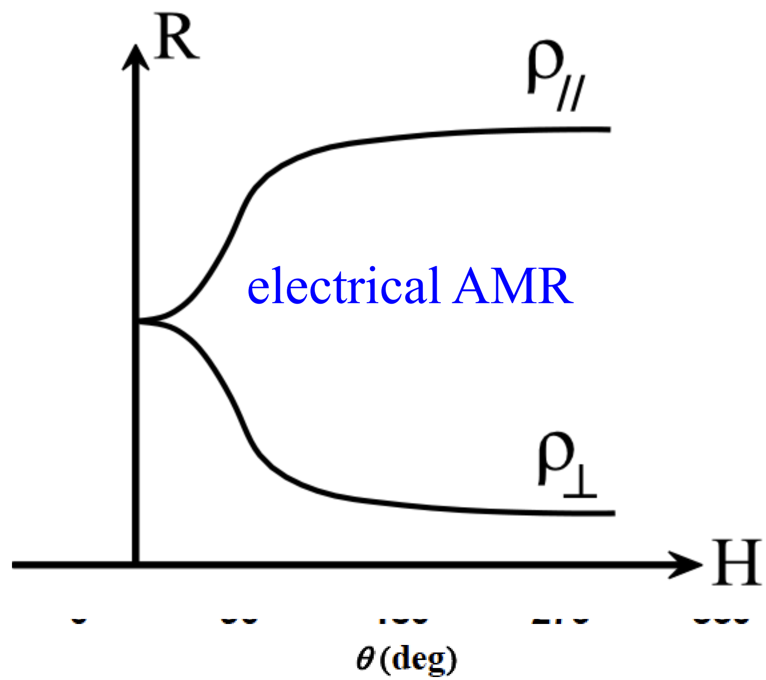

Similar field sensitivity as AMR

$\rho_\perp > \rho_{||}$ opposite to electrical AMR due to Wiedemann-Franz Law

S.D. Bader *et al*. (1991)

Intrinsic spin-dependent **Longitudinal** thermal transport in **substrate-free** samples

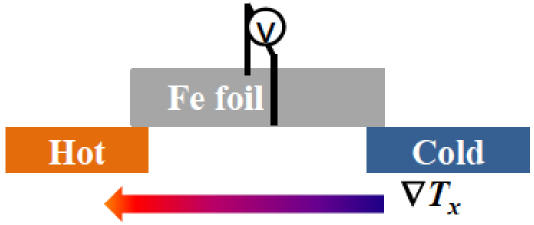

Symmetric in H !

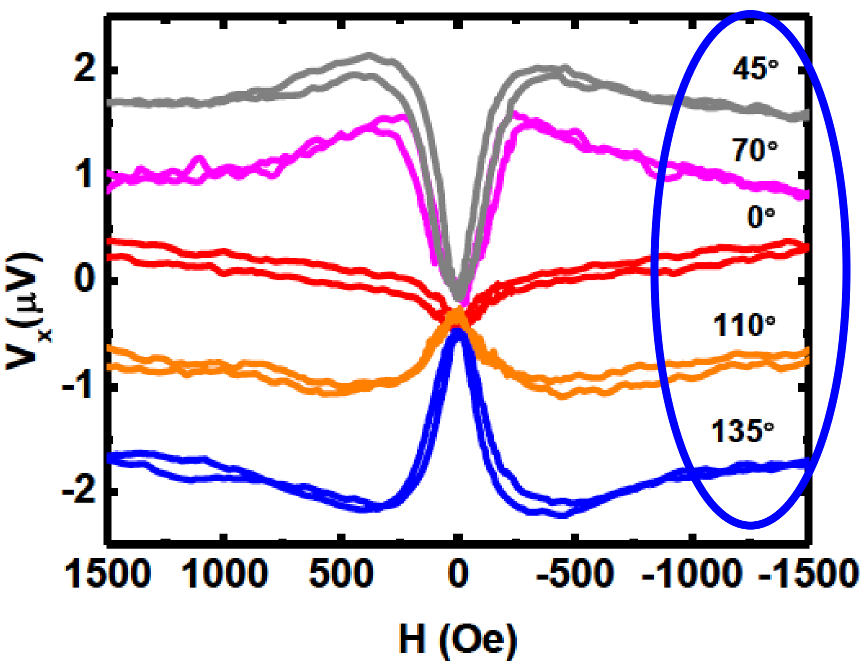

Planar Nernst Effect: sin2θ

Intrinsic spin caloritronic properties with in-plane $\nabla_x T$

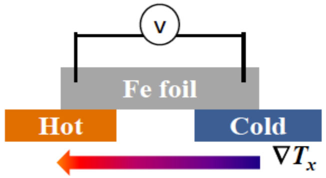

Longitudinal voltage: thermal AMR

$$V_{th} = V_{th\perp} + (V_{th\perp} - V_{th||})\cos^2\theta_M$$

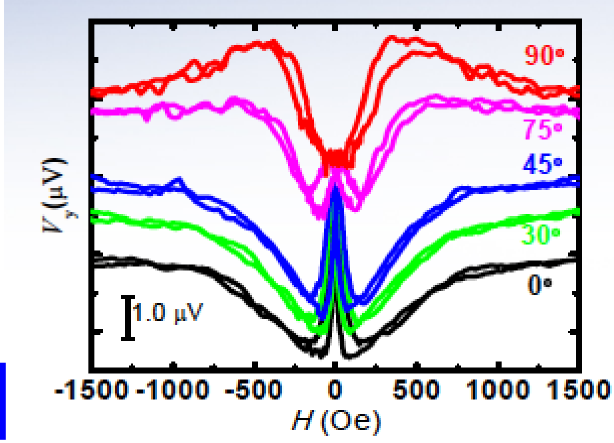

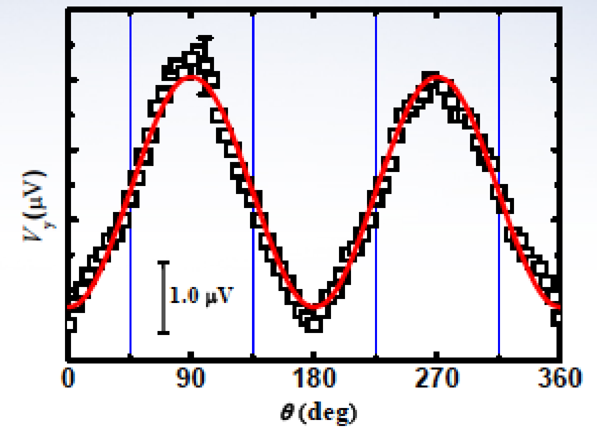

Symmetric in H !

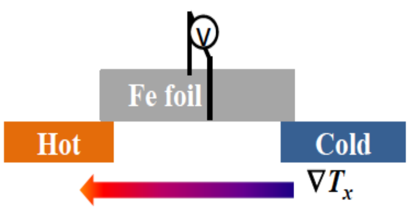

Transverse voltage: Planar Nernst effect

$\sin 2\theta_M$

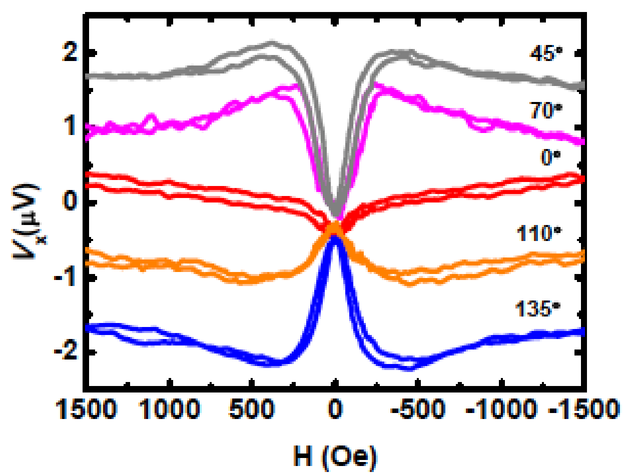

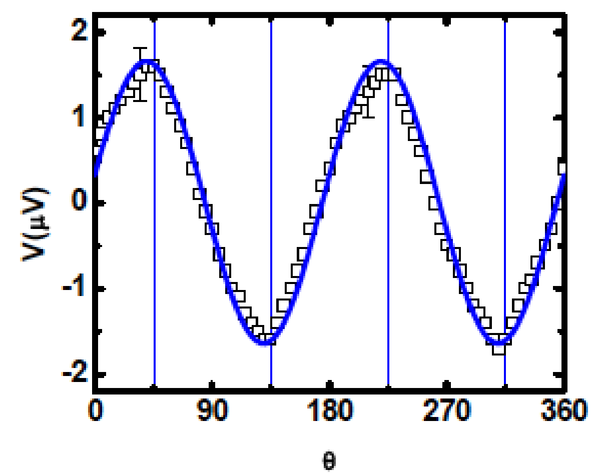

Necessary Signatures of FM film with in-plane $\nabla_x T$

Summary

1. **Thin film/substrate, in-plane ($\nabla_x T$) and perpendicular ($\nabla_z T$)**

Spin Seebeck effect ($\nabla_x T$) with Pt

Anomalous Nernst effect ($\nabla_z T$) with or without Pt

2. V_{ANE} **and** $(V_{SSE})_{Pt}$ are **additive**

If V_{ANE} unknown, $(V_{SSE})_{Pt}$ uncertain

Intrinsic spin Seebeck effect ?

3. **ANE: excellent detector of $\nabla_z T$ and ΔT_z**

4. **Intrinsic spin caloritronics with in-plane $\nabla_x T$ in Fe foils**

Thermal AMR ($cos^2\theta$) Planar Nernst ($sin2\theta$)

Necessary conditions for in-plane $\nabla_x T$ only

outline

- Giant Magnetoresistance, Tunneling Magnetoresistance
- Pure Spin current (no net charge current)
  - Spin Hall, Inverse Spin Hall effects
  - Spin Pumping effect
  - Spin Seebeck effect
- Spin Transfer Torque
- Micro and nano Magnetics

Spin Transfer Torque

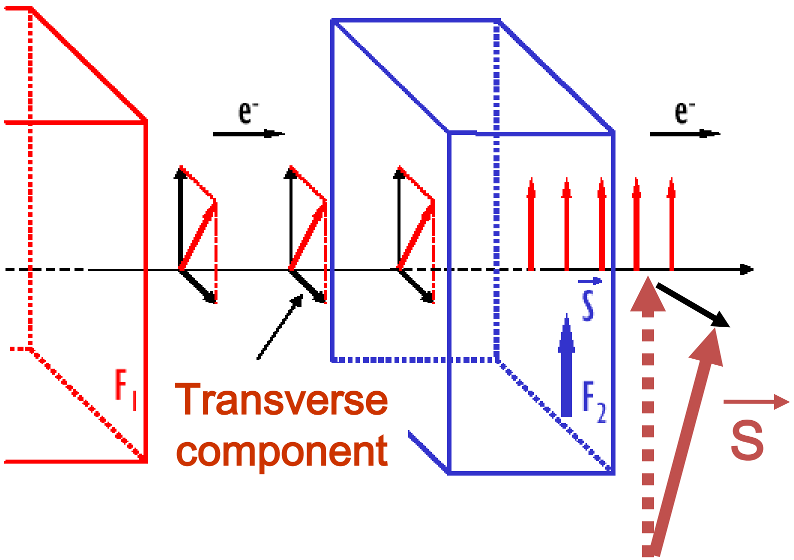

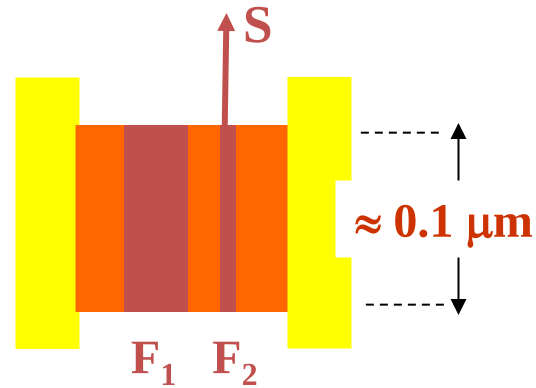

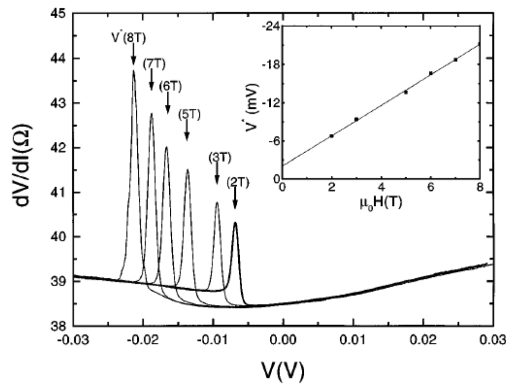

FIG. 1. The point contact $dV/dI(V)$ spectra for a series of magnetic fields (2, 3, 5, 6, 7, and 8 T) revealing an upward step and a corresponding peak in dV/dI at a certain negative bias voltage $V^*(H)$. The inset shows that $V^*(H)$ increases linearly with the applied magnetic field H.

The transverse spin component is lost by the conduction electrons, transferred to the global spin of the layer $\vec{S}$

$$\dot{S}_{1,2} = (I_e g/e)\hat{s}_{1,2} \times (\hat{s}_1 \times \hat{s}_2)$$

Slonczewski JMMM **159**, L1 (1996)

Tsoi et al. PRL **61**, 2472 (1998)

Modified Landau-Lifshitz-Gilbert (LLG) equation

$$\frac{dm}{dt} = -\gamma m \times H_{eff} + \alpha m \times \frac{dm}{dt} + \frac{\gamma \hbar P I}{2e\mu_0 M_S V}(m \times \sigma \times m)$$

Experimantally determined current density ~10^{10}-10^{12}A/m^2

Spin Transfer Torque

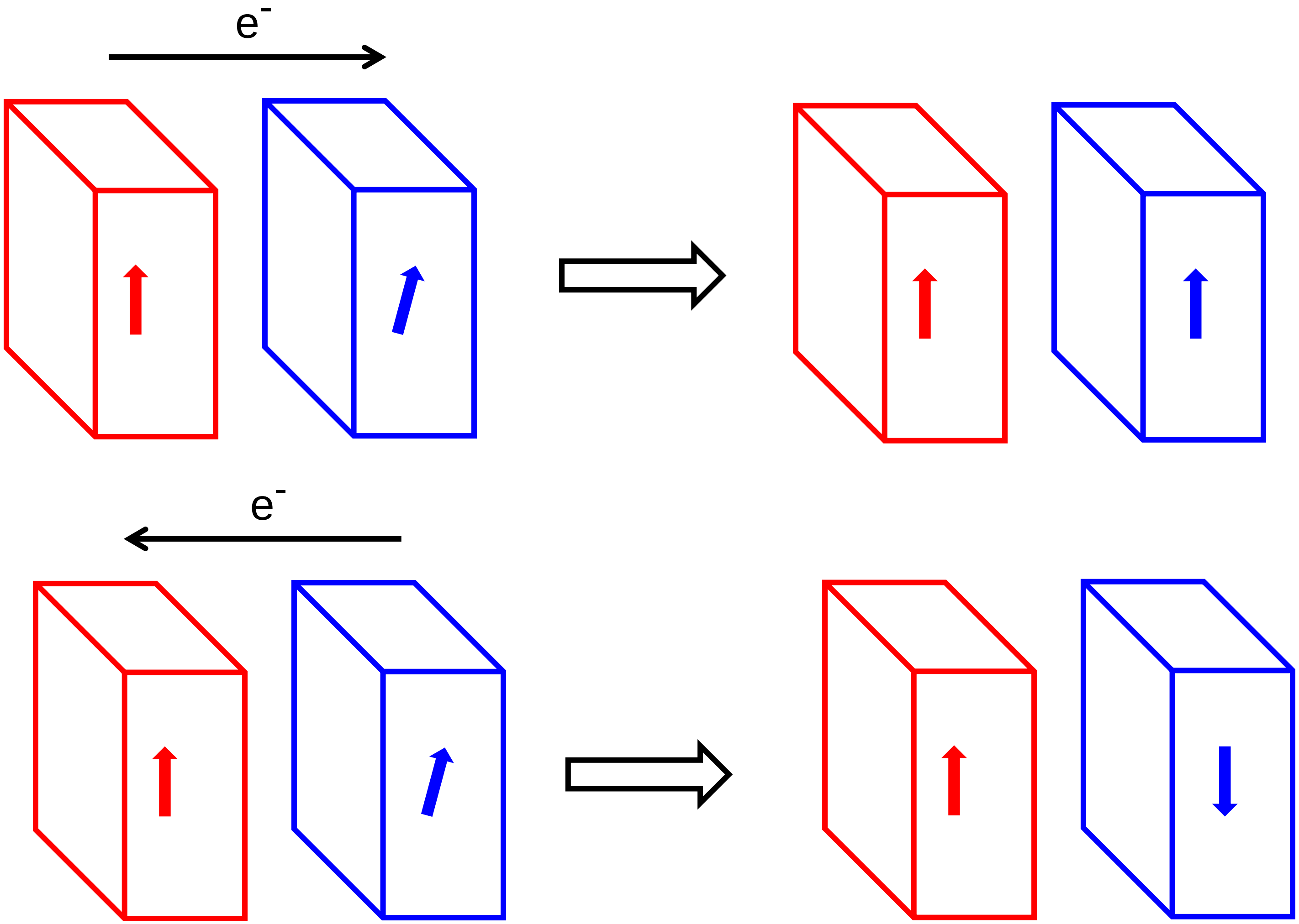

In a trilayer, current direction determines the relative orientation of F_1 and F_2

Spin Transfer Torque

Landau-Lifshitz-Gilbert equation with Spin Transfer Torque terms

Current induced domain wall motion

Passing spin polarized current from Domain A to Domain B⇒B switches

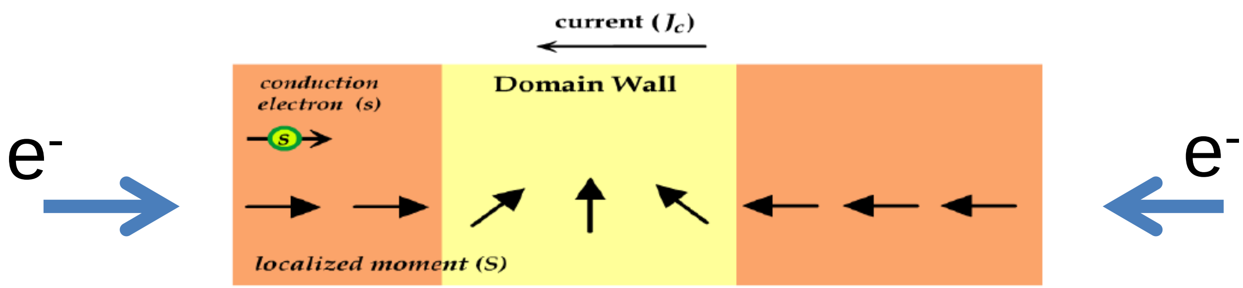

Domain A **Domain B**

$$\frac{\partial \vec{M}}{\partial t} = -\gamma \vec{M} \times \vec{H}_{eff} + \frac{\alpha}{M_s} \vec{M} \times \frac{\partial \vec{M}}{\partial t} + \vec{\mathrm{T}}_{STT}$$

Berger, *JAP* **55**, 1954 (1984)
Tatara *et. al*., *PRL* **92**, 086601 (2004)
Zhang *et. al.*, *PRL* **93**, 127204 (2004)
Thiaville *et. al.*, *Europhys. Lett*. **69**, 990 (2005)
Stiles *et. al.*, *PRB* **75**, 214423 (2007)

Spin Transfer Torque

Landau-Lifshitz-Gilbert equation with Spin Transfer Torque terms

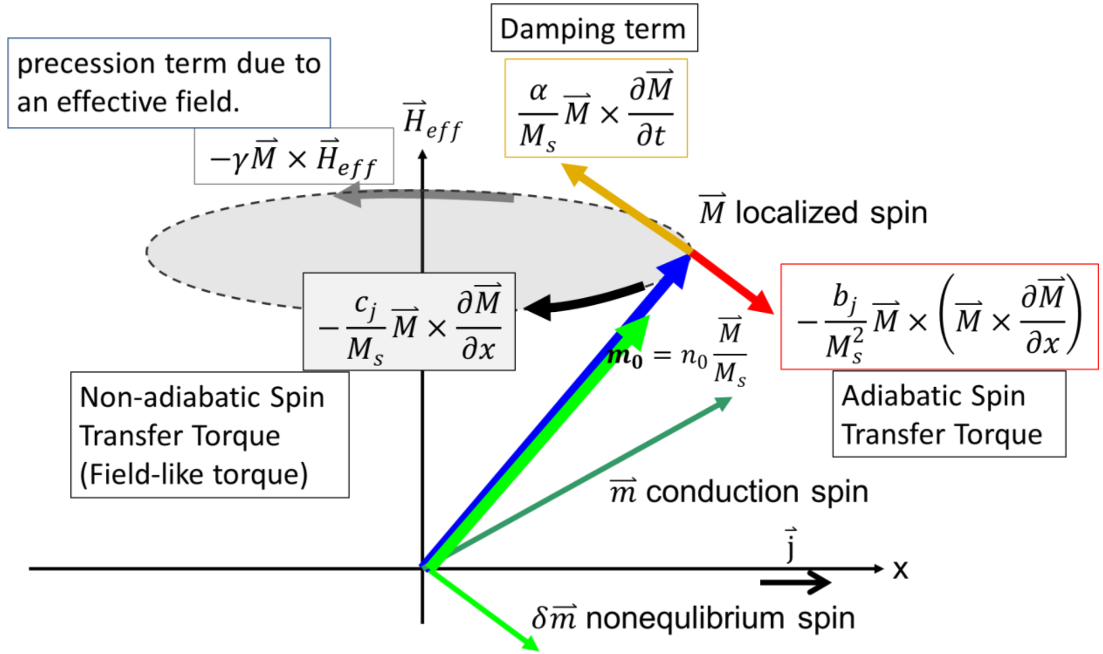

Damping term

Adiabatic Spin Transfer Torque

$$\frac{\partial \vec{M}}{\partial t} = -\gamma \vec{M}\times\vec{H}_{eff} + \frac{\alpha}{M_s}\vec{M}\times\frac{\partial\vec{M}}{\partial t} - \frac{b_j}{M_s^2}\vec{M}\times\left(\vec{M}\times\frac{\partial\vec{M}}{\partial x}\right) - \frac{c_j}{M_s}\vec{M}\times\frac{\partial\vec{M}}{\partial x}$$

$$b_j, c_j \sim JP/t$$

Precessional term due to an effective field.

Non-adiabatic Spin Transfer Torque

Onsager reciprocity relations

X_i generalized forces

J_i generalized currents

$J_i = \sum_j L_{ij} X_j$ linear response

i = {mass, charge, spin, energy, ...}

$\dot{S} = \sum_i X_i J_i$ entropy creation rate

$$L_{ij}\left(\mathbf{m},\mathbf{H}_{ext}\right) = \varepsilon_i \varepsilon_j L_{ji}\left(-\mathbf{m},-\mathbf{H}_{ext}\right)$$

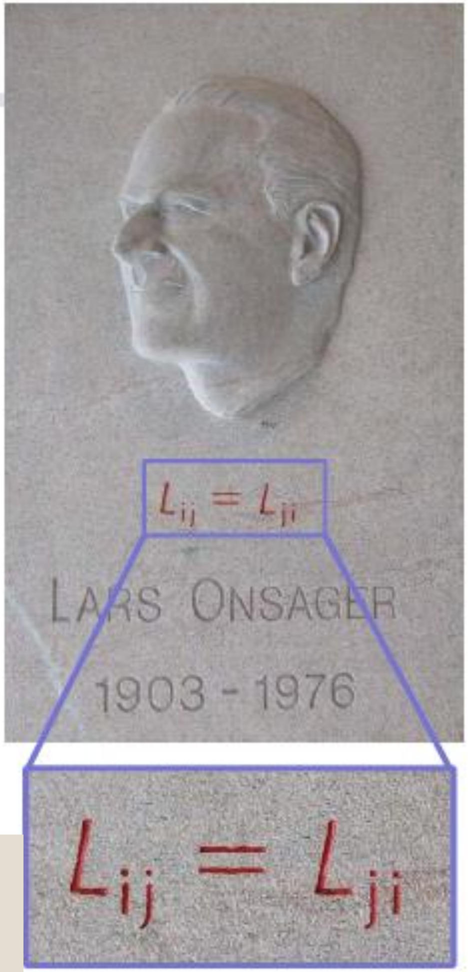

Equality between certain relations between flows and forces out of equilibrium

Currents can induce magnetization excitations

↕

A time-dependent magnetization can induce (charge and spin) currents

Industrial applications

Read head in hard drives

MRAM

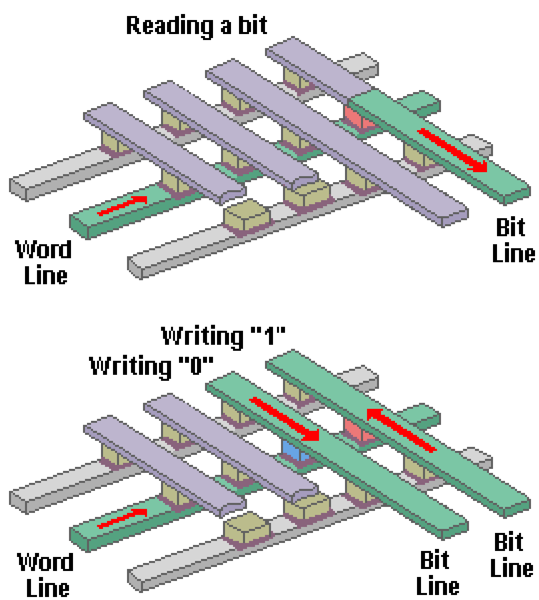

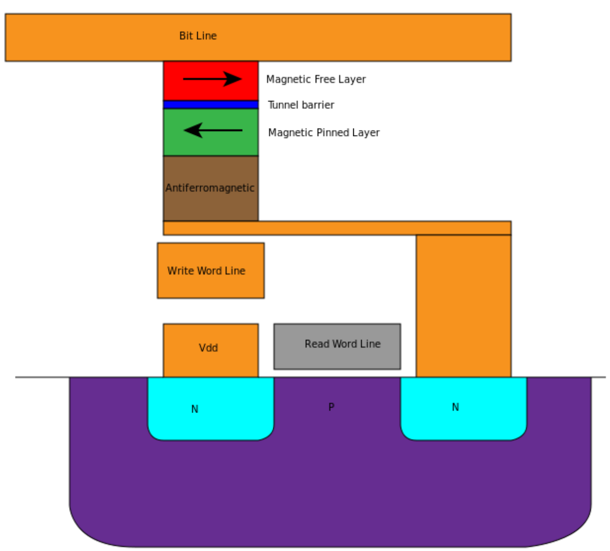

Application of Spin Transfer Torque

Magnetic Domain-Wall Racetrack Memory

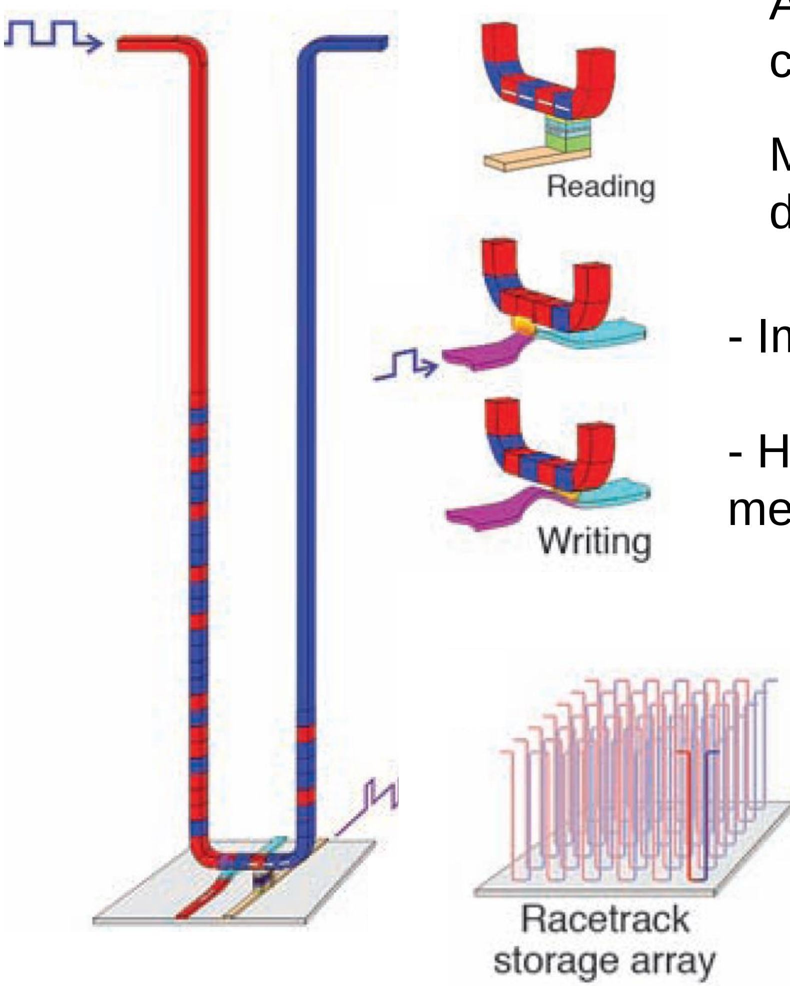

Dr. Stuart S. P. Parkin Science **320**, 190 (2008)

A novel three-dimensional spintronic storage class memory

Magnetic nanowires: information stored in the domain walls

- Immense storage capacity of a hard disk drive

- High reliability and performance of solid state memory (DRAM, FLASH, SRAM...)

→ **Understanding of current induced domain wall (DW) motion**

Application of Spin Transfer Torque

Domain Wall Structures in Permalloy Nanowires

(a)

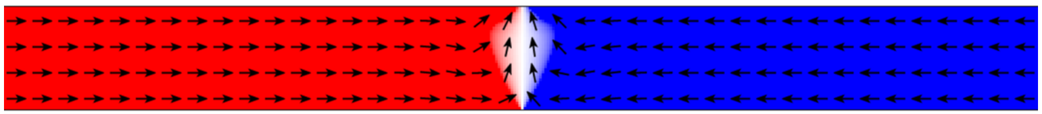

Transvers DW

(b)

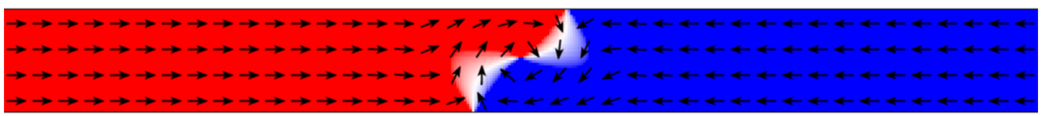

Vortex DW

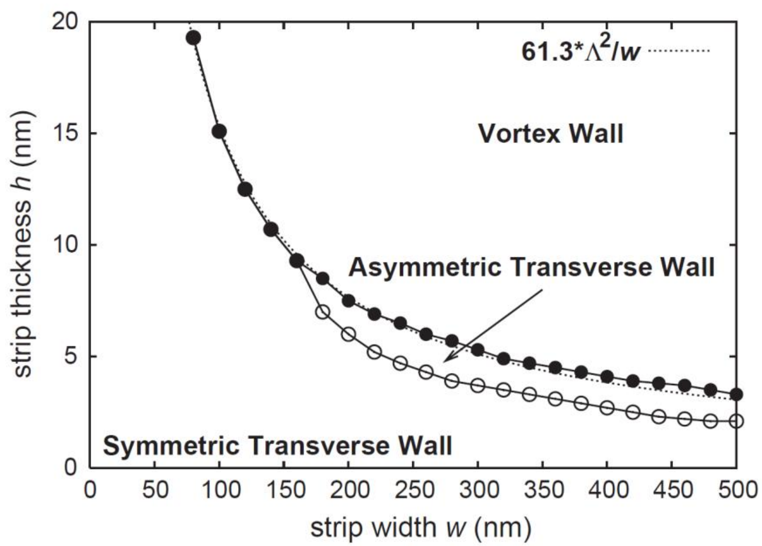

J. Magn. Magn. Mater. **290**, 750 (2005)

DW traps

protrusion

notch

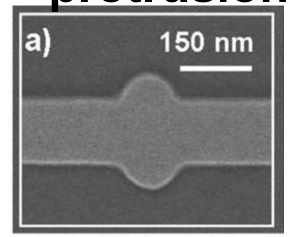

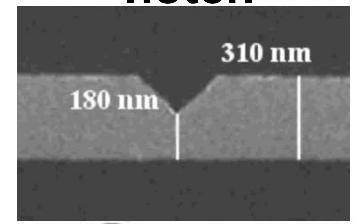

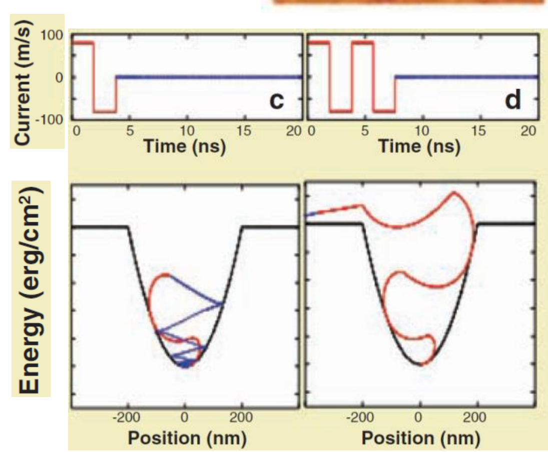

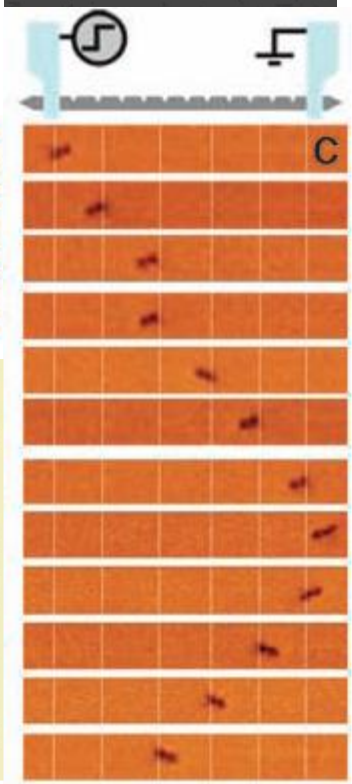

Application of Spin Transfer Torque

DW Oscillators

$j_W < j_a < j_{dep}$

e^- → ← H

Walker breackdown

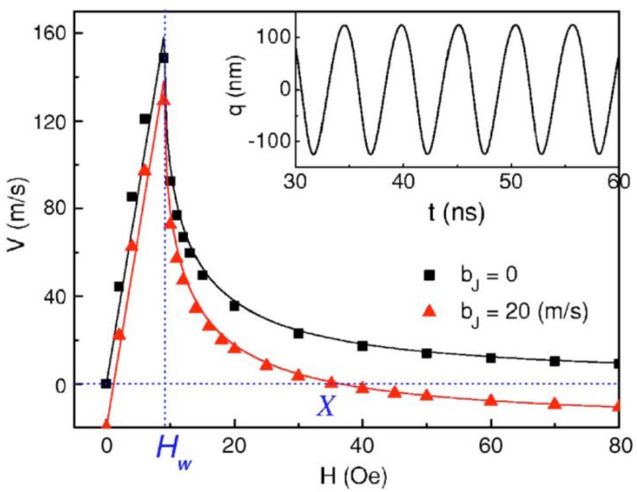

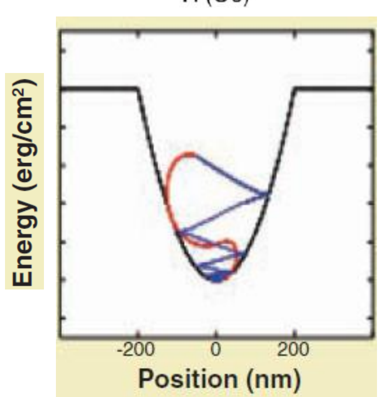

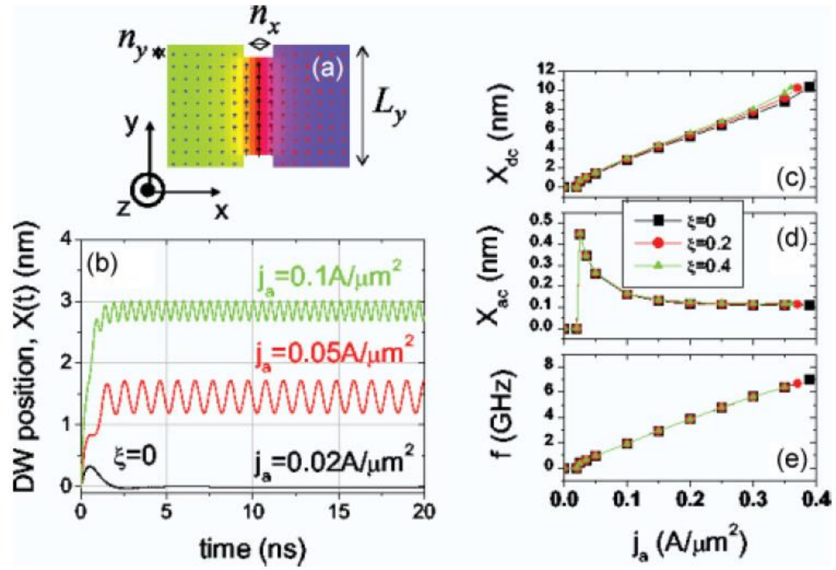

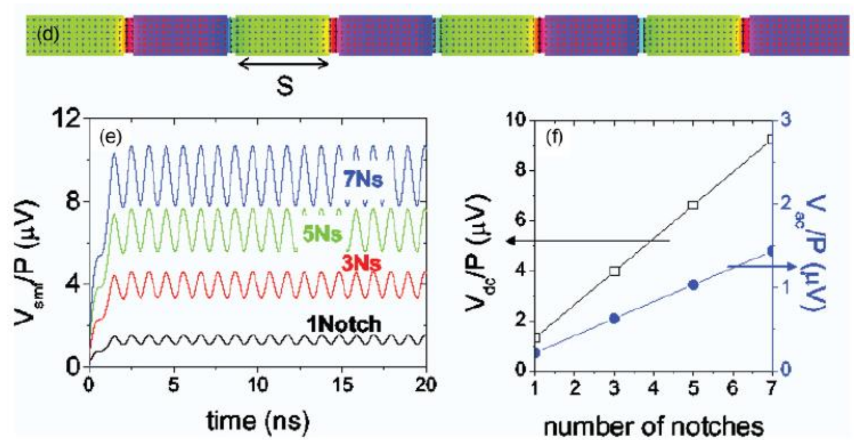

PHYSICAL REVIEW B **83**, 174444 (2011)
Appl. Phys. Lett. **90**, 142508 (2007)

Application of Spin Transfer Torque

AC Current-Induced DW Resonance

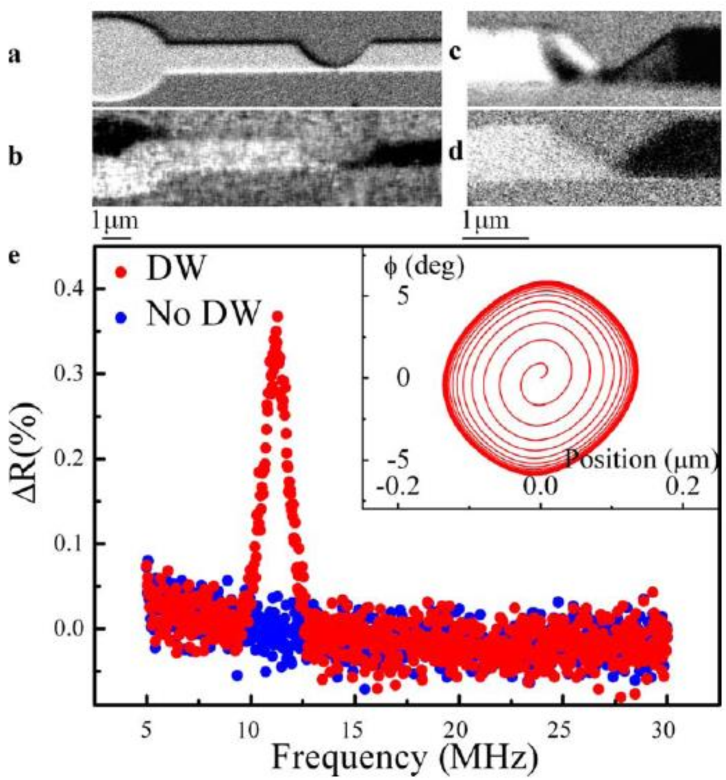

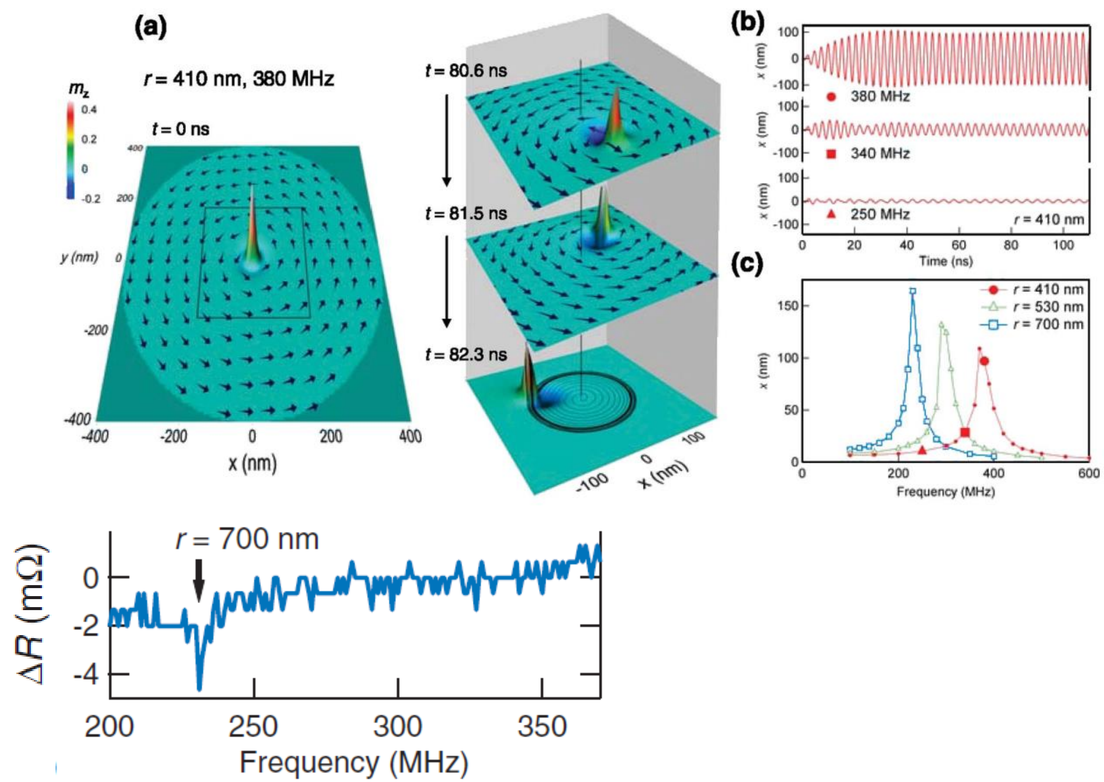

PRB **81**, 060402 (2010), PRL **97**, 107204 (2006)

Application of Spin Transfer Torque

Radio-Frequency DW Oscillators

✖ CPP-nanopillar

AC

DC

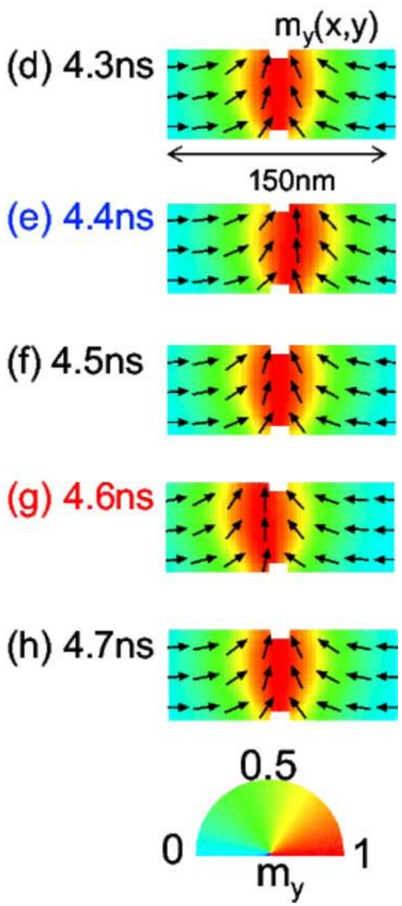

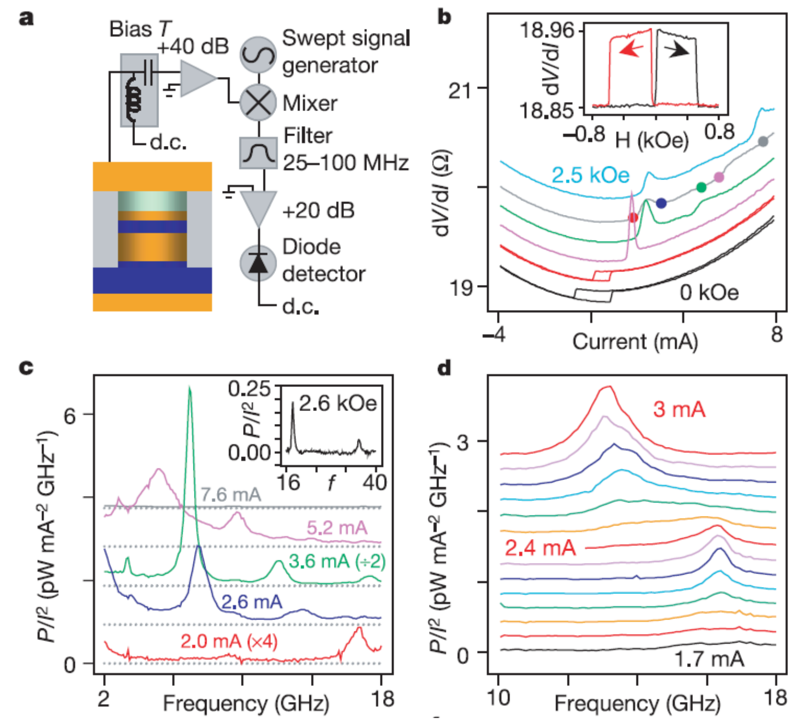

Nature **425**, 380 (2003)

Our works

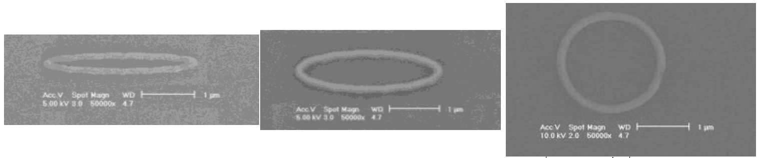

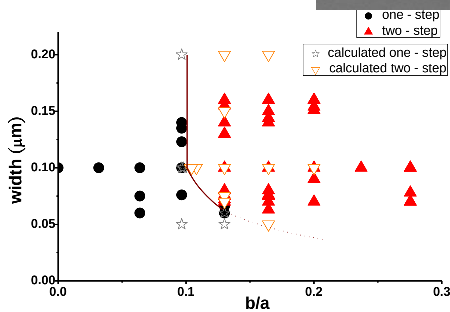

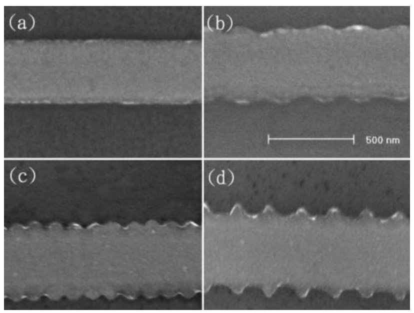

Magnetic nanostructures

- "Quantitative analysis of magnetization reversal in submicron S-patterned structures with narrow constrictions by magnetic force microscopy". APL **86**, 053111 (2005).
- "Observation of Room Temperature Ferromagnetic Behavior in Cluster Free, Co doped HfO_2 Films". APL **91**, 082504 (2007).
- "Variation of magnetization reversal in pseudo-spin-valve elliptical rings". APL **94**, 233103 (2009).
- "Compensation between magnetoresistance and switching current in Co/Cu/Co spin valve pillar structure". APL **96**, 093110 (2010).
- "Exchange bias in spin glass (FeAu)/NiFe thin films". APL **96**, 162502 (2010).
- "Demonstration of edge roughness effect on the magnetization reversal of spin valve submicron wires". APL **97**, 022109 (2010).
- "Current induced localized domain wall oscillators in NiFe/Cu/NiFe submicron wires". APL **101**, 242404 (2012).
- "Inverse spin Hall effect induced by spin pumping into semiconducting ZnO". APL **104**, 052401 (2014).

outline

- Giant Magnetoresistance, Tunneling Magnetoresistance
- Pure Spin current (no net charge current)
    - Spin Hall, Inverse Spin Hall effects
    - Spin Pumping effect
    - Spin Seebeck effect
- Spin Transfer Torque
- Micro and nano Magnetics

Nano Magnetism

Vortex induced by dc current in a circular magnetic spin valve nanopillar

L. J. Chang and S. F. Lee

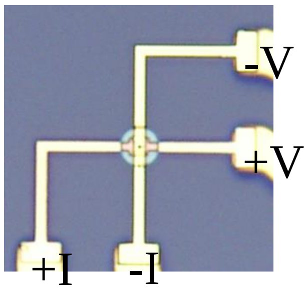

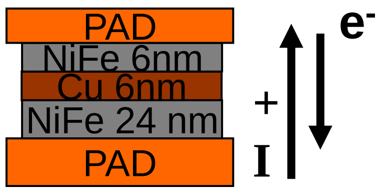

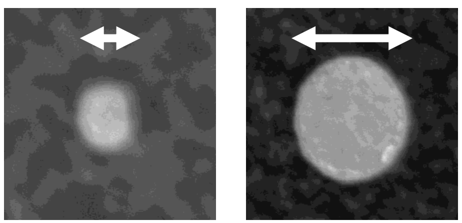

90 nm 380 nm

oommf

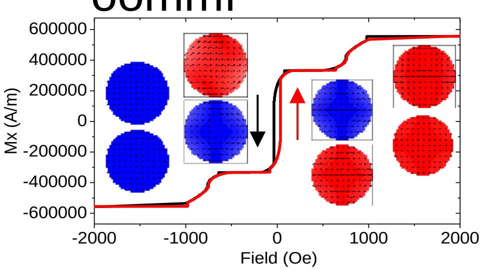

D = 90 nm

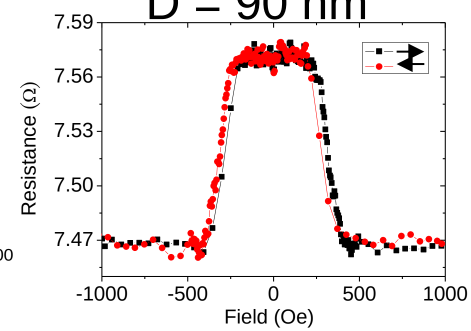

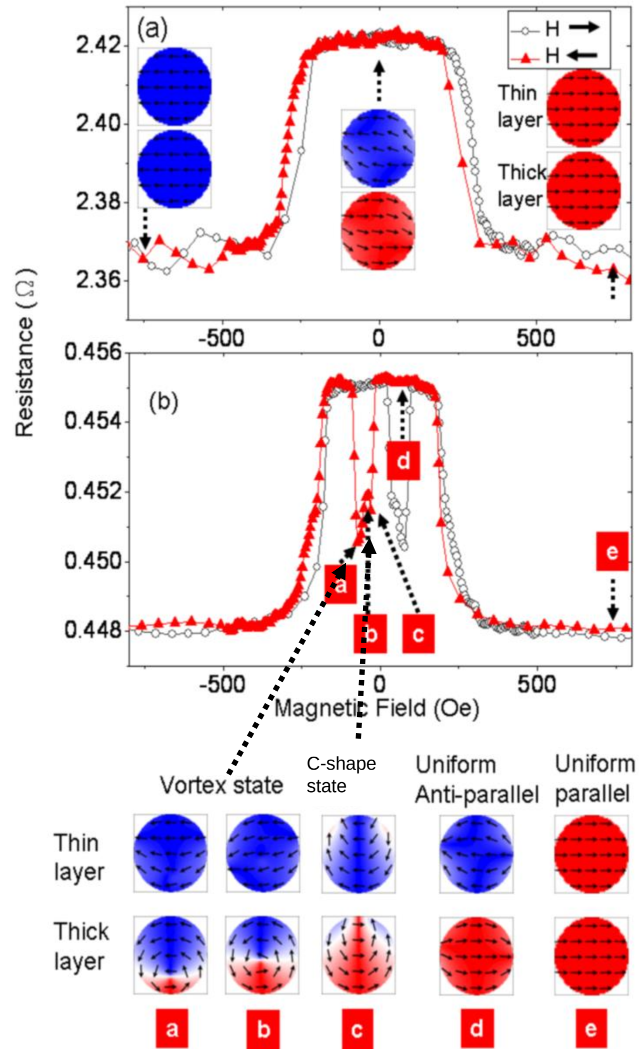

D = 160 nm

D = 380 nm

Current driven vortex nucleation

D = 160 nm H = 0 Oe

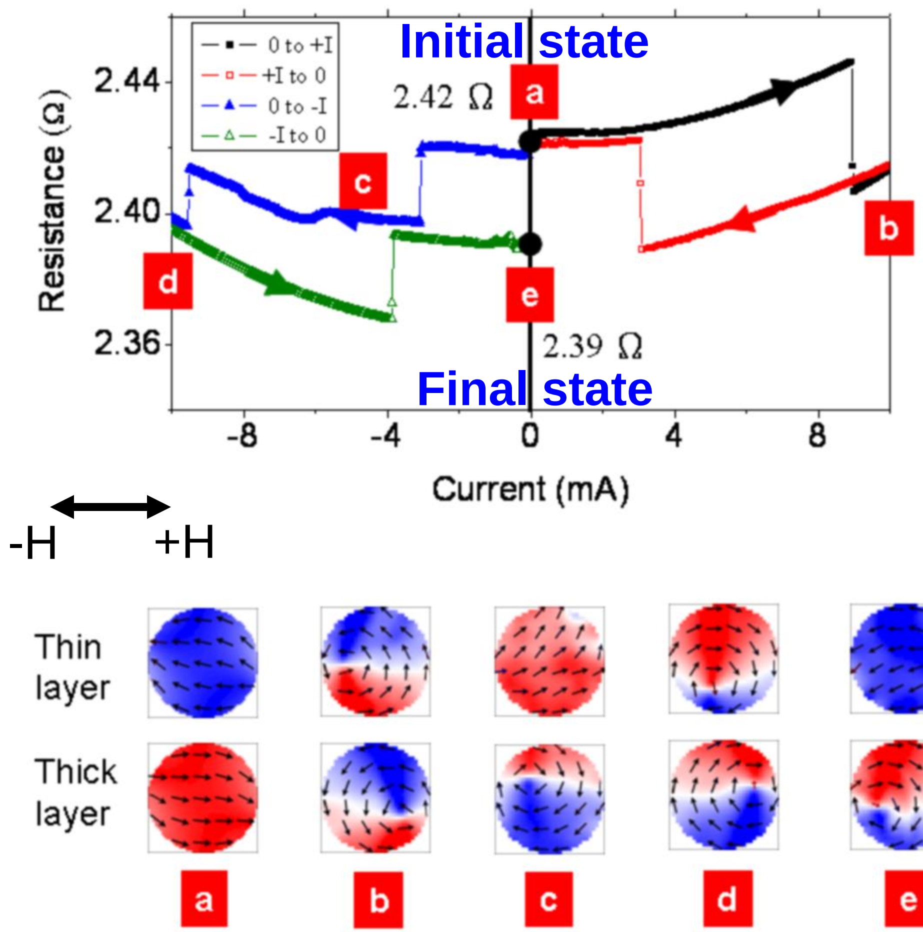

Other research interest include superconductor-magnetic material proximity effect, Ferromagnetic Resonance etc.

Domain wall oscillation in a trapping potential

Theoretical Backgrounds

Resonant DW induced by AC spin-polarized current in Ferromagnetic strips

DW dynamics equation

$$(1+\alpha^2)m\frac{d^2x}{dt^2} = F_p(x) + F_f + F_s + F_d$$

where $m = \frac{2(\mu_0 L_y L_z)}{\gamma_0^2 (N_z - N_y)\Delta_0}$ is the effective DW mass (kg), and the other variables are listed below.

L_y : width of wire (m)

L_z : thickness of wire (m)

μ_0 : permeability ($4\pi \times 10^{-7}$ VsA^{-1}m^{-1})

γ_0 : electron gyromagnetic ratio (2.2×10^5 Vs^{2}m^{-1}kg^{-1})

N_z, N_y : transverse demagnetizing factors

Δ_0 : DW width (m)

x : DW position (m)

Theoretical Backgrounds

Resonant DW induced by AC spin-polarized current in Ferromagnetic strips

pinning force $$F_p(x) = -\frac{\partial V_{pin}(x)}{\partial x} = \begin{cases} -K_N x & (|x| \leq L_N) \\ 0 & (|x| > L_N) \end{cases}$$

L_N : length of pinning potential (m)

where K_N (N/m) is the elastic constant of the DW trap

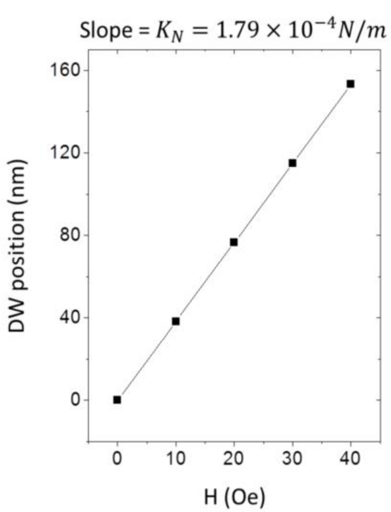

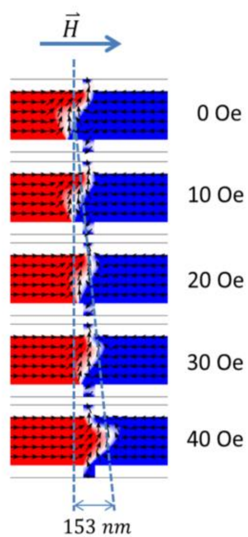

K_N =1.79×10^{-4} N/m.

$m = 5.25 \times 10^{-25}$kg

$$f_r = \frac{1}{2\pi}\sqrt{\frac{K_N}{m}} = \frac{1}{2\pi}\sqrt{\frac{1.79 \times 10^{-4} N/m}{5.25 \times 10^{-25} kg}}$$
$$= 2.93\text{GHz}$$

Theoretical Backgrounds

Resonant DW induced by AC spin-polarized current in Ferromagnetic strips

friction force $F_f = -\left[\alpha m \omega_d \left(1 + \frac{\omega_r^2}{\omega_d^2}\right)\right] \frac{dx(t)}{dt} = -b\,\frac{dx(t)}{dt}$

$\omega_d = \gamma_0 M_s (N_z - N_y)$ ： angular frequency of magnetization oscillations around the demagnetizing field inside the wall.

$\omega_r = 2\pi f_r$ ： angular frequency of free harmonic oscillator.

$$b = \left[\alpha m \omega_d \left(1 + \frac{\omega_r^2}{\omega_d^2}\right)\right] \Rightarrow \frac{b}{m} = \alpha \omega_d \left(1 + \frac{\omega_r^2}{\omega_d^2}\right)$$

$$\omega_d = \gamma_0 M_s (N_z - N_y) = \frac{2(\mu_0 L_y L_z)}{\gamma_0 m \Delta_0} M_s = \frac{2[4\pi\times10^{-7}(VsA^{-1}m^{-1})\cdot400\times10^{-9}(m)\cdot12\times10^{-9}(m)]}{2.2\times10^5(Vs^2m^{-1}kg^{-1})\cdot5.25\times10^{-25}(kg)\cdot100\times10^{-9}(m)}\cdot$$

$$8.6 \times 10^5 \left(\frac{A}{m}\right) = 8.97 \times 10^{11}(s^{-1})$$

$$\Rightarrow \frac{b}{m} = \alpha \omega_d \left(1 + \frac{\omega_r^2}{\omega_d^2}\right) \sim \alpha \omega_d = 0.01 \times 8.97 \times 10^{11}(s^{-1}) = 8.97 \times 10^9(s^{-1})$$

Theoretical Backgrounds

Resonant DW induced by AC spin-polarized current in Ferromagnetic strips

static driving force $F_s = F_H + F_j = m\omega_d\left(\gamma_0\Delta_0 H_a - c_j\right)$

$c_j = \xi b_j$ ： non-adiabatic STT term

time-varying contribution $F_d = F_{H_a} + F_{j_a} = m\left[\alpha\gamma_0\Delta_0\frac{\partial H_a}{\partial t} - (1+\alpha\xi)\frac{\partial b_j}{\partial t}\right]$

$b_j = j_a(t)\frac{\mu_B P}{eM_s(1+\xi^2)}$ ： adiabatic STT term

$j_a(t) = j cos(2\pi f_j t)$ ： AC current dencity

Theoretical Backgrounds

Resonant DW induced by AC spin-polarized current in Ferromagnetic strips

zero external field $H_a = 0$
zero non-adiabatic STT term $c_j = 0$.

$$(1+\alpha^2)m\frac{d^2x}{dt^2} + b\frac{dx(t)}{dt} + K_N x = m(1+\alpha\xi)\frac{j\mu_B P}{eM_s(1+\xi^2)}2\pi f_j \sin(\omega_j t)$$

set $x(t) = A\cos(\omega_j t) + B\sin(\omega_j t)$

$$\frac{dx(t)}{dt} = -A\omega_j\, sin(\omega_j t) + B\omega_j\, cos(\omega_j t)$$

$$\frac{d^2x}{dt^2} = -A\omega_j^2\cos(\omega_j t) - B\omega_j^2\, sin(\omega_j t)$$

Theoretical Backgrounds

Resonant DW induced by AC spin-polarized current in Ferromagnetic strips

$$\begin{bmatrix} \left[K_N-(1+\alpha^2)m\omega_j^2\right] & \left(b\omega_j\right) \\ \left(-\omega_j t\right) & \left[K_N-(1+\alpha^2)m\omega_j^2\right] \end{bmatrix}\begin{bmatrix} A \\ B \end{bmatrix}=\begin{bmatrix} 0 \\ m(1+\alpha\xi)\dfrac{j\mu_B P}{eM_s(1+\xi^2)}\omega_j \end{bmatrix}$$

$$\Rightarrow \mathrm{A}=\frac{m(1+\alpha\xi)\dfrac{j\mu_B P}{eM_s(1+\xi^2)}\omega_j\cdot\left(b\omega_j\right)}{\left[K_N-(1+\alpha^2)m\omega_j^2\right]^2+\left(b\omega_j\right)^2}$$

$$\mathrm{B}=\frac{-m(1+\alpha\xi)\dfrac{j\mu_B P}{eM_s(1+\xi^2)}\omega_j\cdot\left[K_N-(1+\alpha^2)m\omega_j^2\right]}{\left[K_N-(1+\alpha^2)m\omega_j^2\right]^2+\left(b\omega_j\right)^2}$$

Then the particular solution is：

$$x(t) = \sqrt{A^2 + B^2}\cos(\omega_j t - \delta)$$

δ：Phase between the applied current $j_a(t)$ and the DW position $x(t)$ in the stationary regime.

$\delta = \tan^{-1}\left(\frac{B}{A}\right)$

$$A_r = \sqrt{A^2 + B^2}$$

$$= \sqrt{\frac{\left(m(1+\alpha\xi)\frac{j\mu_B P}{eM_s(1+\xi^2)}\omega_j\right)^2 \cdot \left\{\left[K_N - (1+\alpha^2)m\omega_j^2\right]^2 + \left(b\omega_j\right)^2\right\}}{\left\{\left[K_N - (1+\alpha^2)m\omega_j^2\right]^2 + \left(b\omega_j\right)^2\right\}^2}}$$

$$= \frac{j\mu_B P}{eM_s(1+\xi^2)}\sqrt{\frac{(1+\alpha\xi)^2\omega_j^2}{\left[\omega_r^2 - (1+\alpha^2)\omega_j^2\right]^2 + \left(\frac{b}{m}\right)^2\omega_j^2}}$$

$$A_r = \frac{j\mu_B P}{eM_s}\sqrt{\frac{\omega_j^2}{\left[\omega_r^2 - (1+\alpha^2)\omega_j^2\right]^2 + \left(\frac{b}{m}\right)^2 \omega_j^2}} =$$

$$\frac{5\times 10^{12}(A/m^2)\cdot 9.274\times 10^{-24}(Am^2)\cdot 0.4}{1.602\times 10^{-19}(C)\cdot 8.6\times 10^5(A/m)}\sqrt{\frac{\omega_j^2}{[(2\pi\times 2.93\times 10^9(s^{-1}))^2 - \omega_j^2]^2 + (8.97\times 10^9(s^{-1}))^2\cdot \omega_j^2}}$$

$$= 1.34\times 10^2(m/s)\sqrt{\frac{\omega_j^2}{[(2\pi\times 2.93\times 10^9(s^{-1}))^2 - \omega_j^2]^2 + (8.97\times 10^9(s^{-1}))^2\cdot \omega_j^2}}$$

We set the AC current density $j = 5\times 10^{12}(A/m^2)$, Bohr magneton $\mu_B = 9.274\times 10^{-24}(Am^2)$, spin polarization $P = 0.4$, electron charge $e = 1.602\times 10^{-19}$C, width of DW $\Delta_0 = 100(nm)$, NiFe saturation magnetization $M_s = 8.6\times 10^5(A/m)$.

Since the DW resonate with the applied AC current, $\omega_r = \omega_j$. Therefore:

$$\Rightarrow\ 1.34 \times 10^2 \left(\frac{m}{s}\right) \sqrt{\frac{\omega_j^2}{[(2\pi \times 2.93 \times 10^9 (s^{-1}))^2 - \omega_j^2]^2 + \left(8.97 \times 10^9 (s^{-1})\right)^2 \cdot \omega_j^2}}$$

$$= 1.34 \times 10^2 \left(\frac{m}{s}\right) \times \frac{1}{8.97 \times 10^9 (s^{-1})} = 14.9 \times 10^{-9} (m)$$

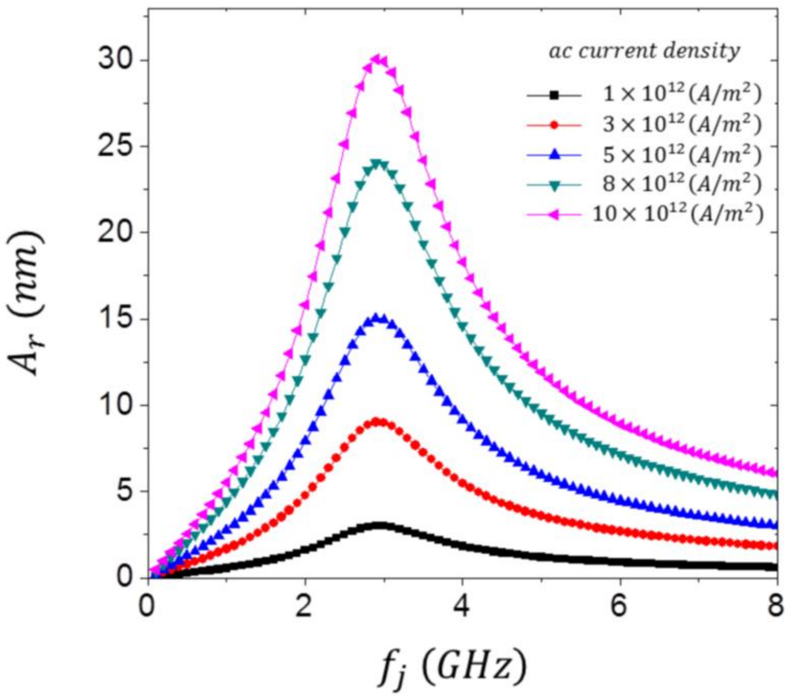

Amplitude of stationary DW oscillations as a function of the frequency of the AC current f_j for $H = 0$ mT, $\xi = 0$, which are given by Eq. (2.37) for five different values of j.

Experiment Methods

four point probe measurement circuit

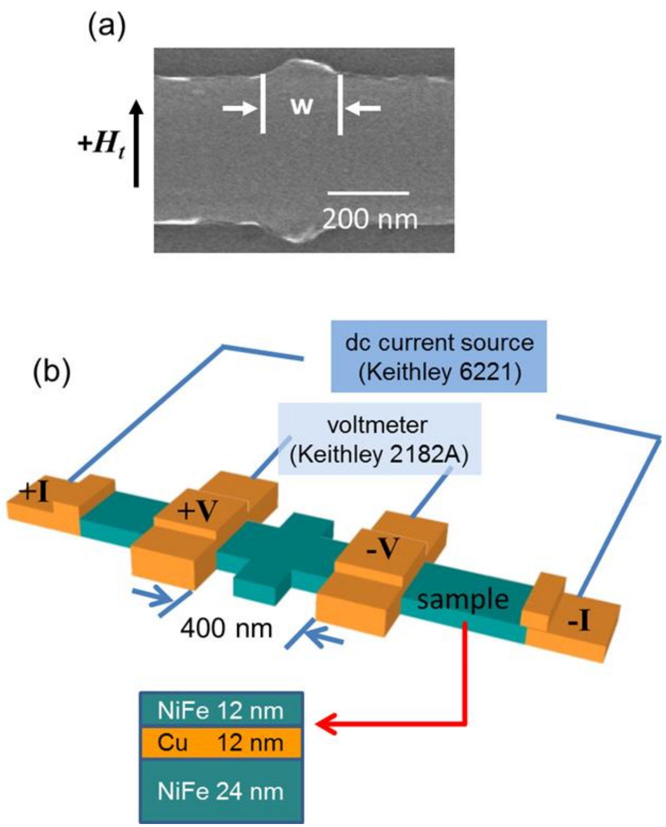

high frequency measurements circuit

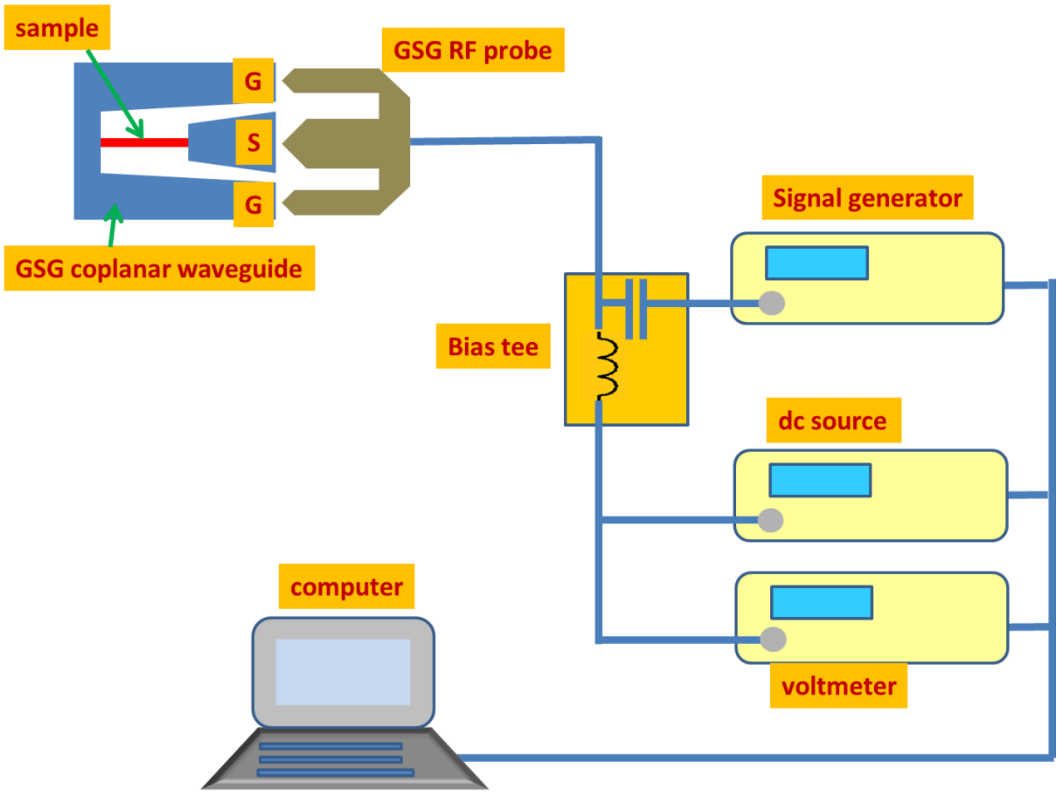

Measurement and simulation results

AC current induced localized domain wall oscillators in NiFe/Cu/NiFe submicron wires

Nucleation of Pinned anti-parallel transverse DW

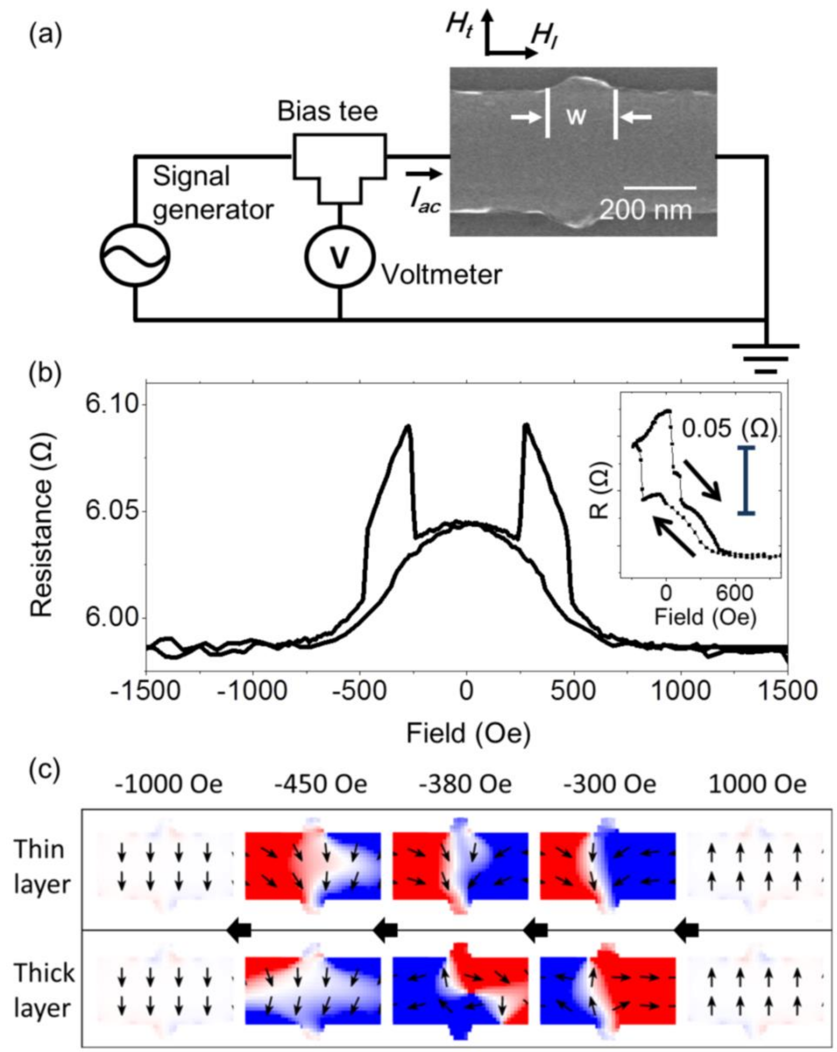

Measurement and simulation results

AC current induced localized domain wall oscillators in NiFe/Cu/NiFe submicron wires

DW resonators for frequency-selective operation

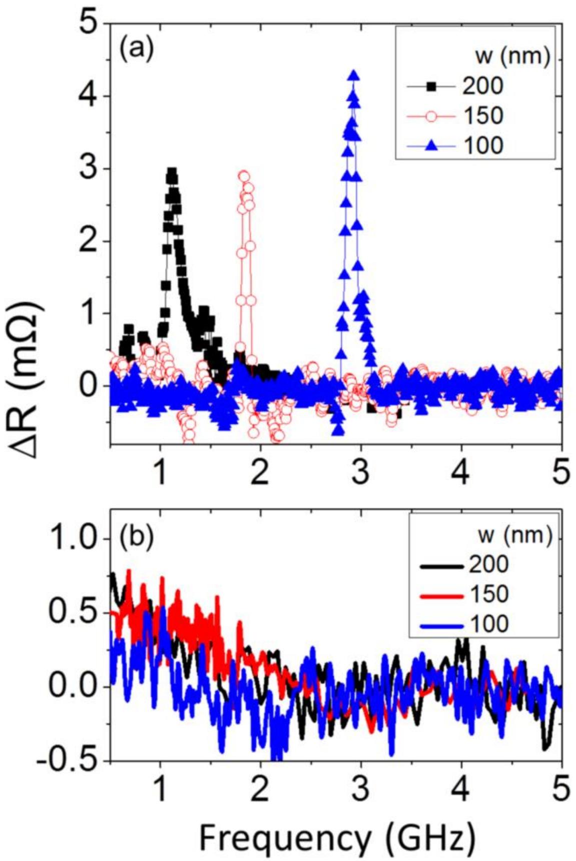

(a) Experimental measurement of the ac current induces resonance excitation of pinned DW trapped at the protrusion. Resistance change as a function of ac excitation current frequency for the submicron wires containing artificial symmetric protrusions with three different widths of protrusion w = 200, 150, and 100 nm. (b) The response curve measured at the saturation field with a uniform state of submicron wires (without DW). The ΔR is observed unchanged with frequency for each of the samples.

Measurement and simulation results

AC current induced localized domain wall oscillators in NiFe/Cu/NiFe submicron wires

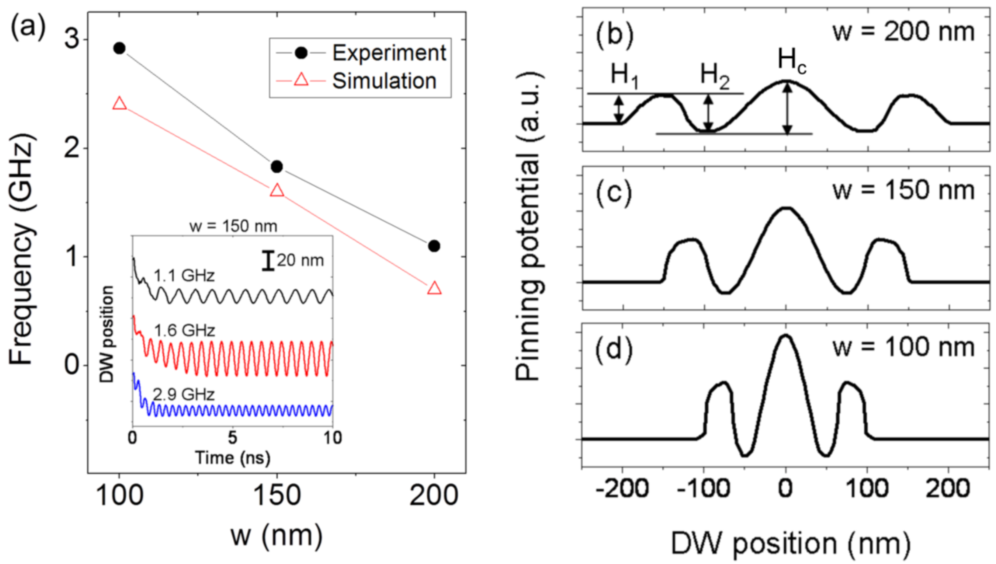

Resonance frequency of pinned DW dependence on the width of trap w, the solid circles and the open triangles indicate the experiment and simulation results respectively. The inset shows the simulated time evolutions of the DW motion with w = 150 nm. (b)-(d) Potential landscape of pinned DW from micromagnetic simulation with three different width of protrusion w = 200, 150, 100 nm.

Measurement and simulation results

Reversible domain wall motion induced by dc current in NiFe/Cu/NiFe submicron wires

Current in-plane

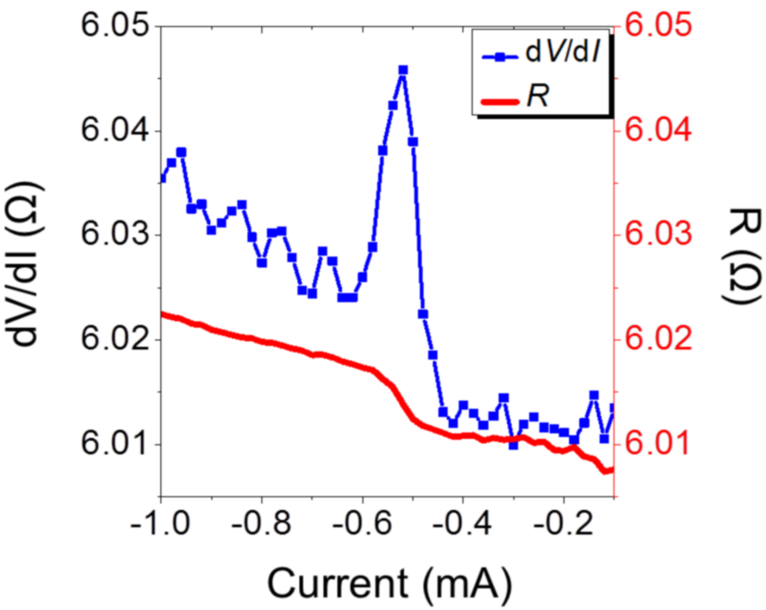

nano-pillar

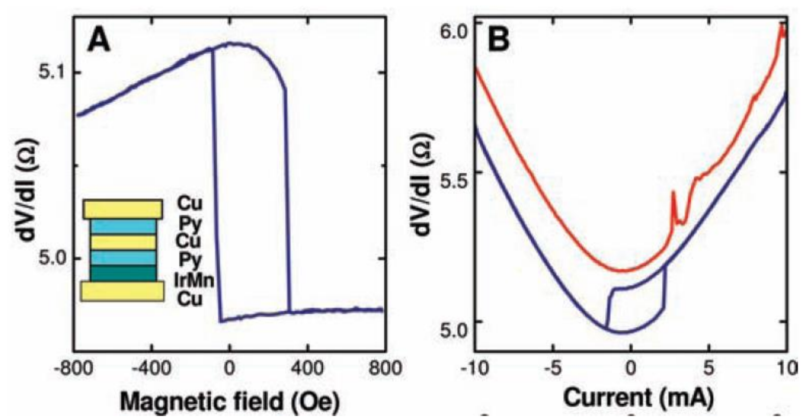

point contact

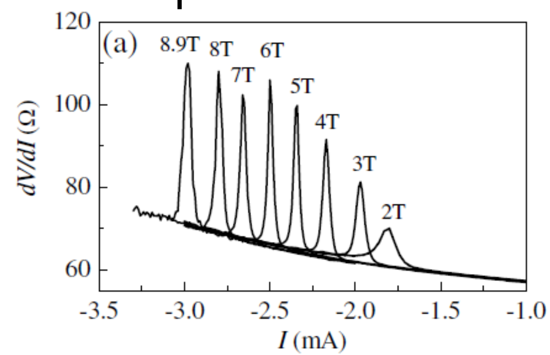

Science **307**, 228 (2005)
PRL **97**, 107204 (2006)

Measurement and simulation results

Reversible domain wall motion induced by dc current in NiFe/Cu/NiFe submicron wires

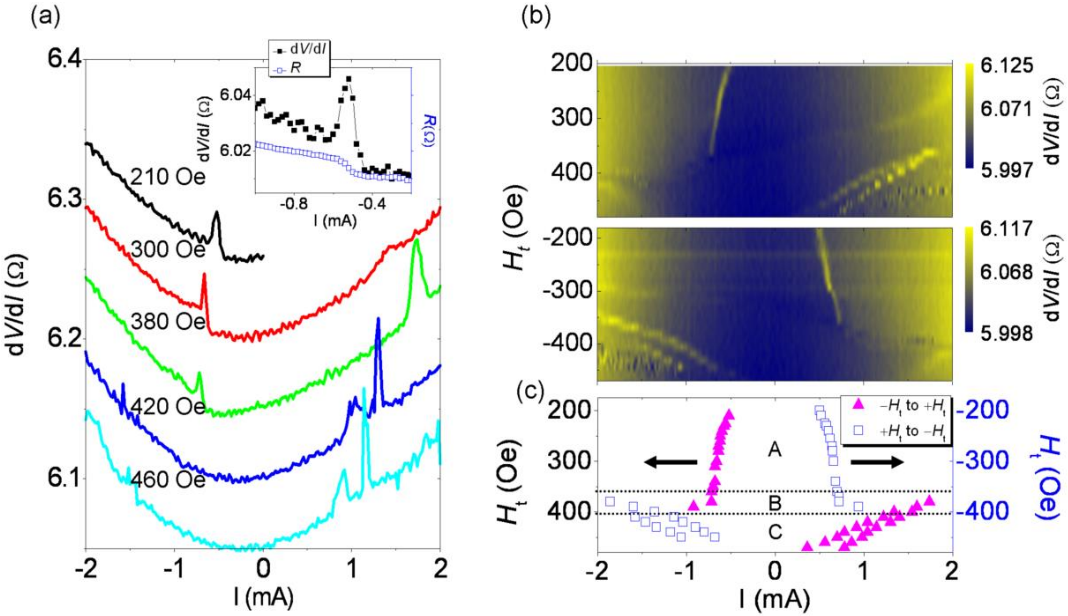

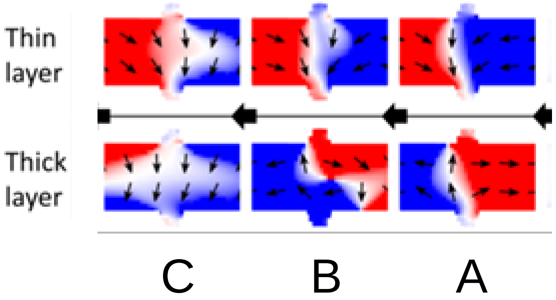

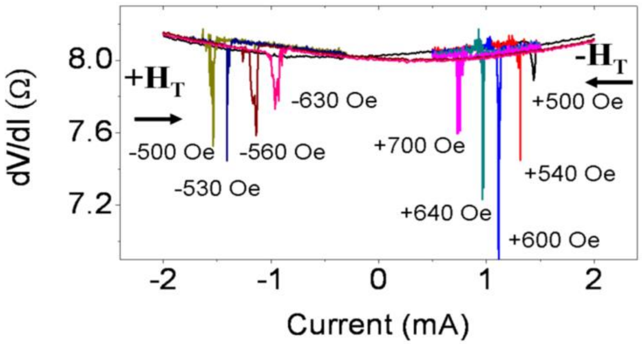

Differential resistance vs. current density at different external transverse fields H_t, enlarged in the inset for V/I vs. j at H_t = 210 Oe. (b) Map of dV/dI versus transverse field and dc current. (c) Critical current I_c vs. H_t.

Measurement and simulation results

Reversible domain wall motion induced by dc current in NiFe/Cu/NiFe submicron wires

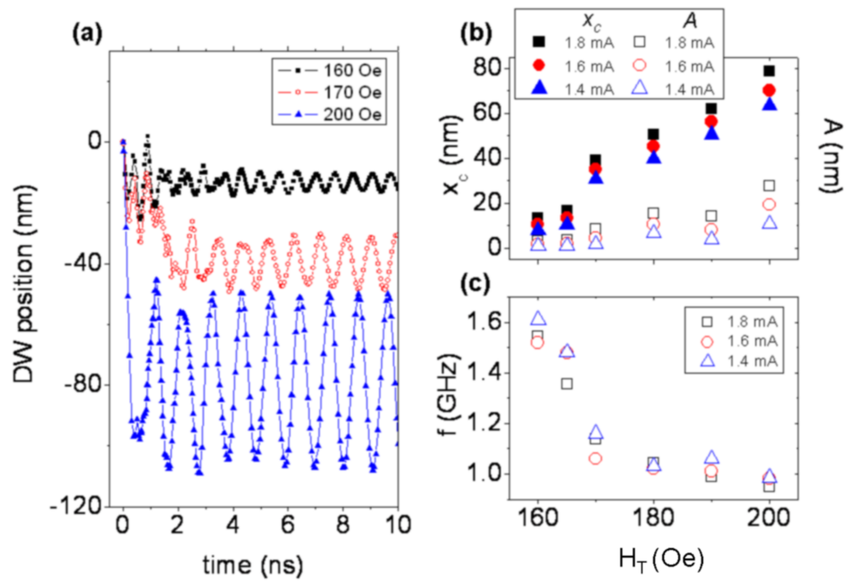

Simulation results of DW position as a function of time under fixed dc current density of 9.7×10^6 A/cm^2 with variation of external transverse field H_t. (b) central position x_c, amplitude A, and (c) frequency of the oscillator vs. H_t with different dc current.

Measurement and simulation results

Reversible domain wall motion induced by dc current in NiFe/Cu/NiFe submicron wires

Series of submicron wires with serial DW traps of artificial symmetric protrusions

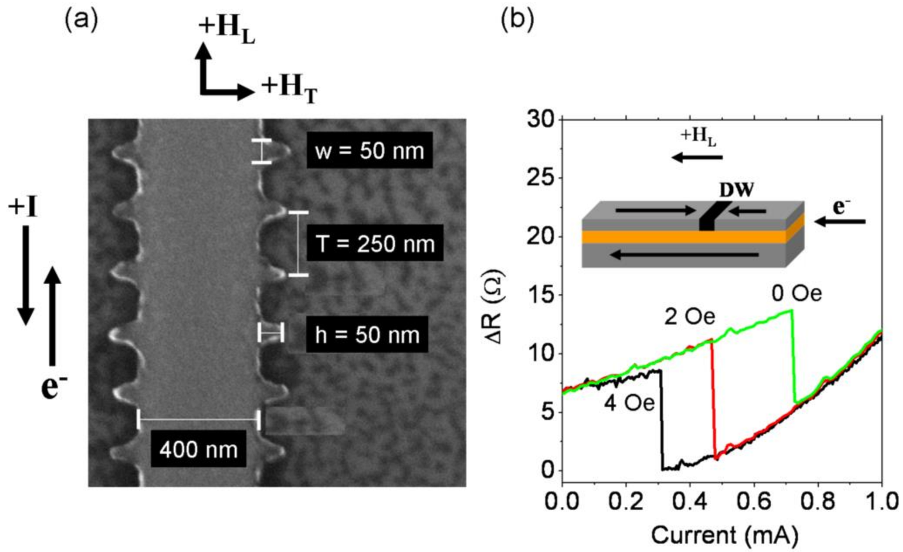

A Scanning electron microscope image of a typical serial-DW-trap sample with the protrusions 50 nm in width and height. The period was 250 nm on either side of the wire. Magnetic field and current directions are specified. (b) Schematic diagram of the sample and the irreversible resistance change from anti-parallel state to parallel state for H_L = 0 (green solid line), 2 (red dash line), and 4 (black dotted line) Oe.

Measurement and simulation results

Reversible domain wall motion induced by dc current in NiFe/Cu/NiFe submicron wires

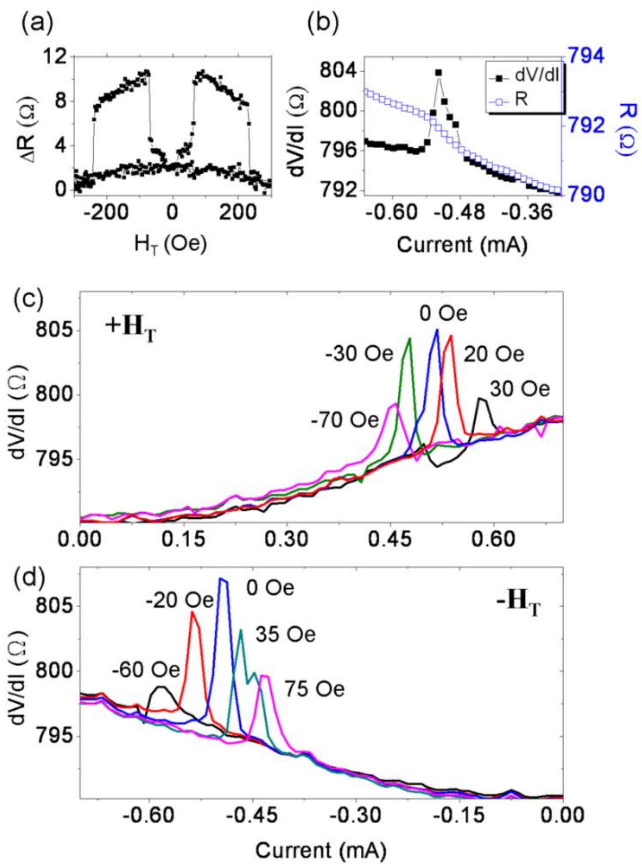

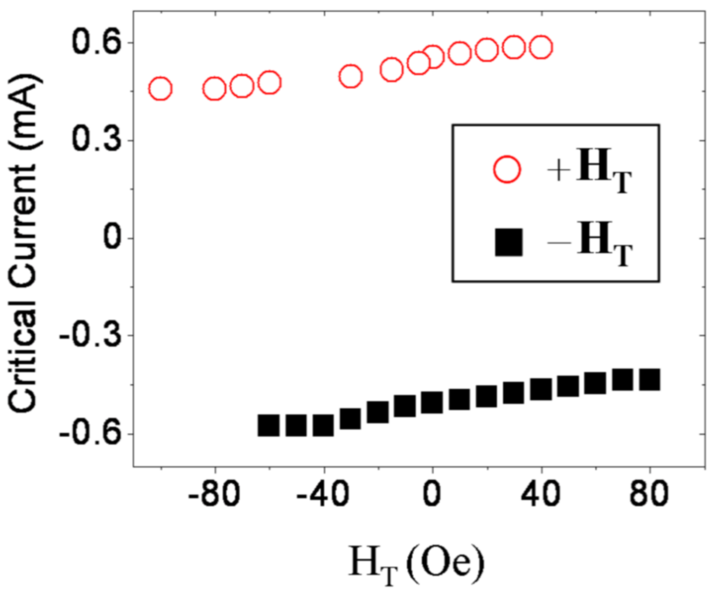

From saturation -3000 (Oe)

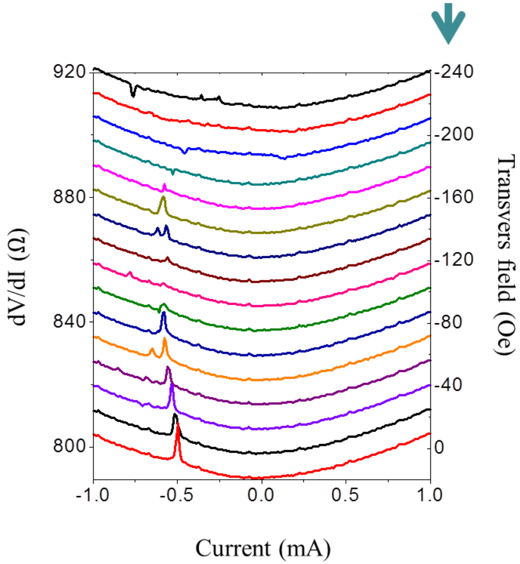

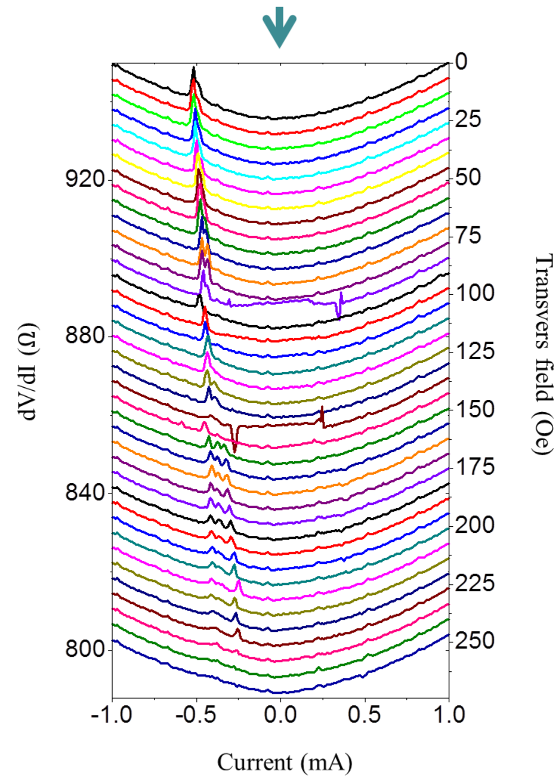

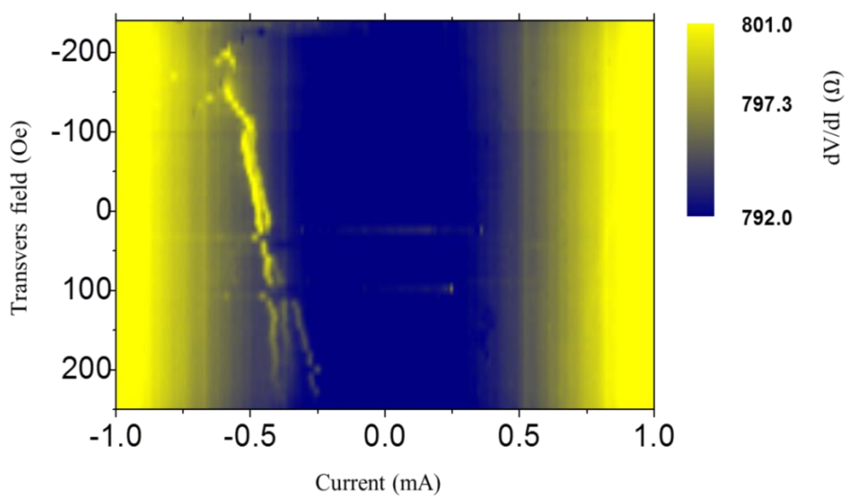

Summary

- DW oscillation with resonance frequency as high as 2.92 GHz and the resonance frequency can be tuned by the width of protrusion.

- The higher resonance frequency for the narrow trap is due to the steeper potential landscape which enhances the restoring force on the pinned DW.

- For the domain wall oscillations induced by injection of a dc current investigated, the observed peak in *dV/dI* associated with the reversible change of magnetoresistance is attributed to the reversible motion of the DW.

Our results on Spin Pumping in ZnO/Py film

co-planar waveguide

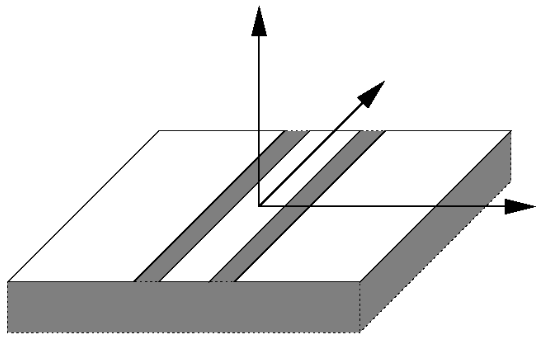

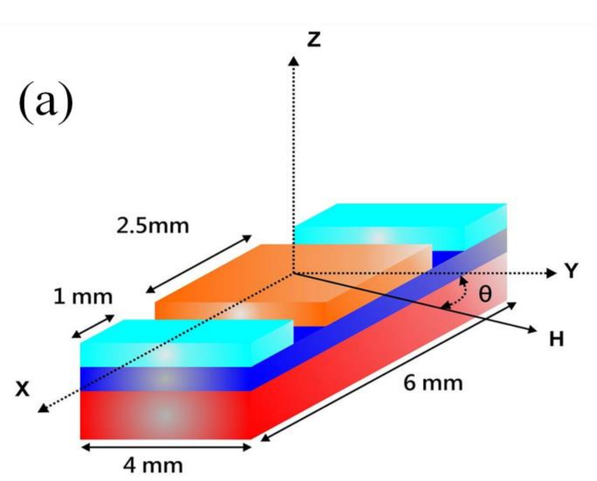

ZnO:
Resistivity 0.014 Ω-cm
carrier concentration 6.09×10^{18} cm^{-3}
mobility 72.9 cm^2/V-s

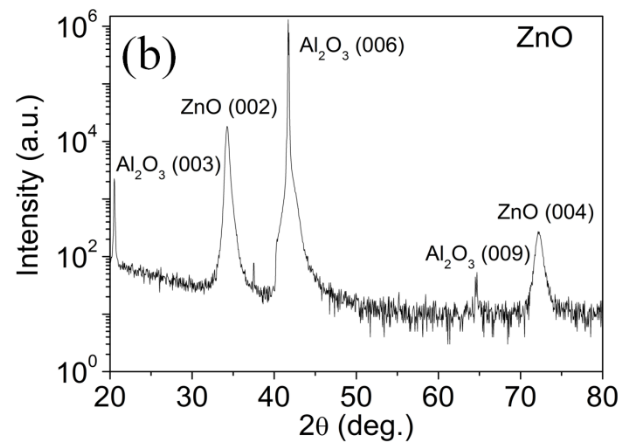

"Inverse spin Hall effect induced by spin pumping into semiconducting ZnO"
APL **104**, 052401 (2014)

The FMR spectra of ZnO/Py samples.

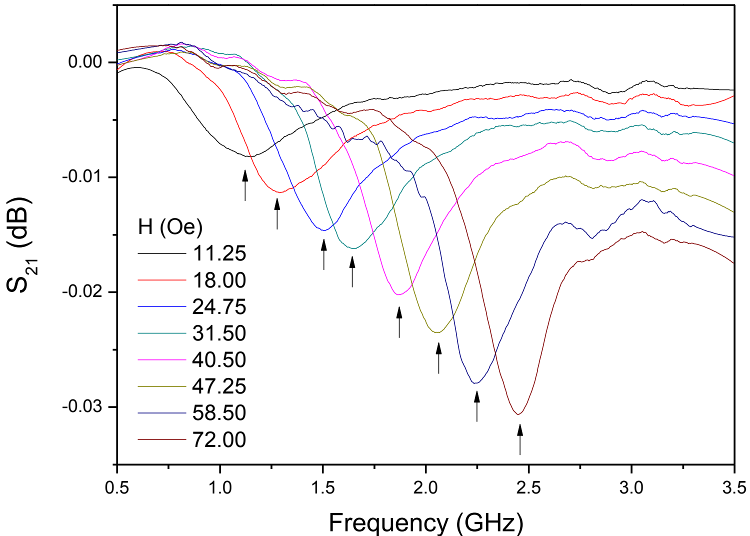

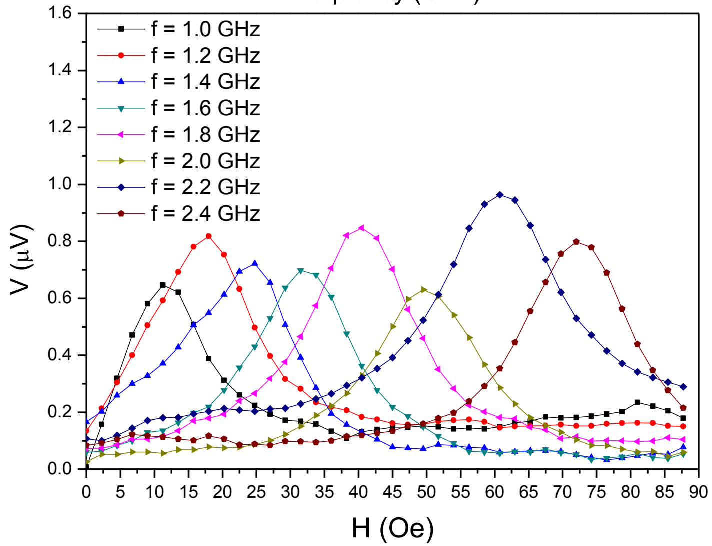

Magnetic field H dependence of electromotive force V measured for the $Ni_{80}Fe_{20}$/ZnO thin film under 50 mW microwave excitation.

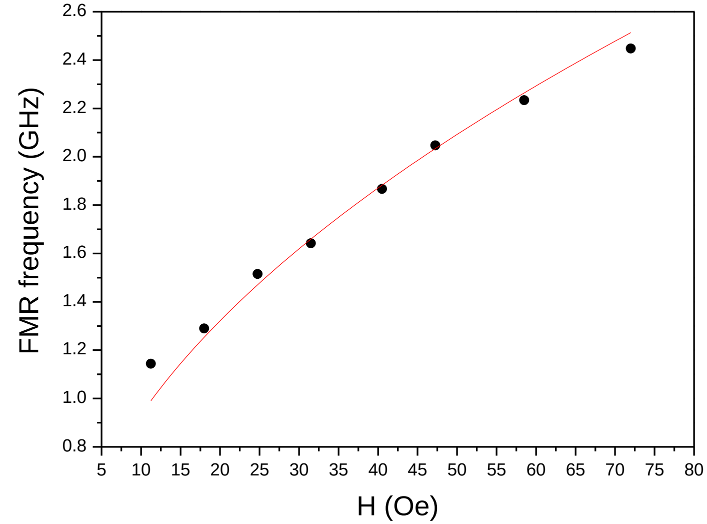

$$(f/\gamma)^2 = H_{FMR}(H_{FMR} + 4\pi M_s)$$

$$V = L\frac{\Delta H^2}{(H-H_0)^2+\Delta H^2} + D\frac{\Delta H(H-H_0)}{(H-H_0)^2+\Delta H^2},$$

Lorentz and dispersive line shapes

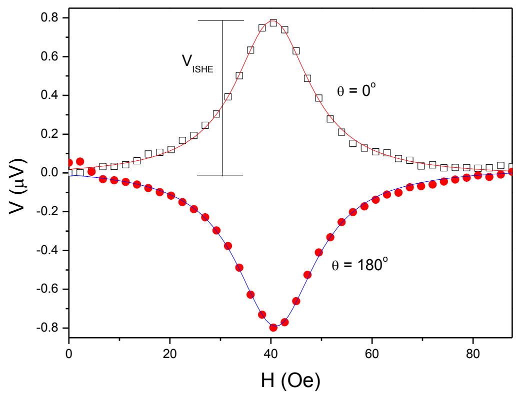

$$\mathbf{E}_{\mathrm{ISHE}} \propto \mathbf{J}_s \times \boldsymbol{\sigma}$$

$$V_{ISHE} = \frac{W_F \theta_{SH} \lambda_N \tanh(\frac{d_N}{2\lambda_N})}{d_N \sigma_N + d_F \sigma_F} (\frac{2e}{\hbar}) j_s^0$$

$$j_s^0 = \frac{g_r^{\uparrow\downarrow} \gamma^2 h_{rf}^2 \hbar [4\pi M_s \gamma + \sqrt{(4\pi M_s)^2 \gamma^2 + 4\omega^2}]}{8\pi\alpha^2 [(4\pi M_s)^2 \gamma^2 + 4\omega^2]}$$

Considering spin back flow,

$$E_y = \frac{2e/\hbar}{\sigma_N d_N + \sigma_F d_F} [j_{1s}^z(0) \theta_{SH}^N \lambda_{sd}^N \tanh \frac{d_N}{2\lambda_{sd}^N} + j_{2s}^z(0) \theta_{SH}^F \lambda_{sd}^F \tanh \frac{d_F}{2\lambda_{sd}^N}]$$

Spin mixing conductance $g_r^{\uparrow\downarrow}$ is the essential parameter to the spin pumping experiment. It refers to the efficiency of generating a spin current

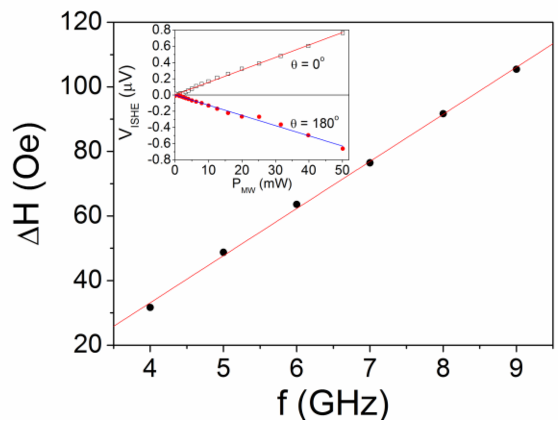

$$\alpha = \frac{g\mu_B}{4\pi M_s d_F} g_r^{\uparrow\downarrow}$$

$$\Delta H_{FMR} = \Delta H_0 + \frac{2\alpha}{\gamma} f$$

$$V_{dc}(H,\theta)=V_{AMR}[L(H)\cos\phi+L'(H)\sin\phi]\sin(2\theta)\sin\theta+V_{ISHE}L(H)\cos\theta$$

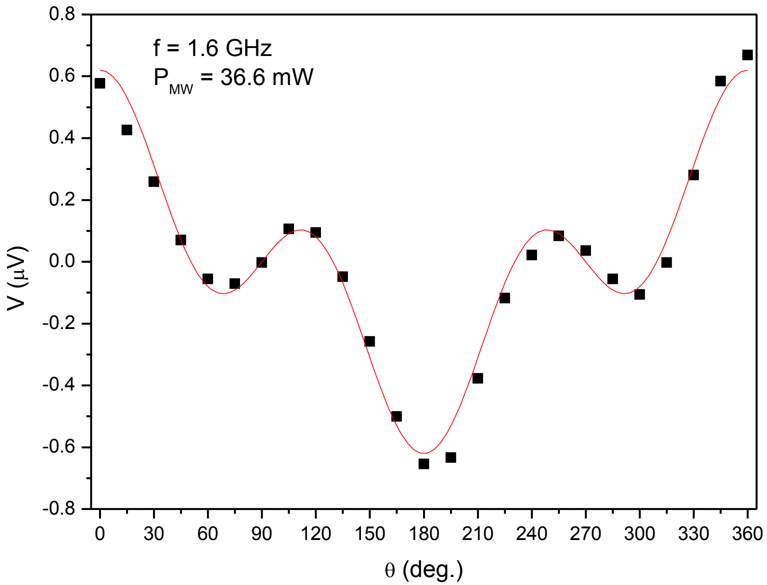

$$L(H)=\frac{\Delta H^2}{(H-H_{FMR})^2+\Delta H^2}$$

$$L'(H)=\frac{\Delta H(H-H_{FMR})}{(H-H_{FMR})^2+\Delta H^2}$$

The in-plane angle θ dependence of the electromotive force V or $Ni_{80}Fe_{20}$ / ZnO thin film. The solid symbols are the experimental data and the red line is the theoretical fitting line.

PHYSICAL REVIEW B **83**, 144402 (2011)

Spin pumping and anisotropic magnetoresistance voltages in magnetic bilayers: Theory and experiment

A. Azevedo,[1,*] L. H. Vilela-Leão,[1] R. L. Rodríguez-Suárez,[2] A. F. Lacerda Santos,[1] and S. M. Rezende[1]
[1]*Departamento de Física, Universidade Federal de Pernambuco, Recife, Pernambuco 50670-901, Brazil*
[2]*Facultad de Física, Pontificia Universidad Católica de Chile, Casilla 306, Santiago, Chile*
(Received 6 June 2010; revised manuscript received 29 January 2011; published 4 April 2011)

$$\mathbf{I}_s^p = \frac{\hbar}{4\pi}\left(\mathrm{Re}g^{\uparrow\downarrow}\mathbf{m}\times\frac{d\mathbf{m}}{dt} + \mathrm{Im}g^{\uparrow\downarrow}\frac{d\mathbf{m}}{dt}\right),$$

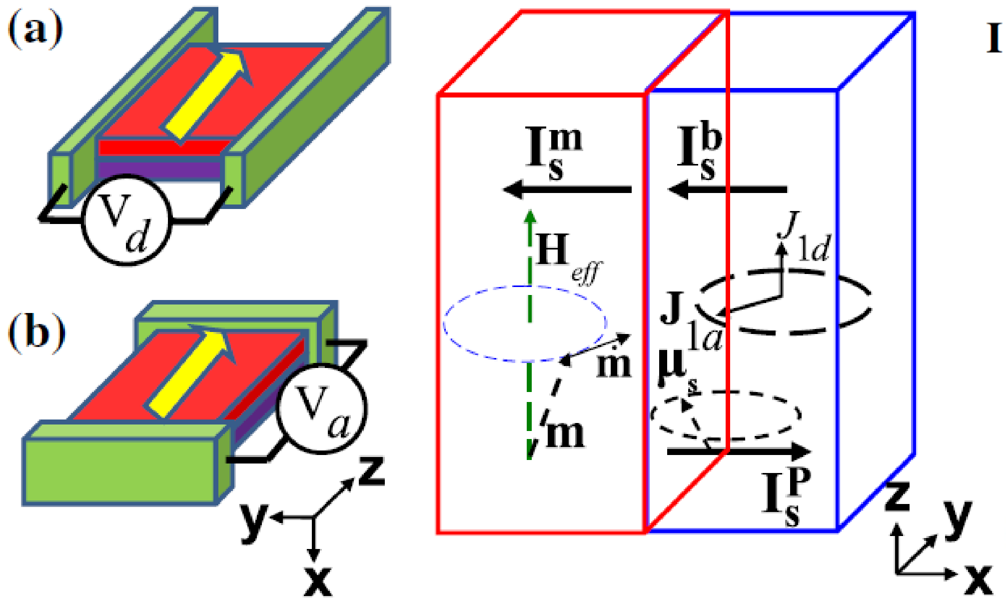

$$\mathbf{I}_s^b = \frac{g}{8\pi}[2p(\mu_0^F - \mu_0^N) + \mu_s^F - \mathbf{m}\cdot\boldsymbol{\mu}_s^N]\mathbf{m} - \frac{\mathrm{Re}g^{\uparrow\downarrow}}{4\pi}\mathbf{m}\times(\boldsymbol{\mu}_s^N\times\mathbf{m}) + \frac{\mathrm{Im}g^{\uparrow\downarrow}}{4\pi}\mathbf{m}\times\boldsymbol{\mu}_s^N$$

$$E_z(t) = \frac{4e/\hbar}{\sigma_N d_N + \sigma_F d_F}\mathrm{Re}\left(\frac{\alpha_N j_{1s}^y(0)}{\kappa_2(\omega)}\tanh\frac{d_N\kappa_2(\omega)}{2} + \alpha_F j_{2s}^y(0)\lambda_{\mathrm{sd}}^F\tanh\frac{d_N}{2\lambda_{\mathrm{sd}}^N}\right),$$

$$E_y = \frac{2e/\hbar}{\sigma_N d_N + \sigma_F d_F}\left[j_{1s}^z(0)\alpha_N\lambda_{\mathrm{sd}}^N\tanh\frac{d_N}{2\lambda_{\mathrm{sd}}^N} + j_{2s}^z(0)\alpha_F\lambda_{\mathrm{sd}}^F\tanh\frac{d_F}{2\lambda_{\mathrm{sd}}^F}\right].$$

Schematic spin battery operated by FMR, for the measurement configurations (a) and (b). The ac (dc) voltage drops along the z (y) direction. The right panel introduces the parameters of the model. The effective field H_{eff} is the sum of the external field H_{ex} and the uniaxial field H_{un}, H_{ex}, and H_{un} point along the z axis. The dc component $J_{1d}(j_{1s}{}^{z})\mathbf{e}_z$ and ac component $\mathbf{J}_{1a}(\mathbf{j}_{1s}{}^{a})$ constitute the spin current $\mathbf{j}_{1s}$.

PRL **110**, 217602 (2013) Spin Backflow and ac Voltage Generation by Spin Pumping and the Inverse Spin Hall Effect

Spin Hall Magnetoresistance

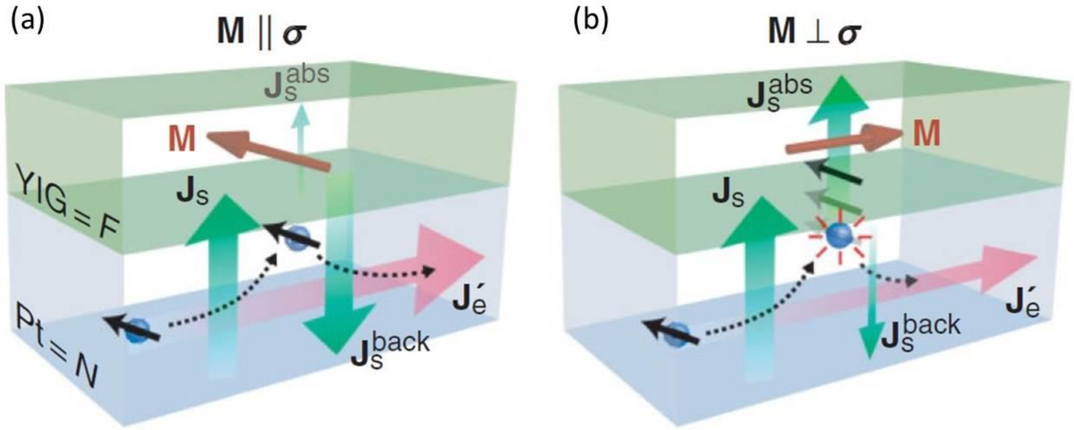

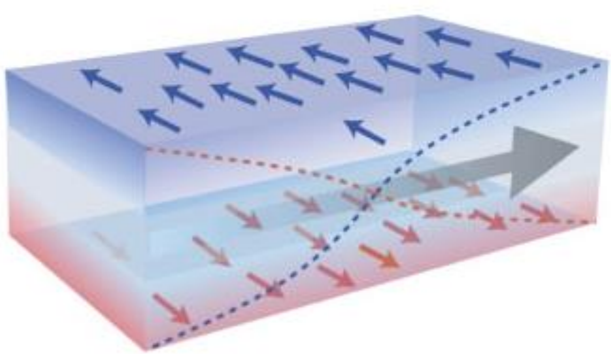

PRL **110**, 206601 (2013) Spin Hall Magnetoresistance Induced by a Nonequilibrium Proximity Effect

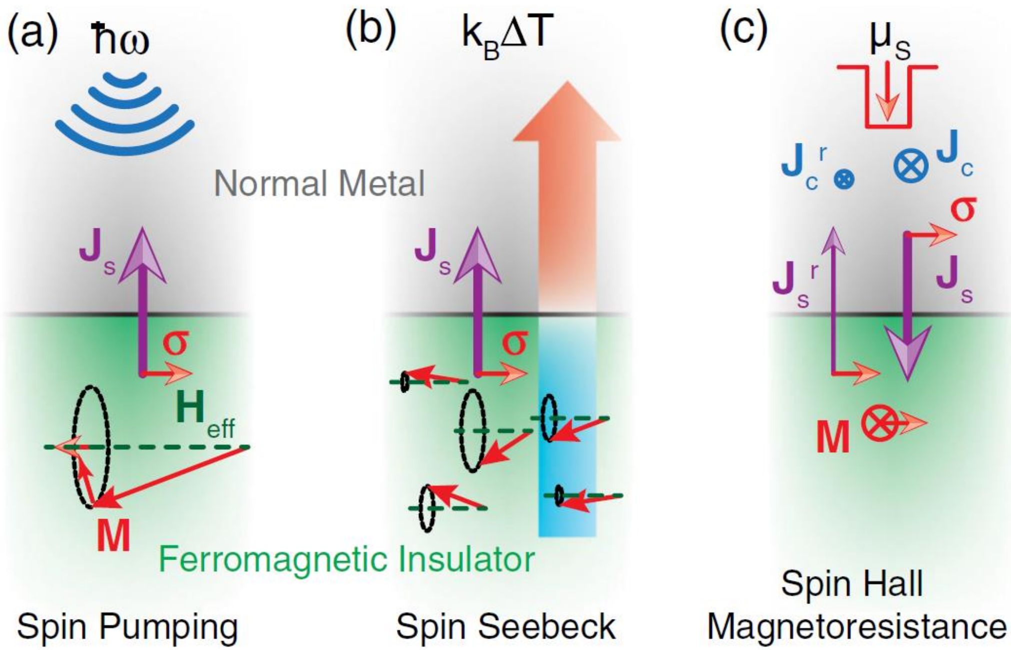

(a),(b) Schematic depictions of the spin pumping and spin Seebeck effects. The magnetization $\boldsymbol{M}$ in the ferromagnet (YIG in our experiments) is excited either resonantly (a) or thermally (b). The $\boldsymbol{M}$ precession around $\boldsymbol{H}_{eff}$ (see text) is damped via the emission of a spin current J_s with polarization $\boldsymbol{\sigma}$ into the normal metal (Pt in our experiments). (c) The spin Hall magnetoresistance is due to the torque exerted on $\boldsymbol{M}$ by an appropriately polarized J_s which yields a change in the reflected spin current J_s^r. The interconversion between J_s (J_s^r) and the charge currents J_c (J_c^r) are due to the (inverse) spin Hall effect in the normal metal.

PRL **111**, 176601 (2013) Experimental Test of the Spin Mixing Interface Conductivity Concept

J. J. Liang (梁君致)
Dept. of Physics, Fu Jen University

D. S. Hung(洪東興)
Dept. of Info. Telecom. Eng.
Ming Chuan University

S. Y. Huang (黃斯衍), C. Yu (于 淳), J. C. Lee(李榮銓), L. J. Chang (張良君), T. W. Chiang (江典蔚), L. K. Lin (林呂圭), Faris B.

Y. C. Chiu (邱昱哲), Y. H. Chiu (邱亦欣) , C. H. Hsieh (謝智勛), C. C. Chang (張哲鈞), L. W. Huang (黃崚瑋)

Summary

Spintronics has involved

- Magnetic materials, metallic multilayers, tunnel junctions, magnetic semiconductors, and (hopefully) room temperature half metal.
- Spin dependent electron transport, spin imbalance induced charge accumulation and relaxation, which transforms into the concept of pure spin current.
- Static and dynamic properties of magnetic nanostructures.

d orbitals

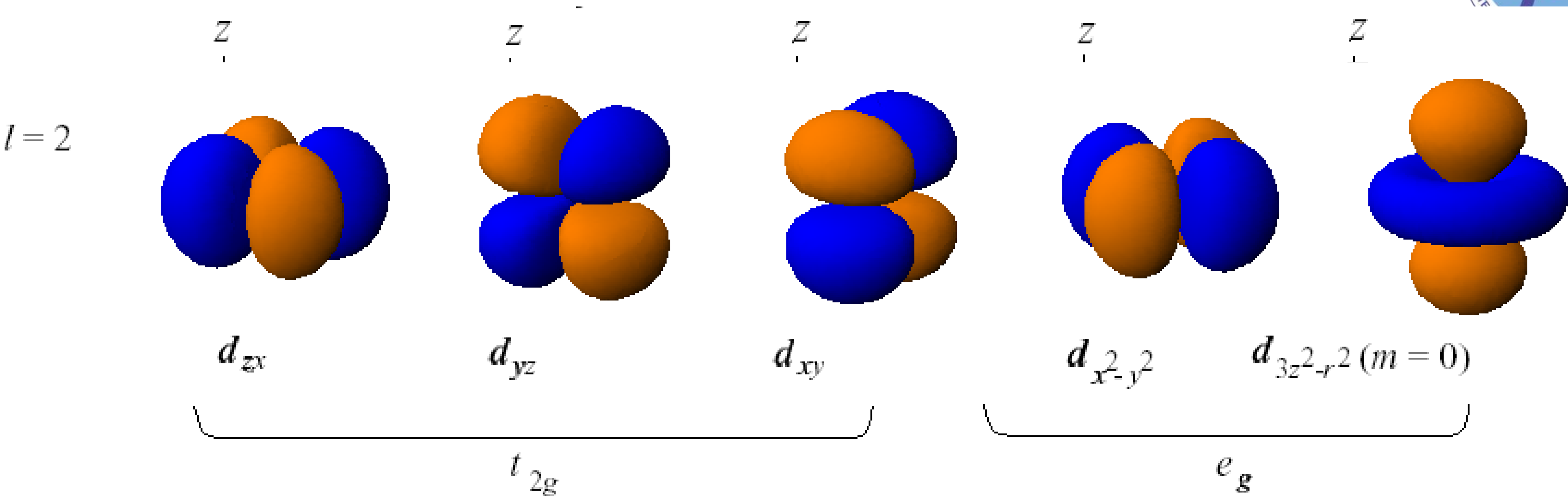

Crystal-field splitting

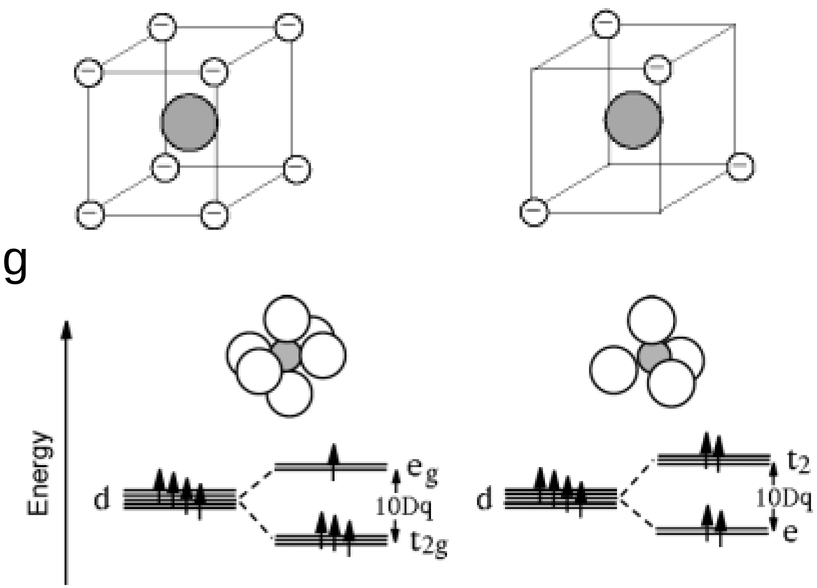

Simulation of Oscillatory Domain Wall Motion Driven by Spin Waves in Perpendicular Magnetic Anisotropy Nanostrip

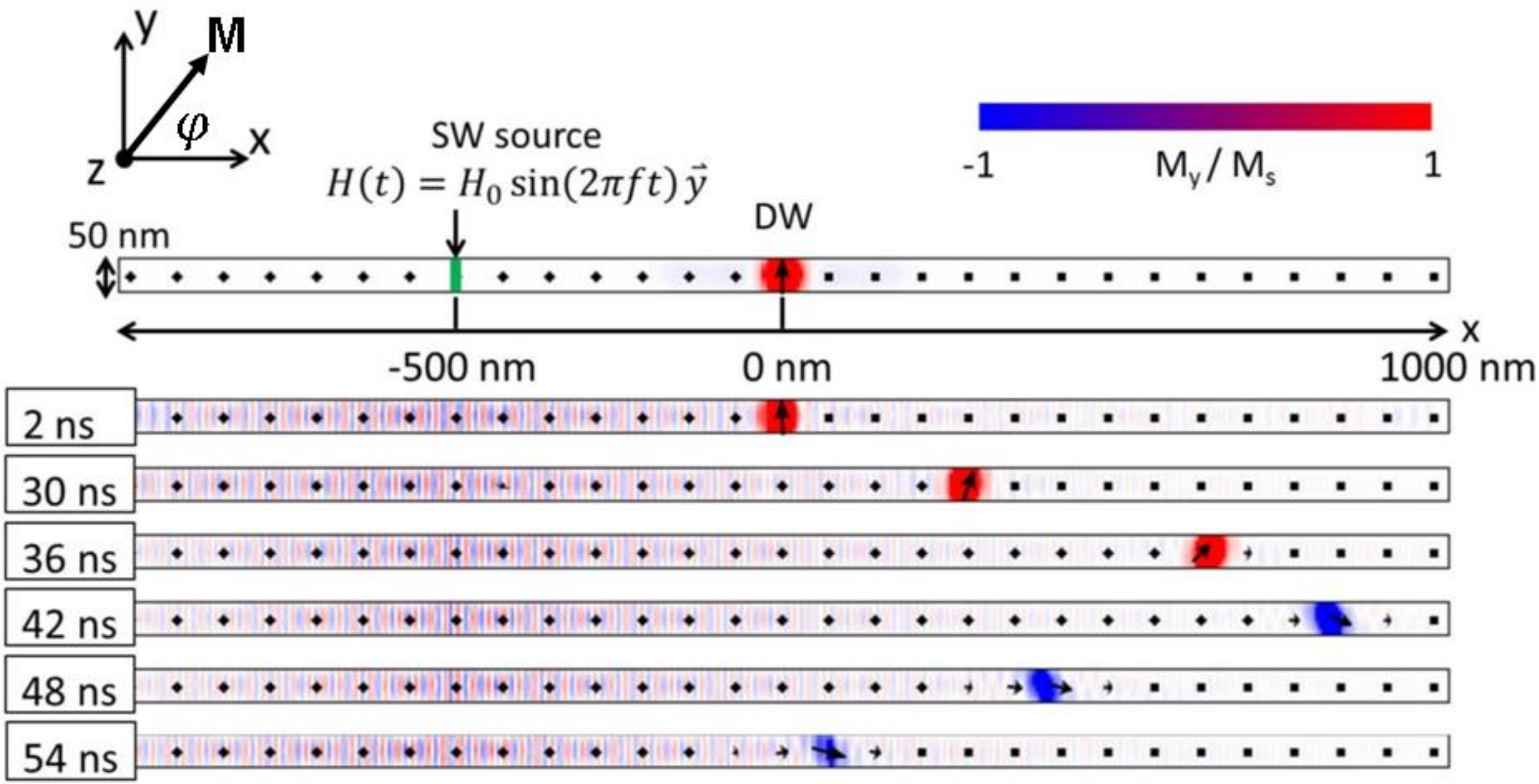

GSG Coplanar Waveguide

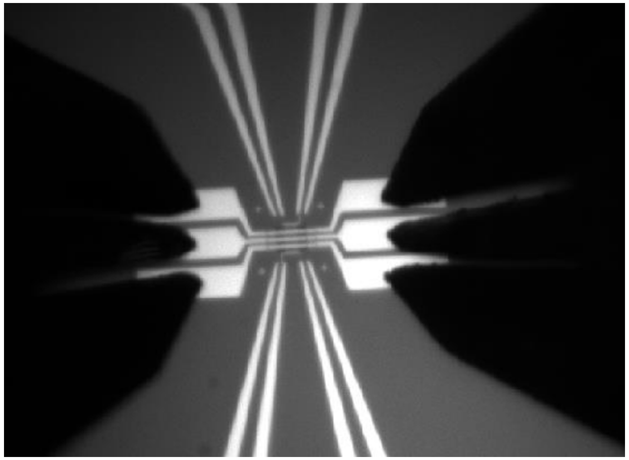

Inverse Spin Hall Effect

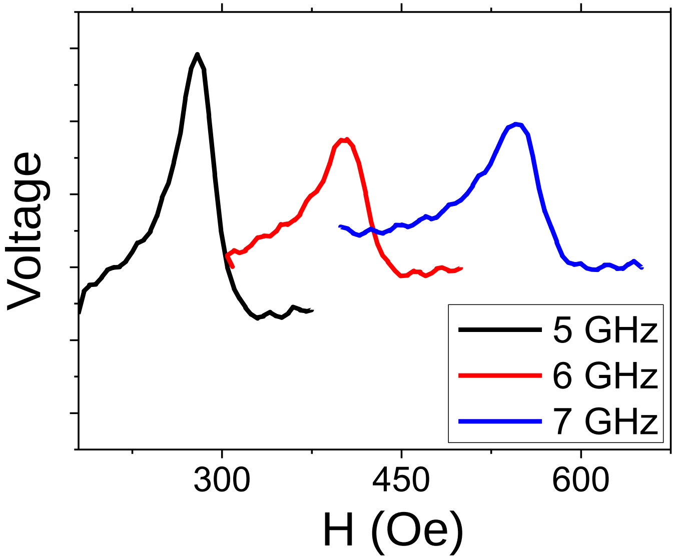

GMR Nanopillar

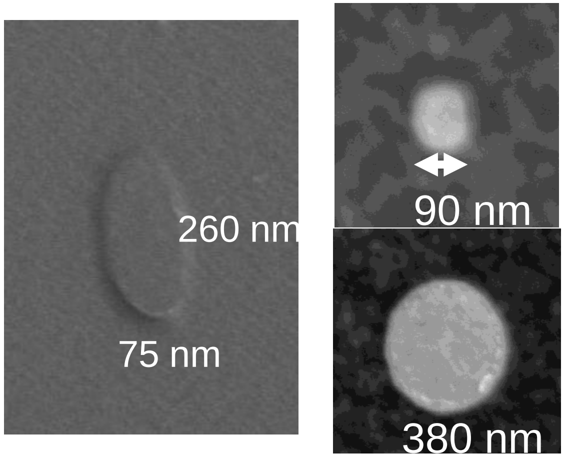

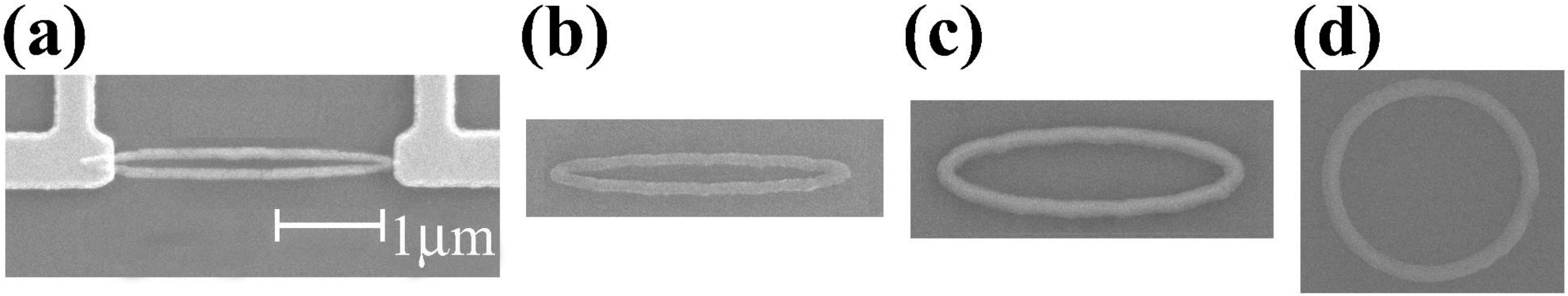
(a)
(b)
(c)
(d)
1μm

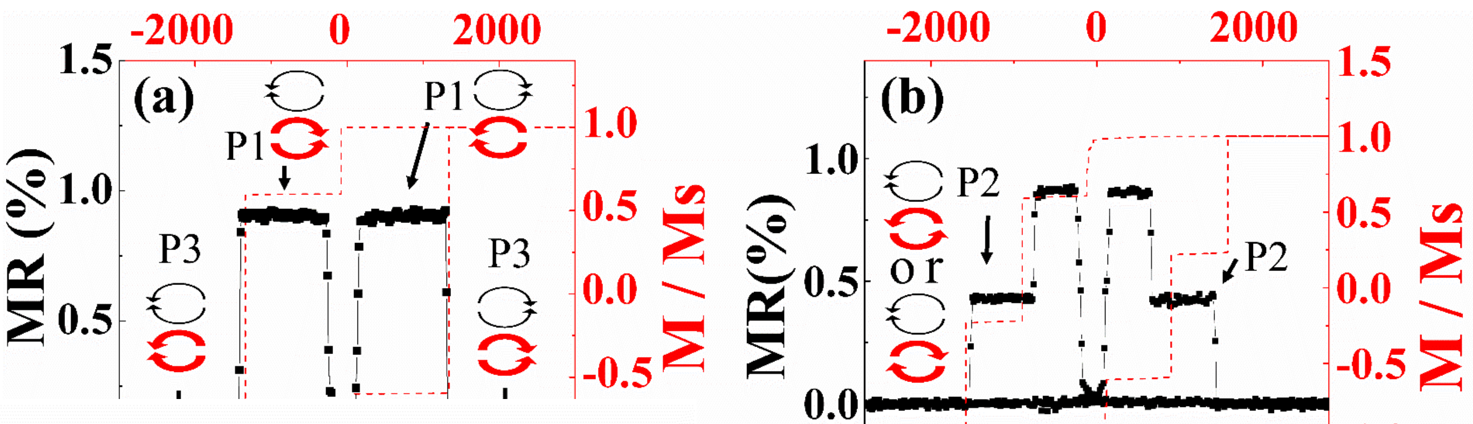
(a)
P1
P1
P3
P3
MR (%)
M / Ms
-2000
0
2000
(b)
P2
or
P2
MR(%)
M / Ms

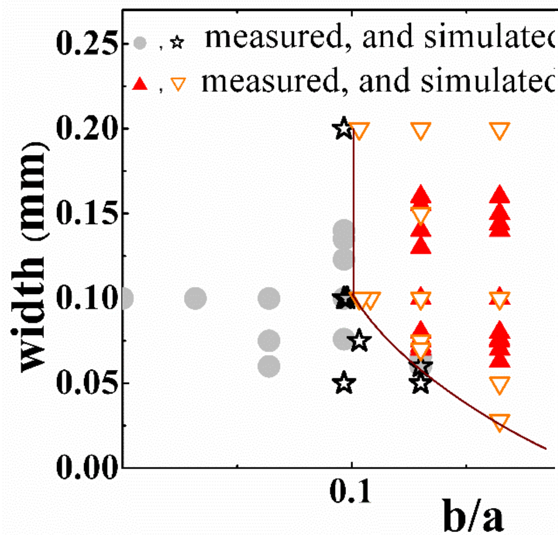
measured, and simulated
measured, and simulated
width (mm)
b/a
0.1

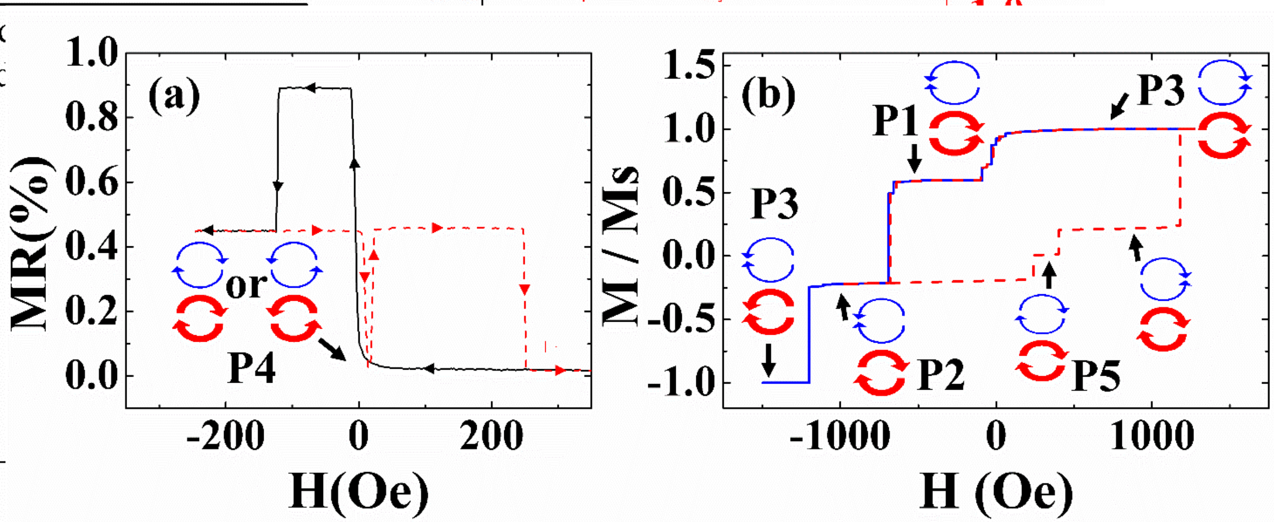
(a)
or
P4
MR(%)
H(Oe)
(b)
P1
P3
P3
P2
P5
M / Ms
H (Oe)

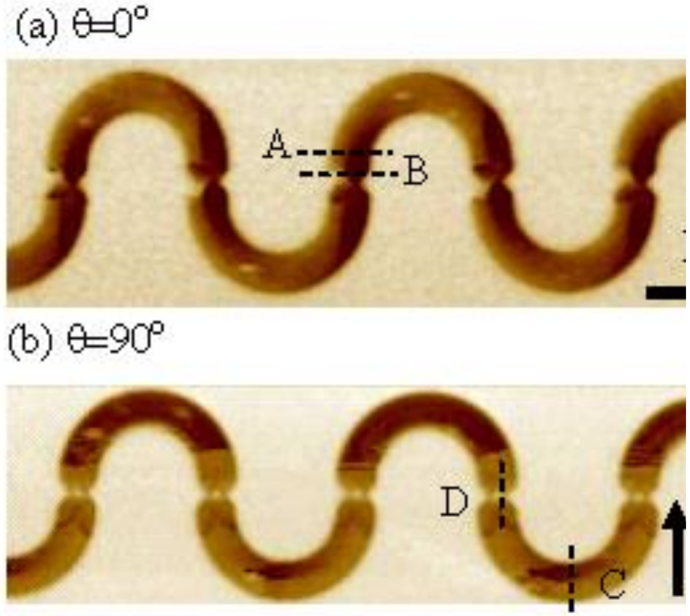
(a) θ=0°
A
B
(b) θ=90°
D
C

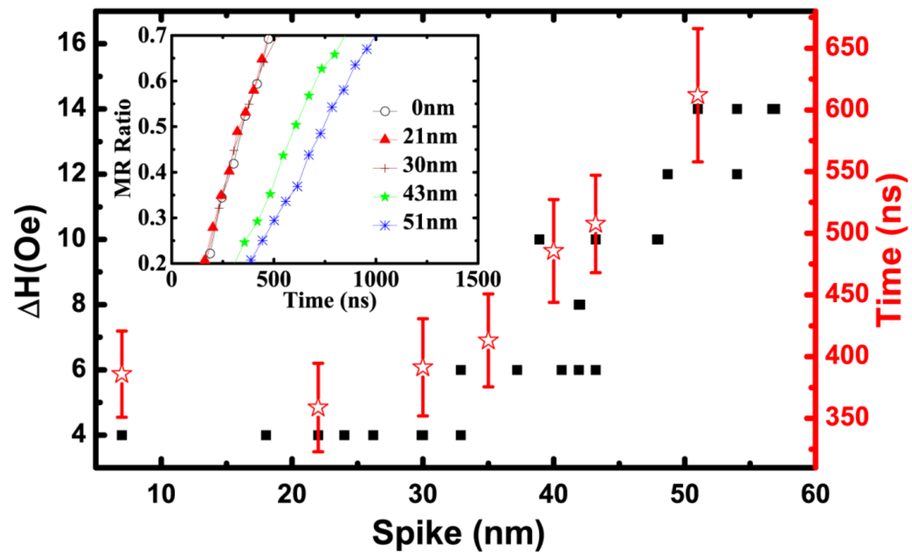
ΔH(Oe)
Time (ns)
Spike (nm)
MR Ratio
Time (ns)
0nm
21nm
30nm
43nm
51nm

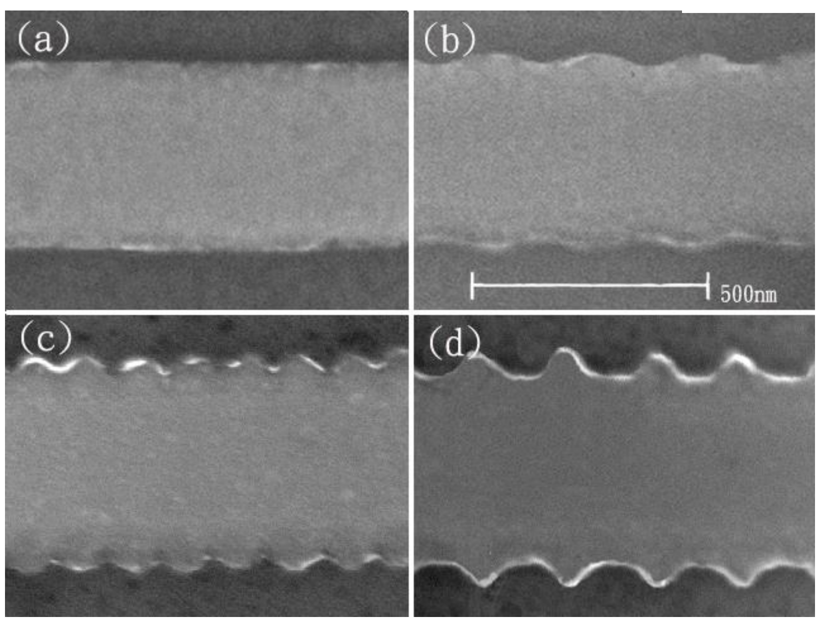
(a)
(b)
500nm
(c)
(d)

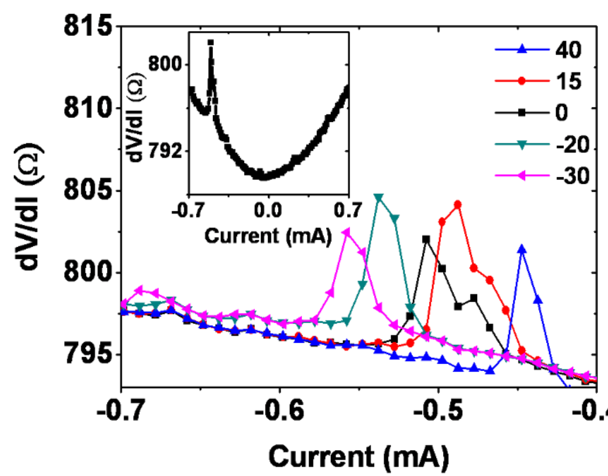
dV/dI (Ω)
Current (mA)
40
15
0
-20
-30
dV/dI (Ω)
Current (mA)

Topological spin textures in the helical magnet $Fe_{0.5}Co_{0.5}Si$.

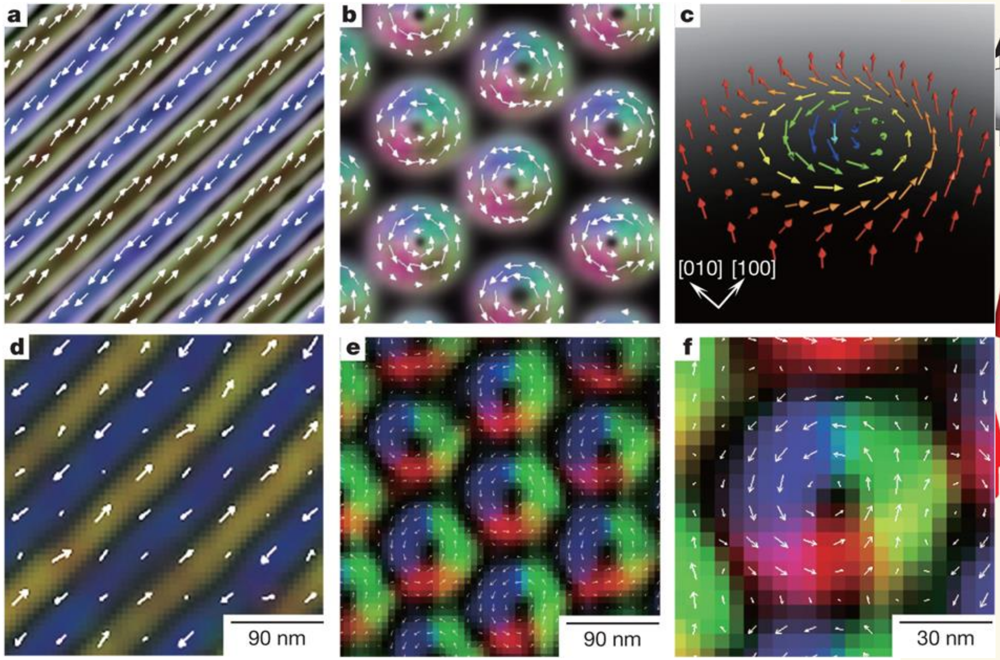

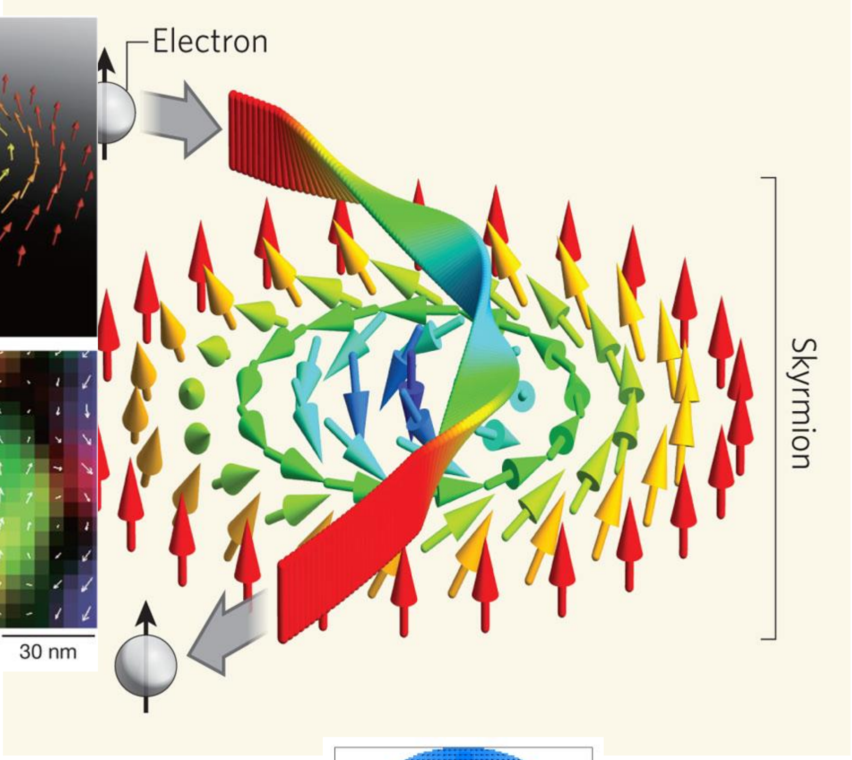

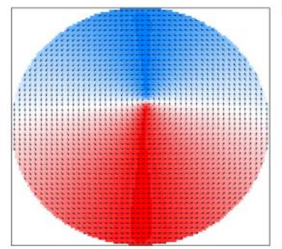

XZ Yu *et al. Nature* **465**, 901-904 (2010) doi:10.1038/nature09124